REPORT DOCUMENTATION PAGE

AFRL-SR-AR-TR-04-

1. REPORT DATE (DD-MM-YYYY)	2. REPORT TYPE		3. DATES COVERED (From - To)
	Final Report		Dec 15, 00 - Dec 14, 03

4. TITLE AND SUBTITLE
Multibody Approach to the Dynamic Analusis of Structures with ActuatedComponents

5a. CONTRACT NUMBER

5b. GRANT NUMBER
F49620-01-1-0038

5c. PROGRAM ELEMENT NUMBER

6. AUTHOR(S)
Dr. Oliver A. Bauchau

5d. PROJECT NUMBER

5e. TASK NUMBER

5f. WORK UNIT NUMBER

7. PERFORMING ORGANIZATION NAME(S) AND ADDRESS(ES)
Gerogia Tech Research Corporation
Gerogia Institute of Technology
Atlanta, GA 30332-0420

8. PERFORMING ORGANIZATION REPORT NUMBER

9. SPONSORING/MONITORING AGENCY NAME(S) AND ADDRESS(ES)
Department of the Air Force   4015 Wilson Blvd.
Air Force Office of Scientific Research   Arlington, VA 22203-1954

10. SPONSOR/MONITOR'S ACRONYM(S)

11. SPONSOR/MONITOR'S REPORT NUMBER(S)

12. DISTRIBUTION/AVAILABILITY STATEMENT

Distribution Statement A: Approved for public release. Distribution unlimited

20040220 311

13. SUPPLEMENTARY NOTES
DODAAD CODE: 1G474
AFOSR Program Manager: Dr. Fariba Farhoo

14. ABSTRACT

High-fidelity, finite-element-based dimensionally reduced models have been constructed for composite plates and shells, including hygrothermal and piezoelectric effects, under the sponsorship of AFOSR. In these models, the smallness of the thickness has been used to advantage to rigorously reduce the original three-dimensional geometrically nonlinear elasticity theory to two-dimensional Reissner-Mindlin type theory for plates and shells. The resulting theory can achieve an accuracy comparable to higher-order layerwise theories at the cost of only a first-order shear deformation theory. The dimensional reduction process and the recovery relations for the original three-dimensional displacements/strains/stresses are implemented in a finite-element code, Variational Asymptotic Plate and Shell Analysis (VAPAS). This program is connected with DYMORE, a nonlinear finite-element based multi-body dynamic code to provide an efficient and accurate simulation capability for space systems involving composite and inflatable components with actuated elements which are required for current and future Air Force missions.

15. SUBJECT TERMS

16. SECURITY CLASSIFICATION OF:			17. LIMITATION OF ABSTRACT	18. NUMBER OF PAGES	19a. NAME OF RESPONSIBLE PERSON
a. REPORT	b. ABSTRACT	c. THIS PAGE			Dr. Oliver A. Bauchau
					19b. TELEPHONE NUMBER (Include area code) 404-894-4763

Standard Form 298 (Rev. 8/98)
Prescribed by ANSI Std. Z39.18

Introduction

This three-year grant was initiated in December 2000. All work done under the auspices of the grant is summarized herein, and the various papers written under grant sponsorship are appended to provide all the technical details. The objective of this research was to provide high-fidelity, finite-element-based simulation capability to assist in the analysis and design of structures for space applications. The importance of such a research stems from the Air Force interest of space structures comprising antennas, solar concentrators, sun shields, struts and booms, and membrane mirrors. Moreover, the various components of these systems often are in relative motion with respect to one another, resulting in variable geometry systems that are truly multi-body in nature. Low-cost, accurate simulation tools are essential for the design, analysis and assessment of such systems. However, efficiency of such a simulation tool can only be achieved through dimensional reduction: it is impractical to treat each structural element as a three-dimensional (3-D) body. Hence, low-order, accurate models are needed to not only provide the elastic constants needed in the finite element representation to calculate the global behavior, but also to provide a unified means to obtain the strain and stress distribution in the structures.

There are two main research aspects in this project: a local through-the-thickness model focuses on the evaluation of elastic constants and displacement/strain/stress recovery, and a finite-element-based, nonlinear flexible multi-body dynamics simulation tools based on those models. The basic research issues that have been addressed under the first aspect are

1. Constructing an accurate Reissner-Mindlin type model for composite plate using the variational asymptotic method (VAM) [1];

2. Constructing of an accurate Reissner-Mindlin type model for composite shells using VAM including both geometrical correction due to initial curvature and transverse shear effects;

3. Developing a geometrically exact nonlinear shear deformation shell theory to be compatible with the models developed;

4. Modeling regular composite plates and shells including hygrothermal effects so that the change of structural behavior due to moisture and temperature can be analyzed;

5. Modeling smart composite plates and shells made with piezoelectric material.

Approach

The variational asymptotic method (VAM) has applied to develop a high-fidelity/low-order model for composite plates and shells. Instead of employing *ad-hoc* assumptions, the VAM relies on the use of the small parameters that are inherent to the structure. This ensures construction of a theory with the minimum complexity for a given level of fidelity. The original 3-D nonlinear problem is formulated based on a set of two-dimensional (2-D) intrinsic variables and warping functions representing the arbitrary deformation of the normal line. Then the VAM is used to rigorously split the 3-D problem into two problems: a nonlinear, 2-D, plate or shell analysis over the reference surface to obtain the global deformation and a one-dimensional (1-D) linear analysis through the thickness to provide the 2-D generalized constitutive law and the recovering relations to approximate

2

Multi-body Approach to the Dynamic Analysis of Space Structures with Actuated Components Final Report: AFOSR Grant F49620-01-1-0038

Olivier A. Bauchau, Professor
Project Director and Co-Principal Investigator
e-mail: olivier.bauchau@ae.gatech.edu
phone: 404-894-0042; fax: (404) 894-2760
and
Dewey H. Hodges, Professor
Co-Principal Investigator
e-mail: dewey.hodges@ae.gatech.edu
phone: 404-894-8201; fax: (404) 894-2760

School of Aerospace Engineering
Georgia Institute of Technology, Atlanta, Georgia 30332-0150

Summary

High-fidelity, finite-element-based dimensionally reduced models have been constructed for composite plates and shells, including hygrothermal and piezoelectric effects, under the sponsorship of AFOSR. In these models, the smallness of the thickness has been used to advantage to rigorously reduce the original three-dimensional geometrically nonlinear elasticity theory to two-dimensional Reissner-Mindlin type theory for plates and shells. The resulting theory can achieve an accuracy comparable to higher-order layerwise theories at the cost of only a first-order shear deformation theory. The dimensional reduction process and the recovery relations for the original three-dimensional displacements/strains/stresses are implemented in a finite-element code, Variational Asymptotic Plate and Shell Analysis (VAPAS). This program is connected with DYMORE, a nonlinear finite-element based multi-body dynamic code to provide an efficient and accurate simulation capability for space systems involving composite and inflatable components with actuated elements which are required for current and future Air Force missions.

the original 3-D results. The non-uniqueness of asymptotic theory correct up to a certain order is used to cast the obtained asymptotically correct second-order energy into a Reissner-Mindlin type model to account for transverse shear deformation. All the developed theories are implemented in a finite element code, Variational Asymptotic Plate and Shell Analysis (VAPAS). Results from VAPAS have been compared with the exact solutions available in the literature, classical lamination theory and first-order shear-deformation theory to demonstrate the accuracy and power of the developed theory.

Work Accomplished

Asymptotic Construction of Composite Plate Model

The development starts with formulation of 3-D anisotropic elasticity problem in which the deformation of the reference surface is expressed in terms of intrinsic 2-D variables. The VAM is then used to rigorously split this 3-D problem into a linear 1-D analysis and a nonlinear 2-D "plate" analysis accounting for transverse shear deformation. The through-the-thickness analysis provides a constitutive law between the generalized, two-dimensional strains and stress resultants as well as recovering relations to approximately but accurately express the 3-D displacement, strain and stress fields in terms of plate variables calculated in the "plate" analysis. It is known that more than one theory may exist that is asymptotically correct to a given order. This non-uniqueness is used to cast a strain energy functional that is asymptotically correct through the second order into a simple "Reissner-Mindlin" type plate theory. Although it is not possible in general to construct an asymptotically correct Reissner-Mindlin type composite plate theory, an optimization procedure is used to drive the present theory as close to being asymptotically correct as possible while maintaining the simplicity of the Reissner-Mindlin formulation. This theory is firstly formulated analytically and reported on an ASME conference [2] and later archived in [3]. Later, for the purpose to connecting with 2-D finite-element analysis code and efficiency for multilayer analysis, a finite-element formulation is developed and published in [4].

Asymptotic Construction of Composite Shell Model

A rigorous and systematic dimensional reduction of a shell-like structure is undertaken. Instead of the transverse shear refinement we have for plates, an accurate shell model will also include the geometry correction due to the initial curvatures of the shell structure. There are two main small parameters, h/l and h/R, where h is the thickness of the shell, l is the wavelength of in-plane deformation and R is the minimum radius of curvature for the shell structure. The asymptotic orders of these two small parameters are carefully chosen so that an energy asymptotically correct up to the first order of h/R and the second order of h/l has been successfully constructed. Our studies [5, 6] show that the constructed model can predict the stress distribution through the thickness very accurately for shall shells. Improvement to this theory can be made to include the second order of h/R so that deep shells can also be accurately modeled. A 2-D geometrically exact nonlinear shear deformation shell theory [7] has been developed to be consistent with the Reissner-Mindlin type model constructed. A complete set of kinematical and intrinsic equilibrium equations are derived for shells undergoing large displacements and rotations but with small, 2-D generalized

3

strains. The large rotation is represented by the general finite rotation is along the normal line. It is shown that the rotation of the frame about the normal line is not zero and that it can be expressed in terms of other global deformation variables. It is also shown that only five equilibrium equations can be derived in this manner because the component of virtual rotation about the normal is not independent.

A Thermolelastic Composite Plate Model

Composite structures are more sensitive and vulnerable to temperature change than their isotropic counterpart because the thermal expansion coefficients of different constituents of the material are usually dramatically different from each other resulting in high stresses due to sudden temperature change. The analysis including thermal effects is much more involved than that for isothermal conditions. A Reissner-Mindlin type plate model capable of performing a thermoelastic stress analysis of laminated composite plates has been constructed by the VAM. It is shown in [8] that although the resulting theory is of the simple Reissner-Mindlin form, it has an accuracy comparable to a higher-order layerwise theory. The hygro effect due to moisture to composite plates can also handled in exactly the same procedure except one has to replace the thermal expansion coefficients with hygroscopic expansion coefficients and temperature with moisture.

A Thermopiezoelastic Composite Plate Model

A Reissner-Mindlin type model for analyzing laminated smart composite plates including piezo-electric layers under mechanical, thermal and electric loads has been developed. This model can analyze the one-way coupling between structure and thermal, electric field. The non-mechanical stress resultants due to temperature and actuation can be predicted using this model. This theory has been implemented into the computer program VAPAS and validated against published exact solutions for simple problems. As reported in [9, 10], the recovered 3-D stress distribution due to temperature, or electricity has a good agreement with the exact solutions.

A Thermopiezoelastic Composite Shell Model

Finally, the above developed thermopiezoelastic model for smart plates is extended to model smart shells made embedded with piezoelectric layers. All the effects due to temperature, electricity, initial curvature and transverse shear are represented in this model. This model is also implemented in the computer program VAPAS and a paper giving the results has been accepted for presentation at the 2004 AIAA SDM conference [11].

Multibody Modeling of Shells and Membranes

The classical approach to the numerical simulation of flexible multibody systems proceeds in two steps: first, the equations of motion of the system are written in a convenient form, then general purpose Differential Algebraic Equations (DAE) solvers are used to integrate these equations in the time domain. General purpose DAE integrators are specifically designed for effectively dealing with the dual differential/algebraic nature of the equations but are otherwise unaware of the specific features and characteristics of the equations being solved.

4

The equations governing nonlinear flexible multibody systems with shells and membranes present very specific features. First, they are characterized by linear and rotational tensorial fields describing kinematic (displacements, velocities) and co-kinematic (forces, momenta) quantities. Second, nonlinearities can arise from several sources: large displacements and finite rotations (geometric nonlinearities), or nonlinear constitutive laws for the deformable components of the system (material nonlinearities). Third, a distinguishing feature of multibody systems is the presence of joints which impose different types of kinematic constraints between the various bodies of the system. More often than not, constraints are modeled via the Lagrange multipliers technique that imposes the nonlinear algebraic constraints on the system. Fourth, the exact solution of the equations of motion implies the preservation of a number of dynamic invariants, such as energy and momenta. Fifth, when the elastic bodies of the system are modeled by means of an appropriate spatial discretization process, such as the finite element method, high frequency modes are introduced in the system. Finally, when dealing with shells and membranes, the ratio of in-plane to out-of-plane frequencies is extremely high, leading to very stiff systems.

While standard approaches perform adequately for a number of simulations, problems can arise when modeling flexible, nonlinear multibody systems involving shells and membranes. In this case, robust algorithms that satisfy precise *requirements* should be *designed* for the time integration of such systems. A formulation of time integrators for shells and membranes was developed that satisfies the following requirements: *nonlinear unconditional stability* of the scheme, a *rigorous treatment of all nonlinearities*, the *exact satisfaction of the constraints*, and the presence of *high frequency numerical dissipation*. The proof of nonlinear unconditional stability stems from two physical characteristics of multibody systems that will be reflected in the numerical scheme: the preservation of the total mechanical energy, and the vanishing of the work performed by constraint forces. Numerical dissipation is obtained by letting the solution drift from the constant energy manifold in a controlled manner in such a way that at each time step, energy can be dissipated but not created.

A novel integration scheme for nonlinear dynamics of geometrically exact shells was developed based on the inextensible director assumption. The new algorithm is designed so as to imply the strict decay of the system total mechanical energy at each time step, and consequently unconditional stability is achieved in the nonlinear regime. Furthermore, the scheme features tunable high frequency numerical damping and it is therefore stiffly accurate. The method is tested for a finite element spatial formulation of shells based on mixed interpolations of strain tensorial components and on a two-parameter representation of director rotations. The robustness of the scheme is illustrated with the help of numerical examples presented at conferences [12, 13] and later published in a paper [14].

Next, these algorithms were extended to deal with the complexities associated with multibody systems. Results were first presented at conferences [15, 16] and later published in papers [17, 18] addressing various aspects of the problem. The modeling of cables and membranes was addressed in [19].

Conclusions and Suggestions

A rigorous framework to construct accurate model for composite plates and shells has been established under this grant using the variational asymptotic method. Models constructed this way can

not only provide accurate 2-D constitutive model for plate or shell analysis but also a consistent way to recover the original 3-D displacement/strain/stress fields. All the theories developed have been implemented in the computer program VAPAS. VAPAS has been connected with DYMORE to provide an efficient yet accurate simulation for complex aerospace systems.

More work needs to be done to verify the developed and implemented thermopiezoelastic model for smart shells against available published results. And also the developed shell models could be improved by constructing an energy asymptotically correct up to the second order in h/R. However, this requires significant research effort and would also require the development of shell models capable of providing the required inputs to such models.

Acknowledgements

Additional Project Personnel

Dr. Jou-Young Choi: Graduate Research Assistant; received Ph.D. in December 2002, presently Post Doctoral Fellow, Georgia Tech.

Dr. Wenbin Yu: Graduate Research Assistant; received Ph.D. in May 2002, Post Doctoral Fellow at Georgia Tech through August 2003; presently Assistant Professor, Department of Mechanical and Aerospace Engineering, Utah State University.

References

[1] Berdichevsky, V. L., "Variational-Asymptotic Method of Constructing a Theory of Shells," *PMM*, Vol. 43, No. 4, 1979, pp. 664 – 687.

[2] Yu, W., Hodges, D. H., and Volovoi, V. V., "Asymptotic Construction of Reissner-like Models for Composite Plates with Accurate Strain Recovery," *Proceedings of the 2001 ASME International Mechanical Engineering Congress and Exposition, New York, Paper No. IMECE2001/AD-23766, AD-vol. 65, AMD-vol. 249*, Nov. 11 – 16, 2001, pp. 189 – 206.

[3] Yu, W., Hodges, D. H., and Volovoi, V. V., "Asymptotic Construction of Reissner-like Models for Composite Plates with Accurate Strain Recovery," *International Journal of Solids and Structures*, Vol. 39, No. 20, 2002, pp. 5185 – 5203 (Appendix A).

[4] Yu, W., Hodges, D. H., and Volovoi, V. V., "Asymptotically Accurate 3-D Recovery from Reissner-like Composite Plate Finite Elements," *Computers and Structures*, Vol. 81, No. 7, 2003, pp. 439–454 (Appendix B).

[5] Yu, W., Hodges, D. H., and Volovoi, V. V., "Asymptotic Construction of a Reissner-like Composite Shell Model with Accurate Three-Dimensional Recovery," *Proceedings of the 43rd Structures, Structural Dynamics, and Materials Conference*, Denver, Colorado, Apr. 22 – 25, 2002, Paper AIAA-2002-1657.

[6] Yu, W., Hodges, D. H., and Volovoi, V. V., "Asymptotic Generalization of Reissner-Mindlin Theory: Accurate Three-Dimensional Recovery for Composite Shells," *Computer Methods in Applied Mechanics and Engineering*, Vol. 191, No. 44, 2002, pp. 4971–5112 (Appendix C).

[7] Yu, W. and Hodges, D. H., "A Geometrically Nonlinear Shear Deformation Theory for Composite Shells," *Journal of Applied Mechanics*, 2004, to appear (Appendix D).

[8] Yu, W. and Hodges, D. H., "An Asymptotic Approach for Thermoelastic Analysis of Laminated Composite Plates," *Journal of Engineering Mechanics*, 2004, to appear (Appendix E).

[9] Yu, W. and Hodges, D. H., "Asymptotic Construction of a Thermopiezoelastic Model for Smart Composite Plates," *Proceedings of the 44rd Structures, Structural Dynamics and Materials Conference*, Norfolk, Virginia, April 7 – 10, 2003.

[10] Yu, W. and Hodges, D. H., "A Simple Thermopiezoelastic Model for Composite Plates with Accurate Stress Recovery," *Smart Materials and Structures*, 2003, submitted (Appendix F).

[11] Yu, W. and Hodges, D. H., "A Simple Thermopiezoelastic Model for Composite Plates with Accurate Stress Recovery," *Proceedings of the 45th Structures, Structural Dynamics and Materials Conference*, AIAA, 2004, to appear.

[12] Bauchau, O.A., Choi J.Y. and Bottasso C.L.: " Energy Decaying Scheme for Nonlinear Dynamics of Shells," *Proceeding of the Second European Conference on Computational Mechanics*, Cracow, Poland, June 26-29, 2001. Volume 1, pp 44 – 45.

[13] Bottasso, C.L. and Bauchau, O.A.: "Geometrically Exact Shell Dynamics by an Energy Decaying Scheme," *Proceedings of the Sixth U.S. National Congress on Computational Mechanics*, Dearborn, Michigan, Aug. 1 – 3, 2001. pp 708 – 709.

[14] Bottasso, C.L., Bauchau, O.A. and Choi, J.Y., "An Energy Decaying Scheme for Nonlinear Dynamics of Shells," *Computer Methods in Applied Mechanics and Engineering*, Vol. 191, pp 3099 – 3121, 2002 (Appendix G).

[15] Bauchau, O.A. and Bottasso, C.L.: "On the Modeling of Shells in Multibody Dynamics," *Proceeding of the First MIT Conference on Computational Fluid and Solid Mechanics*, Cambridge, Massachusetts, June 12-15, 2001. Volume 1, pp 58 – 60. Editor: K.J. Bathe.

[16] Bauchau, O.A., Choi, J.Y. and Bottasso, C.L.: "On the Modeling of Shells in Multibody Dynamic," *Proceedings of the 18th Biennial Conference on Mechanical Vibration and Noise*, Pittsburgh Pennsylvania, Sep. 9 – 12, 2001. Paper DETC2001/VIB-21339.

7

[17] Bauchau, O.A., Choi, J.Y. and Bottasso, C.L., "Time Integrators for Shells in Multibody Dynamics," *Computers and Structures*, Vol. 80, 2002, pp. 871 – 889 (Appendix H).

[18] Bauchau, O.A., Choi, J.Y. and Bottasso, C.L., "On the Modeling of Shells in Multibody Dynamics," *Multibody System Dynamics*, Vol. 8, No. 4, 2002, pp. 459 – 489 (Appendix I).

[19] Bauchau O.A. and Choi J.Y.: "Dynamic Simulation of Cables and Membranes," *Proceedings of the Fifth World Congress on Computational Mechanics*, Vienna, Austria, July 7 – 12, 2002. pp. 262 – 270.

Georgia Tech | Research Corporation

Georgia Institute of Technology
Office of Sponsored Programs
Atlanta, Georgia 30332-0420 U.S.A.

January 21, 2004
In reply refer to: E-16-T09

Ms. Wendy Veon
AFOSR/PK
4015 Wilson Blvd
Room 713
Arlington, VA 22203-1954

Subject: Final Performance Report
Project Director(s): Dr. Oliver A. Bauchau
Telephone No.: (404) 894-0042
Contract No.: F49620-01-1-0038
Prime No: N/A
"MULTIBODY APPROACH TO THE DYNAMIC ANALYSIS
OF STRUCRTURES WITH ACTUATED..."
Period Covered: December 15, 2000 – March 14, 2004

The subject report is forwarded in conformance with the contract/grant specifications.

Should you have any questions or comments regarding this report(s), please contact the Project Director or the undersigned at 404-894-4763.

Sincerely,

Thelma Woods
Customer Service Representative

Addressee: 1 copy
1 copy to:DTIC
1 copy to: ONR-RR

Multi-body Approach to the Dynamic Analysis of Space Structures with Actuated Components Final Report: AFOSR Grant F49620-01-1-0038

Olivier A. Bauchau, Professor
Project Director and Co-Principal Investigator
e-mail: olivier.bauchau@ae.gatech.edu
phone: 404-894-0042; fax: (404) 894-2760
and
Dewey H. Hodges, Professor
Co-Principal Investigator
e-mail: dewey.hodges@ae.gatech.edu
phone: 404-894-8201; fax: (404) 894-2760

School of Aerospace Engineering
Georgia Institute of Technology, Atlanta, Georgia 30332-0150

Summary

High-fidelity, finite-element-based dimensionally reduced models have been constructed for composite plates and shells, including hygrothermal and piezoelectric effects, under the sponsorship of AFOSR. In these models, the smallness of the thickness has been used to advantage to rigorously reduce the original three-dimensional geometrically nonlinear elasticity theory to two-dimensional Reissner-Mindlin type theory for plates and shells. The resulting theory can achieve an accuracy comparable to higher-order layerwise theories at the cost of only a first-order shear deformation theory. The dimensional reduction process and the recovery relations for the original three-dimensional displacements/strains/stresses are implemented in a finite-element code, Variational Asymptotic Plate and Shell Analysis (VAPAS). This program is connected with DYMORE, a nonlinear finite-element based multi-body dynamic code to provide an efficient and accurate simulation capability for space systems involving composite and inflatable components with actuated elements which are required for current and future Air Force missions.

Introduction

This three-year grant was initiated in December 2000. All work done under the auspices of the grant is summarized herein, and the various papers written under grant sponsorship are appended to provide all the technical details. The objective of this research was to provide high-fidelity, finite-element-based simulation capability to assist in the analysis and design of structures for space applications. The importance of such a research stems from the Air Force interest of space structures comprising antennas, solar concentrators, sun shields, struts and booms, and membrane mirrors. Moreover, the various components of these systems often are in relative motion with respect to one another, resulting in variable geometry systems that are truly multi-body in nature. Low-cost, accurate simulation tools are essential for the design, analysis and assessment of such systems. However, efficiency of such a simulation tool can only be achieved through dimensional reduction: it is impractical to treat each structural element as a three-dimensional (3-D) body. Hence, low-order, accurate models are needed to not only provide the elastic constants needed in the finite element representation to calculate the global behavior, but also to provide a unified means to obtain the strain and stress distribution in the structures.

There are two main research aspects in this project: a local through-the-thickness model focuses on the evaluation of elastic constants and displacement/strain/stress recovery, and a finite-element-based, nonlinear flexible multi-body dynamics simulation tools based on those models. The basic research issues that have been addressed under the first aspect are

1. Constructing an accurate Reissner-Mindlin type model for composite plate using the variational asymptotic method (VAM) [1];

2. Constructing of an accurate Reissner-Mindlin type model for composite shells using VAM including both geometrical correction due to initial curvature and transverse shear effects;

3. Developing a geometrically exact nonlinear shear deformation shell theory to be compatible with the models developed;

4. Modeling regular composite plates and shells including hygrothermal effects so that the change of structural behavior due to moisture and temperature can be analyzed;

5. Modeling smart composite plates and shells made with piezoelectric material.

Approach

The variational asymptotic method (VAM) has applied to develop a high-fidelity/low-order model for composite plates and shells. Instead of employing *ad-hoc* assumptions, the VAM relies on the use of the small parameters that are inherent to the structure. This ensures construction of a theory with the minimum complexity for a given level of fidelity. The original 3-D nonlinear problem is formulated based on a set of two-dimensional (2-D) intrinsic variables and warping functions representing the arbitrary deformation of the normal line. Then the VAM is used to rigorously split the 3-D problem into two problems: a nonlinear, 2-D, plate or shell analysis over the reference surface to obtain the global deformation and a one-dimensional (1-D) linear analysis through the thickness to provide the 2-D generalized constitutive law and the recovering relations to approximate

the original 3-D results. The non-uniqueness of asymptotic theory correct up to a certain order is used to cast the obtained asymptotically correct second-order energy into a Reissner-Mindlin type model to account for transverse shear deformation. All the developed theories are implemented in a finite element code, Variational Asymptotic Plate and Shell Analysis (VAPAS). Results from VAPAS have been compared with the exact solutions available in the literature, classical lamination theory and first-order shear-deformation theory to demonstrate the accuracy and power of the developed theory.

Work Accomplished

Asymptotic Construction of Composite Plate Model

The development starts with formulation of 3-D anisotropic elasticity problem in which the deformation of the reference surface is expressed in terms of intrinsic 2-D variables. The VAM is then used to rigorously split this 3-D problem into a linear 1-D analysis and a nonlinear 2-D "plate" analysis accounting for transverse shear deformation. The through-the-thickness analysis provides a constitutive law between the generalized, two-dimensional strains and stress resultants as well as recovering relations to approximately but accurately express the 3-D displacement, strain and stress fields in terms of plate variables calculated in the "plate" analysis. It is known that more than one theory may exist that is asymptotically correct to a given order. This non-uniqueness is used to cast a strain energy functional that is asymptotically correct through the second order into a simple "Reissner-Mindlin" type plate theory. Although it is not possible in general to construct an asymptotically correct Reissner-Mindlin type composite plate theory, an optimization procedure is used to drive the present theory as close to being asymptotically correct as possible while maintaining the simplicity of the Reissner-Mindlin formulation. This theory is firstly formulated analytically and reported on an ASME conference [2] and later archived in [3]. Later, for the purpose to connecting with 2-D finite-element analysis code and efficiency for multilayer analysis, a finite-element formulation is developed and published in [4].

Asymptotic Construction of Composite Shell Model

A rigorous and systematic dimensional reduction of a shell-like structure is undertaken. Instead of the transverse shear refinement we have for plates, an accurate shell model will also include the geometry correction due to the initial curvatures of the shell structure. There are two main small parameters, h/l and h/R, where h is the thickness of the shell, l is the wavelength of in-plane deformation and R is the minimum radius of curvature for the shell structure. The asymptotic orders of these two small parameters are carefully chosen so that an energy asymptotically correct up to the first order of h/R and the second order of h/l has been successfully constructed. Our studies [5, 6] show that the constructed model can predict the stress distribution through the thickness very accurately for shall shells. Improvement to this theory can be made to include the second order of h/R so that deep shells can also be accurately modeled. A 2-D geometrically exact nonlinear shear deformation shell theory [7] has been developed to be consistent with the Reissner-Mindlin type model constructed. A complete set of kinematical and intrinsic equilibrium equations are derived for shells undergoing large displacements and rotations but with small, 2-D generalized

strains. The large rotation is represented by the general finite rotation is along the normal line. It is shown that the rotation of the frame about the normal line is not zero and that it can be expressed in terms of other global deformation variables. It is also shown that only five equilibrium equations can be derived in this manner because the component of virtual rotation about the normal is not independent.

A Thermolelastic Composite Plate Model

Composite structures are more sensitive and vulnerable to temperature change than their isotropic counterpart because the thermal expansion coefficients of different constituents of the material are usually dramatically different from each other resulting in high stresses due to sudden temperature change. The analysis including thermal effects is much more involved than that for isothermal conditions. A Reissner-Mindlin type plate model capable of performing a thermoelastic stress analysis of laminated composite plates has been constructed by the VAM. It is shown in [8] that although the resulting theory is of the simple Reissner-Mindlin form, it has an accuracy comparable to a higher-order layerwise theory. The hygro effect due to moisture to composite plates can also handled in exactly the same procedure except one has to replace the thermal expansion coefficients with hygroscopic expansion coefficients and temperature with moisture.

A Thermopiezoelastic Composite Plate Model

A Reissner-Mindlin type model for analyzing laminated smart composite plates including piezo-electric layers under mechanical, thermal and electric loads has been developed. This model can analyze the one-way coupling between structure and thermal, electric field. The non-mechanical stress resultants due to temperature and actuation can be predicted using this model. This theory has been implemented into the computer program VAPAS and validated against published exact solutions for simple problems. As reported in [9, 10], the recovered 3-D stress distribution due to temperature, or electricity has a good agreement with the exact solutions.

A Thermopiezoelastic Composite Shell Model

Finally, the above developed thermopiezoelastic model for smart plates is extended to model smart shells made embedded with piezoelectric layers. All the effects due to temperature, electricity, initial curvature and transverse shear are represented in this model. This model is also implemented in the computer program VAPAS and a paper giving the results has been accepted for presentation at the 2004 AIAA SDM conference [11].

Multibody Modeling of Shells and Membranes

The classical approach to the numerical simulation of flexible multibody systems proceeds in two steps: first, the equations of motion of the system are written in a convenient form, then general purpose Differential Algebraic Equations (DAE) solvers are used to integrate these equations in the time domain. General purpose DAE integrators are specifically designed for effectively dealing with the dual differential/algebraic nature of the equations but are otherwise unaware of the specific features and characteristics of the equations being solved.

The equations governing nonlinear flexible multibody systems with shells and membranes present very specific features. First, they are characterized by linear and rotational tensorial fields describing kinematic (displacements, velocities) and co-kinematic (forces, momenta) quantities. Second, nonlinearities can arise from several sources: large displacements and finite rotations (geometric nonlinearities), or nonlinear constitutive laws for the deformable components of the system (material nonlinearities). Third, a distinguishing feature of multibody systems is the presence of joints which impose different types of kinematic constraints between the various bodies of the system. More often than not, constraints are modeled via the Lagrange multipliers technique that imposes the nonlinear algebraic constraints on the system. Fourth, the exact solution of the equations of motion implies the preservation of a number of dynamic invariants, such as energy and momenta. Fifth, when the elastic bodies of the system are modeled by means of an appropriate spatial discretization process, such as the finite element method, high frequency modes are introduced in the system. Finally, when dealing with shells and membranes, the ratio of in-plane to out-of-plane frequencies is extremely high, leading to very stiff systems.

While standard approaches perform adequately for a number of simulations, problems can arise when modeling flexible, nonlinear multibody systems involving shells and membranes. In this case, robust algorithms that satisfy precise *requirements* should be *designed* for the time integration of such systems. A formulation of time integrators for shells and membranes was developed that satisfies the following requirements: *nonlinear unconditional stability* of the scheme, a *rigorous treatment of all nonlinearities*, the *exact satisfaction of the constraints*, and the presence of *high frequency numerical dissipation*. The proof of nonlinear unconditional stability stems from two physical characteristics of multibody systems that will be reflected in the numerical scheme: the preservation of the total mechanical energy, and the vanishing of the work performed by constraint forces. Numerical dissipation is obtained by letting the solution drift from the constant energy manifold in a controlled manner in such a way that at each time step, energy can be dissipated but not created.

A novel integration scheme for nonlinear dynamics of geometrically exact shells was developed based on the inextensible director assumption. The new algorithm is designed so as to imply the strict decay of the system total mechanical energy at each time step, and consequently unconditional stability is achieved in the nonlinear regime. Furthermore, the scheme features tunable high frequency numerical damping and it is therefore stiffly accurate. The method is tested for a finite element spatial formulation of shells based on mixed interpolations of strain tensorial components and on a two-parameter representation of director rotations. The robustness of the scheme is illustrated with the help of numerical examples presented at conferences [12, 13] and later published in a paper [14].

Next, these algorithms were extended to deal with the complexities associated with multibody systems. Results were first presented at conferences [15, 16] and later published in papers [17, 18] addressing various aspects of the problem. The modeling of cables and membranes was addressed in [19].

Conclusions and Suggestions

A rigorous framework to construct accurate model for composite plates and shells has been established under this grant using the variational asymptotic method. Models constructed this way can

not only provide accurate 2-D constitutive model for plate or shell analysis but also a consistent way to recover the original 3-D displacement/strain/stress fields. All the theories developed have been implemented in the computer program VAPAS. VAPAS has been connected with DYMORE to provide an efficient yet accurate simulation for complex aerospace systems.

More work needs to be done to verify the developed and implemented thermopiezoelastic model for smart shells against available published results. And also the developed shell models could be improved by constructing an energy asymptotically correct up to the second order in h/R. However, this requires significant research effort and would also require the development of shell models capable of providing the required inputs to such models.

Acknowledgements

Additional Project Personnel

Dr. Jou-Young Choi: Graduate Research Assistant; received Ph.D. in December 2002, presently Post Doctoral Fellow, Georgia Tech.

Dr. Wenbin Yu: Graduate Research Assistant; received Ph.D. in May 2002, Post Doctoral Fellow at Georgia Tech through August 2003; presently Assistant Professor, Department of Mechanical and Aerospace Engineering, Utah State University.

References

[1] Berdichevsky, V. L., "Variational-Asymptotic Method of Constructing a Theory of Shells," *PMM*, Vol. 43, No. 4, 1979, pp. 664 – 687.

[2] Yu, W., Hodges, D. H., and Volovoi, V. V., "Asymptotic Construction of Reissner-like Models for Composite Plates with Accurate Strain Recovery," *Proceedings of the 2001 ASME International Mechanical Engineering Congress and Exposition, New York, Paper No. IMECE2001/AD-23766, AD-vol. 65, AMD-vol. 249*, Nov. 11 – 16, 2001, pp. 189 – 206.

[3] Yu, W., Hodges, D. H., and Volovoi, V. V., "Asymptotic Construction of Reissner-like Models for Composite Plates with Accurate Strain Recovery," *International Journal of Solids and Structures*, Vol. 39, No. 20, 2002, pp. 5185 – 5203 (Appendix A).

[4] Yu, W., Hodges, D. H., and Volovoi, V. V., "Asymptotically Accurate 3-D Recovery from Reissner-like Composite Plate Finite Elements," *Computers and Structures*, Vol. 81, No. 7, 2003, pp. 439–454 (Appendix B).

[5] Yu, W., Hodges, D. H., and Volovoi, V. V., "Asymptotic Construction of a Reissner-like Composite Shell Model with Accurate Three-Dimensional Recovery," *Proceedings of the 43rd Structures, Structural Dynamics, and Materials Conference*, Denver, Colorado, Apr. 22 – 25, 2002, Paper AIAA-2002-1657.

[6] Yu, W., Hodges, D. H., and Volovoi, V. V., "Asymptotic Generalization of Reissner-Mindlin Theory: Accurate Three-Dimensional Recovery for Composite Shells," *Computer Methods in Applied Mechanics and Engineering*, Vol. 191, No. 44, 2002, pp. 4971–5112 (Appendix C).

[7] Yu, W. and Hodges, D. H., "A Geometrically Nonlinear Shear Deformation Theory for Composite Shells," *Journal of Applied Mechanics*, 2004, to appear (Appendix D).

[8] Yu, W. and Hodges, D. H., "An Asymptotic Approach for Thermoelastic Analysis of Laminated Composite Plates," *Journal of Engineering Mechanics*, 2004, to appear (Appendix E).

[9] Yu, W. and Hodges, D. H., "Asymptotic Construction of a Thermopiezoelastic Model for Smart Composite Plates," *Proceedings of the 44rd Structures, Structural Dynamics and Materials Conference*, Norfolk, Virginia, April 7 – 10, 2003.

[10] Yu, W. and Hodges, D. H., "A Simple Thermopiezoelastic Model for Composite Plates with Accurate Stress Recovery," *Smart Materials and Structures*, 2003, submitted (Appendix F).

[11] Yu, W. and Hodges, D. H., "A Simple Thermopiezoelastic Model for Composite Plates with Accurate Stress Recovery," *Proceedings of the 45th Structures, Structural Dynamics and Materials Conference*, AIAA, 2004, to appear.

[12] Bauchau, O.A., Choi J.Y. and Bottasso C.L.: " Energy Decaying Scheme for Nonlinear Dynamics of Shells," *Proceeding of the Second European Conference on Computational Mechanics*, Cracow, Poland, June 26-29, 2001. Volume 1, pp 44 – 45.

[13] Bottasso, C.L. and Bauchau, O.A.: "Geometrically Exact Shell Dynamics by an Energy Decaying Scheme," *Proceedings of the Sixth U.S. National Congress on Computational Mechanics*, Dearborn, Michigan, Aug. 1 – 3, 2001. pp 708 – 709.

[14] Bottasso, C.L., Bauchau, O.A. and Choi, J.Y., "An Energy Decaying Scheme for Nonlinear Dynamics of Shells," *Computer Methods in Applied Mechanics and Engineering*, Vol. 191, pp 3099 – 3121, 2002 (Appendix G).

[15] Bauchau, O.A. and Bottasso, C.L.: "On the Modeling of Shells in Multibody Dynamics," *Proceeding of the First MIT Conference on Computational Fluid and Solid Mechanics, Cambridge, Massachusetts, June 12-15, 2001*. Volume 1, pp 58 – 60. Editor: K.J. Bathe.

[16] Bauchau, O.A., Choi, J.Y. and Bottasso, C.L.: "On the Modeling of Shells in Multibody Dynamic," *Proceedings of the 18th Biennial Conference on Mechanical Vibration and Noise*, Pittsburgh Pennsylvania, Sep. 9 – 12, 2001. Paper DETC2001/VIB-21339.

[17] Bauchau, O.A., Choi, J.Y. and Bottasso, C.L., "Time Integrators for Shells in Multibody Dynamics," *Computers and Structures*, Vol. 80, 2002, pp. 871 – 889 (Appendix H).

[18] Bauchau, O.A., Choi, J.Y. and Bottasso, C.L., "On the Modeling of Shells in Multibody Dynamics," *Multibody System Dynamics*, Vol. 8, No. 4, 2002, pp. 459 – 489 (Appendix I).

[19] Bauchau O.A. and Choi J.Y.: "Dynamic Simulation of Cables and Membranes," *Proceedings of the Fifth World Congress on Computational Mechanics*, Vienna, Austria, July 7 – 12, 2002. pp. 262 – 270.

A Geometrically Nonlinear Shear Deformation Theory for Composite Shells

Wenbin Yu[*] and **Dewey H. Hodges**[†]

Georgia Institute of Technology, Atlanta, Georgia 30332-0150

A geometrically nonlinear shear deformation theory has been developed for elastic shells to accommodate a constitutive model suitable for composite shells when modeled as a two-dimensional continuum. A complete set of kinematical and intrinsic equilibrium equations are derived for shells undergoing large displacements and rotations but with small, two-dimensional, generalized strains. The large rotation is represented by the general finite rotation of a frame embedded in the undeformed configuration, of which one axis is along the normal line. The unit vector along the normal line of the undeformed reference surface is not in general normal to the deformed reference surface because of transverse shear. It is shown that the rotation of the frame about the normal line is not zero and that it can be expressed in terms of other global deformation variables. Based on a generalized constitutive model obtained from an asymptotic dimensional reduction from the three-dimensional energy, and in the form of a Reissner-Mindlin type theory, a set of intrinsic equilibrium equations and boundary conditions follow. It is shown that only five equilibrium equations can be derived in this manner because the component of virtual rotation about the normal is not independent. It is shown, however, that these equilibrium equations contain terms that cannot be obtained without the use of all three components of the finite rotation vector.

Introduction

For an elastic three-dimensional (3-D) continuum, there are two types of nonlinearity: geometrical and physical. A theory is geometrically nonlinear if the kinematical (strain-displacement) relations are nonlinear but the constitutive (stress-strain) relations are linear. This kind of theory allows large displacements and rotations with the restriction that strain must be small. A physically (or materially) nonlinear theory is necessary for biological, rubber-like or inflatable structures where the strain cannot be considered small, and a nonlinear constitutive law is needed to relate the stress and strain. Although this classification seems obvious and clear for a structure modeled as a 3-D continuum, it becomes somewhat ambiguous to model dimensionally reducible structures – structures have one or two dimensions much smaller than the other(s) such as beams, plates and

---

[*]Post Doctoral Fellow, School of Aerospace Engineering.
[†]Professor, School of Aerospace Engineering. Member, ASME.

shells [1] – using reduced one-dimensional (1-D) or two-dimensional (2-D) models. A nonlinear constitutive law for the reduced structural model can in some circumstances be obtained from the reduction of a geometrically nonlinear 3-D theory. For example, in the so-called Wagner or trapeze effect [2–5], the effective torsional rigidity is increased due to axial force. This physically nonlinear 1-D model stems from a purely geometrically nonlinear theory at the 3-D level. On the other hand, the present paper focuses on a geometrically nonlinear analysis at the 3-D level which becomes a geometrically nonlinear analysis at the two-dimensional 2-D as well. That is, the 2-D generalized strain-displacement relations are nonlinear while the 2-D generalized stress-strain relations turn out to be linear.

A shell is a 3-D body with a relatively small thickness and a smooth reference surface. The feature of the small thickness attracts researchers to simplify their analyses by reducing the original 3-D problem to a 2-D problem by taking advantage of the thinness. By comparison with the original 3-D problem, an exact shell theory does not exist. Dimensional reduction is an inherently approximate process. Shell theory is a very old subject, since the vibration of a bell was attempted by Euler even before elasticity theory was well established [6]. Even so, shell theory still receives a lot of attention from modern researchers because it is used so extensively in so many engineering applications. Moreover, many shells are now made with advanced materials that have only recently become available.

Generally speaking, shell theories can be classified according to *direct*, *derived* and *mixed* approaches. The direct approach, which originated with the Cosserat brothers [7], models a shell directly as a 2-D "orientated" continuum. Naghdi [8] provided an extensive review of this kind of approach. Although the direct approach is elegant and able to account for transverse and normal strains and rotations associated with couple stresses, it nowhere connects with the fact that a shell is a 3-D body and thus completely isolates itself from 3-D continuum mechanics. This could be the main reason that this approach has not been much appreciated in the engineering community. One of the complaints of these approaches that they are difficult for numerical implementation has been answered by Simo and his co-workers by providing an efficient formulation "free from mathematical complexities and suitable for large scale computation" [9, 10]. And more recently a similar theory was developed by Ibrahimbegovic [11] to include drilling rotations so that not-so-smooth shell structures can be analyzed conveniently. However, the main complaint remains that these approaches lack a meaningful way to find the constitutive models "which can only be experienced and formulated properly in our 3-D real world" [12]. Reissner [13] developed a very general nonlinear shell theory introducing twelve generalized strains by considering the dynamics of stress resultants and couples on the reference surface as the basis. He gracefully avoided the awkwardness of finding a proper constitutive model by pointing out two possible means to establish them. It is recommended in [13] that one could either design experiments to determine the

constitutive constants without explicit reference to the 3-D nature of the structure or derive an appropriate 2-D model from the given knowledge of the constitutive relations for the real 3-D model of the structure.

Derived approaches reduce the original 3-D elasticity problem into a 2-D problem to be solved over the reference surface. Such reductions are usually carried out in one of two ways. The most common approach is to assume *a priori* the distribution of 3-D quantities through the thickness and then to construct a 2-D strain energy per unit area by integrating the 3-D energy per unit volume through the thickness. Remarkably, classical (also known as Kirchhoff-Love type theory), first-order shear deformation (also known as Reissner-Mindlin type theory), higher-order, and layer-wise shell theories all fall into this category, including the theories proposed by Reddy [14], for example. Another approach is to apply an asymptotic method to expand all quantities into an asymptotic series of the thickness coordinate, so that a sequence of 2-D problems can be solved according to the different orders.

The mixed approach is used in [15] based on the argument that all the 3-D elasticity equations except the constitutive relations are independent of the material properties, such as the kinematical relations, equilibrium of momentum and forces. The constitutive law must be determined experimentally, and hence it is avoidable that it is approximate. Libai and Simmonds [15] obtain exact shell equations for the balance of momentum, heat flow and an entropy inequality from the 3-D continuum mechanics via integration through the thickness. An analogous 2-D constitutive law is postulated due to the fact that even 3-D constitutive laws are inexact.

There is a sense in which the present approach can also be considered as mixed. The 2-D constitutive model is obtained by the Variational Asymptotic Method (VAM) [16] such that the 2-D energy is as close to an asymptotic approximation of the original 3-D energy as possible [17]. The process of constructing the constitutive model defines the reference surface and the kinematics of this surface are geometrically exact formulated in an intrinsic format. The 2-D equilibrium equations are obtained from the 2-D energy with the knowledge of the variations of the generalized strains. The only approximate part of our 2-D shell theory is the constitutive law which is not postulated but is mathematically obtained by VAM.

Shell Kinematics

The equations of 2-D shell theory are written over the domain of the reference surface, on which every point can be represented by a position vector r in the undeformed configuration and R in the deformed configuration (see Fig. 1) with respect to a fixed point O in the space. A set of two curvilinear coordinates, x_α, are required to located a point on the reference surface. The coordinates are so-called *convected* coordinates such that every point of the configuration has the same coordinates during the deformation. (Here and throughout the paper Latin indices assume 1,

2, 3; and Greek indices assume values 1 and 2. Dummy indices are summed over their range except where explicitly indicated.) Without loss of generality, x_α are chosen to be the lines of curvatures of the surface to simplify the formulation. For the purpose of representing finite rotations, an orthonormal triad $\mathbf{b}_i$ is introduced for the initial configuration, such that

$$\mathbf{b}_\alpha = \mathbf{a}_\alpha / A_\alpha \quad \mathbf{b}_3 = \mathbf{b}_1 \times \mathbf{b}_2 \tag{1}$$

where $\mathbf{a}_\alpha$ is the set of base vectors associated with x_α and A_α are the Lamé parameters, defined as

$$\mathbf{a}_\alpha = \mathbf{r}_{,\alpha} \quad A_\alpha = \sqrt{\mathbf{a}_\alpha \cdot \mathbf{a}_\alpha} \tag{2}$$

From the differential geometry of the surface and following [13] and [18] one can express the derivatives of $\mathbf{b}_i$ as

$$\mathbf{b}_{i,\alpha} = A_\alpha \mathbf{k}_\alpha \times \mathbf{b}_i \tag{3}$$

where $\mathbf{k}_\alpha$ is the curvature vector measured in $\mathbf{b}_i$ with the components

$$k_\alpha = \lfloor -k_{\alpha 2} \quad k_{\alpha 1} \quad k_{\alpha 3} \rfloor^T \tag{4}$$

in which $k_{\alpha 3}$ refers to out-of-plane curvatures. We note that $k_{12} = k_{21} = 0$ because the coordinates are the lines of curvatures. The geodesic curvatures $k_{\alpha 3}$ can be expressed in terms of the Lamé parameters as

$$k_{13} = -\frac{A_{1,2}}{A_1 A_2} \quad k_{23} = \frac{A_{2,1}}{A_1 A_2} \tag{5}$$

When the shell deforms, the particle that had position vector $\mathbf{r}$ in the undeformed state now has position vector $\mathbf{R}$ in the deformed shell. The triad $\mathbf{b}_i$ rotates to be $\mathbf{B}_i$. The rotation relating these two triads can be arbitrarily large and represented in the form of a matrix of direction cosines $C(x_\alpha)$ so that

$$\mathbf{B}_i = C_{ij}\mathbf{b}_j \quad C_{ij} = \mathbf{B}_i \cdot \mathbf{b}_j \tag{6}$$

A definition of the 2-D generalized strain measures is needed for the purpose of formulating this problem in an intrinsic form. Following [13] and [18], they can be defined as

$$\mathbf{R}_{,\alpha} = A_\alpha (\mathbf{B}_\alpha + \epsilon_{\alpha\beta}\mathbf{B}_\beta + 2\gamma_{\alpha 3}\mathbf{B}_3) \tag{7}$$

and

$$\mathbf{B}_{i,\alpha} = A_\alpha(-K_{\alpha 2}\mathbf{B}_1 + K_{\alpha 1}\mathbf{B}_2 + K_{\alpha 3}\mathbf{B}_3) \times \mathbf{B}_i \tag{8}$$

where $\epsilon_{\alpha\beta}$ are the 2-D in-plane strains, and K_{ij} are the curvatures of the deformed surface, which

are the summation of curvatures of undeformed geometry k_{ij} and curvatures introduced by the deformation κ_{ij}, and $\gamma_{\alpha3}$ are the transverse strains because $\mathbf{B}_3$ is not normal to the reference surface after deformation. Please note that the 2-D generalized strain measures are defined by Eqs. (7) and (8) in an intrinsic fashion, the symmetry of the inplane strain measures such that $\epsilon_{12} = \epsilon_{21}$ does not hold automatically. Nevertheless, one is free to set $\epsilon_{12} = \epsilon_{21}$, i.e.

$$\frac{\mathbf{B}_1 \cdot \mathbf{R}_{,2}}{A_2} = \frac{\mathbf{B}_2 \cdot \mathbf{R}_{,1}}{A_1} \tag{9}$$

which is a constraint used in [17] to make the 3-D formulation unique.

At this point sufficient preliminary information has been obtained to develop a geometrically nonlinear shell theory.

Compatibility Equations

It is well known that a rigid body in 3-D space has only six degrees of freedom. Thus, the kinematics of an element of the deformed shell reference surface can be expressed in terms of *at most* six independent quantities: three measures of displacement, say $\mathbf{u} \cdot \mathbf{b}_i$, and three measures of the rotation of $\mathbf{B}_i$ (since the global rotation tensor $\mathbf{C}$, which brings $\mathbf{b}_i$ into $\mathbf{B}_i$, can be expressed in terms of three independent quantities). However, we have the eleven 2-D strain measures ϵ_{11}, $2\epsilon_{12}$, ϵ_{22}, $2\gamma_{\alpha3}$, $\kappa_{\alpha3}$, and $\kappa_{\alpha3}$ as defined in Eqs. (7) and (8). Thus, they are not independent; there are some compatibility equations among these eleven quantities. In [19] and [13] appropriate compatibility equations are derived by first enforcing the equalities

$$\mathbf{R}_{,12} = \mathbf{R}_{,21} \tag{10}$$

and

$$\mathbf{B}_{i,12} = \mathbf{B}_{i,21} \tag{11}$$

These two vector equations lead to six independent compatibility equations equivalent to a form of those found in [13]. These equations are rewritten here for convenience in the present notation. First, from the $\mathbf{B}_3$ components of Eq. (10), we obtain

$$(1 + \epsilon_{22})\kappa_{12} - (1 + \epsilon_{11})\kappa_{21} = \frac{(A_2 2\gamma_{23})_{,1}}{A_1 A_2} - \frac{(A_1 2\gamma_{13})_{,2}}{A_1 A_2} + \epsilon_{12}(K_{22} - K_{11}) \tag{12}$$

Next, from the $\mathbf{B}_\alpha$ components of Eq. (10) we obtain two equations for $\alpha=1$ and 2, respectively, as

$$(1 + \epsilon_{22})K_{13} - \epsilon_{12}K_{23} = \frac{(A_2\epsilon_{12})_{,1}}{A_1 A_2} - \frac{[A_1(1 + \epsilon_{11})]_{,2}}{A_1 A_2} - 2\gamma_{13}\kappa_{21} + 2\gamma_{23}K_{11}$$

$$(1 + \epsilon_{11})K_{23} - \epsilon_{12}K_{13} = \frac{[A_2(1 + \epsilon_{22})]_{,1}}{A_1 A_2} - \frac{(A_1 \epsilon_{12})_{,2}}{A_1 A_2} - 2\gamma_{13}K_{22} + 2\gamma_{23}\kappa_{12} \tag{13}$$

Finally, from the three components of Eq. (11) we have nine identities. However, there are only three independent equations, given by

$$\frac{(A_1 K_{11})_{,2}}{A_1 A_2} - \frac{(A_2 \kappa_{21})_{,1}}{A_1 A_2} + K_{13}K_{22} - \kappa_{12}K_{23} = 0$$

$$\frac{(A_1 \kappa_{12})_{,2}}{A_1 A_2} - \frac{(A_2 K_{22})_{,1}}{A_1 A_2} + K_{23}K_{11} - \kappa_{21}K_{13} = 0$$

$$\frac{(A_2 K_{23})_{,1}}{A_1 A_2} - \frac{(A_1 K_{13})_{,2}}{A_1 A_2} + K_{11}K_{22} - \kappa_{12}\kappa_{21} = 0 \tag{14}$$

There are now eleven quantities which are related by six compatibility equations. This means that these strain measures can be determined in terms of *only five* independent quantities – *not six*.

In the process of dimensional reduction of [17] to find an accurate constitutive model for composite shells, the authors encountered the question whether one should include κ_{21} and κ_{12} as two different generalized strain measures. This was determined by the following argument. Let us denote a new twist measure $2\omega = \kappa_{12} + \kappa_{21}$. From Eq. (12) the difference between κ_{21} and κ_{12} can be obtained as

$$\frac{\kappa_{12} - \kappa_{21}}{2} = \frac{\frac{(A_2 2\gamma_{23})_{,1} - (A_1 2\gamma_{13})_{,2}}{A_1 A_2} + \epsilon_{12}(K_{22} - K_{11}) + \omega(\epsilon_{11} - \epsilon_{22})}{(2 + \epsilon_{11} + \epsilon_{22})} \tag{15}$$

This difference is clearly $O(\frac{\varepsilon h}{l^2})$ or $O(\frac{\varepsilon}{R})$ disregarding the nonlinear terms (ε is the order of generalized strains, h is the thickness of the shell, l is the wavelength of in-plane deformation and R is the characteristic radius of shell). One can show that it contributes terms that are $O(\frac{\varepsilon h^2}{l^2} \frac{h}{R})$ or $O(\frac{\varepsilon h^2}{R^2})$ to the strains. Clearly, such terms will not be counted in a physically linear theory with only correction up to the order of h/R and $(h/l)^2$.

Eqs. (13) can be solved for the in-plane curvatures κ_{13} and κ_{23}, and Eq. (15) can be used to express κ_{12} and κ_{21} in terms of ω. Now, using these expressions, one can rewrite the *three* Eqs. (14) entirely in terms of the *eight* strain measures ϵ_{11}, $2\epsilon_{12}$, ϵ_{22}, $2\gamma_{13}$, $2\gamma_{23}$, κ_{11}, 2ω, and κ_{22}. This confirms that *only five independent measures of displacement and rotation are necessary to define these strain measures* as we will demonstrate conclusively below by deriving such measures.

Global Displacement and Rotation Variables

There is no unique choice for the global deformation variables. For this reason, the importance (not to mention the beauty) of an intrinsic formulation is widely appreciated. On the other hand, for the purpose of understanding the displacement field more fully, for practical computational algo-

rithms, and for easy derivation of virtual strain-displacement relations, it is expedient to introduce a suitable set of displacement measures.

The displacement measures we choose are derived by expressing $\mathbf{R}$ in terms of $\mathbf{r}$ plus a displacement vector so that

$$\mathbf{R}(x_1, x_2) = \mathbf{r}(x_1, x_2) + u_i \mathbf{b}_i \tag{16}$$

Differentiating both sides of Eq. (16) with respect to x_α, and making use of Eq. (7), one can obtain the identity

$$\mathbf{B}_\alpha + \epsilon_{\alpha\beta} \mathbf{B}_\beta + 2\gamma_{\alpha 3} \mathbf{B}_3 = \mathbf{b}_\alpha + u_{i;\alpha} \mathbf{b}_i + u_i \mathbf{k}_\alpha \times \mathbf{b}_i \tag{17}$$

where $(\ )_{;\alpha} = \frac{1}{A_\alpha} \frac{\partial (\ )}{\partial \alpha}$. The above formula allows the determination of the strain measures $\epsilon_{\alpha\beta}$ and $2\gamma_{\alpha 3}$ in terms of C, u_i and the derivatives of u_i. Introducing column matrices $u = \lfloor u_1 \ u_2 \ u_3 \rfloor^T$, $e_1 = \lfloor 1 \ 0 \ 0 \rfloor^T$, $e_2 = \lfloor 0 \ 1 \ 0 \rfloor^T$, $\gamma_1 = \lfloor \epsilon_{11} \ \epsilon_{12} \ 2\gamma_{13} \rfloor^T$, and $\gamma_2 = \lfloor \epsilon_{21} \ \epsilon_{22} \ 2\gamma_{23} \rfloor^T$, we can obtain the following identity in matrix form

$$e_\alpha + \gamma_\alpha = C(e_\alpha + u_{;\alpha} + \widetilde{k_\alpha} u) \tag{18}$$

where C is the matrix of direction cosines from Eq. (6) and k_α is defined in Eq. (4).

Rodrigues parameters [20] can be used as rotation measures to allow a compact expression of C. These are derived based on Euler's theorem, which shows that any rotation can be represented as a rotation of magnitude Θ about a line parallel to a unit vector $\mathbf{e}$. Defining the Rodrigues parameters $\rho_i = 2\mathbf{e} \cdot \mathbf{b}_i \tan\left(\frac{\Theta}{2}\right)$ and arranging these in a column matrix $\rho = \lfloor \rho_1 \ \rho_2 \ \rho_3 \rfloor^T$, the matrix C can simply be written as

$$C = \frac{\left(1 - \frac{\rho^T \rho}{4}\right) I - \widetilde{\rho} + \frac{\rho \rho^T}{2}}{1 + \frac{\rho^T \rho}{4}} \tag{19}$$

where $\widetilde{(\ )}_{ij} = -e_{ijk}(\ )_k$. Let us also denote the direction cosines of $\mathbf{B}_3$ by

$$C_{3i} = \delta_{3i} + \theta_i \tag{20}$$

Hodges [21] has shown that, given the third row of C, the Rodrigues parameters can be uniquely

expressed in terms of θ_i as

$$\rho_1 = \frac{\rho_3\theta_1 - 2\theta_2}{2 + \theta_3}$$

$$\rho_2 = \frac{\rho_3\theta_2 + 2\theta_1}{2 + \theta_3}$$

$$\rho_3 = 2\tan\left(\frac{\phi_3}{2}\right) \tag{21}$$

where ρ_3 can be understood as a change of variables to simplify later parts of the derivation. Later on we will discuss the meaning of ϕ_3 for a special case. Finally, it is noted that the three rotational parameters θ_i are not independent but instead satisfy the constraint

$$\theta_1^2 + \theta_2^2 + (1 + \theta_3)^2 = 1 \tag{22}$$

When Eq. (21) is substituted into Eq. (19), the resulting elements of C can be expressed as functions of θ_i and ϕ_3

$$C_{11} = \frac{(2 + \theta_3 - \theta_1^2)\cos\phi_3 - \theta_1\theta_2\sin\phi_3}{2 + \theta_3}$$

$$C_{12} = \frac{(2 + \theta_3 - \theta_2^2)\sin\phi_3 - \theta_1\theta_2\cos\phi_3}{2 + \theta_3}$$

$$C_{13} = -\theta_1\cos\phi_3 - \theta_2\sin\phi_3$$

$$C_{21} = \frac{-(2 + \theta_3 - \theta_1^2)\sin\phi_3 - \theta_1\theta_2\cos\phi_3}{2 + \theta_3}$$

$$C_{22} = \frac{(2 + \theta_3 - \theta_2^2)\cos\phi_3 + \theta_1\theta_2\sin\phi_3}{2 + \theta_3}$$

$$C_{23} = \theta_1\sin\phi_3 - \theta_2\cos\phi_3$$

$$C_{31} = \theta_1$$

$$C_{32} = \theta_2$$

$$C_{33} = 1 + \theta_3 \tag{23}$$

This representation reduces to those of [22] when considering small, finite rotations. There is an apparent singularity in the present scheme when $\theta_3 = -2$ (*i.e.*, when the shell deforms in such a way that B_3 is pointed in the opposite direction of b_3). This should pose no practical problem, however, since $\theta_1 = \theta_2 = 0$ for that condition, and none of the kinematical relations become infinite in the limit as $\theta_3 \to -2$.

When these expressions for the direction cosines are substituted into Eq. (18), explicit expres-

sions for the strain measures can be found as

$$\epsilon_{11} = \left[\frac{(2 + \theta_3 - \theta_1^2)(1 + u_{1;1} - k_{13}u_2 + k_{11}u_3) - \theta_1\theta_2(u_{2;1} + k_{13}u_1)}{2 + \theta_3} + \theta_1(k_{11}u_1 - u_{3;1})\right]\cos\phi_3$$

$$+ \left[\frac{(2 + \theta_3 - \theta_2^2)(u_{2;1} + k_{13}u_1) - \theta_1\theta_2(1 + u_{1;1} - k_{13}u_2 + k_{11}u_3)}{2 + \theta_3} + \theta_2(k_{11}u_1 - u_{3;1})\right]\sin\phi_3 - 1$$

$$\epsilon_{22} = \left[\frac{(2 + \theta_3 - \theta_2^2)(1 + u_{2;2} + k_{23}u_1 + k_{22}u_3) - \theta_1\theta_2(u_{1;2} - k_{23}u_2)}{2 + \theta_3} - \theta_2(u_{3;2} - k_{22}u_2)\right]\cos\phi_3$$

$$+ \left[\frac{(2 + \theta_3 - \theta_1^2)(k_{23}u_2 - u_{1;2}) + \theta_1\theta_2(1 + u_{2;2} + k_{23}u_1 + k_{22}u_3)}{2 + \theta_3} + \theta_1(u_{3;2} - k_{22}u_2)\right]\sin\phi_3 - 1$$

$$\epsilon_{12} = \left[\frac{(2 + \theta_3 - \theta_2^2)(u_{2;1} + k_{13}u_1) - \theta_1\theta_2(1 + u_{1;1} - k_{13}u_2 + k_{11}u_3)}{2 + \theta_3} + \theta_2(k_{11}u_1 - u_{3;1})\right]\cos\phi_3$$

$$- \left[\frac{(2 + \theta_3 - \theta_1^2)(1 + u_{1;1} - k_{13}u_2 + k_{11}u_3) - \theta_1\theta_2(u_{2;1} + k_{13}u_1)}{2 + \theta_3} + \theta_1(k_{11}u_1 - u_{3;1})\right]\sin\phi_3$$

$$\epsilon_{21} = \left[\frac{(2 + \theta_3 - \theta_1^2)(u_{1;2} - k_{23}u_2) + \theta_1\theta_2(1 + u_{2;2} + k_{23}u_1 + k_{22}u_3)}{2 + \theta_3} + \theta_1(u_{3;2} - k_{22}u_2)\right]\cos\phi_3$$

$$+ \left[\frac{(2 + \theta_3 - \theta_2^2)(1 + u_{2;2} + k_{23}u_1 + k_{22}u_3) - \theta_1\theta_2(u_{1;2} - k_{23}u_2)}{2 + \theta_3} - \theta_2(u_{3;2} - k_{22}u_2)\right]\sin\phi_3$$

$$2\gamma_{13} = \theta_1(1 + u_{1;1} - k_{13}u_2 + k_{11}u_3) + \theta_2(u_{2;1} + k_{13}u_1) + (1 + \theta_3)(u_{3;1} - k_{11}u_1)$$

$$2\gamma_{23} = \theta_1(u_{1;2} - k_{23}u_2) + \theta_2(1 + u_{2;2} + k_{23}u_1 + k_{22}u_3) + (1 + \theta_3)(u_{3;2} - k_{22}u_2)$$

$$(24)$$

These expressions explicitly depend on $\sin\phi_3$ and $\cos\phi_3$. It is evident that one can choose ϕ_3 so that $\epsilon_{12} = \epsilon_{21}$, yielding

$$\tan\phi_3 = \frac{n_1 + \theta_2^2(u_{2;1} + k_{13}u_1) - \theta_1^2(u_{1;2} - k_{23}u_2) + \theta_1\theta_2\left[u_{1;1} - u_{2;2} + (k_{11} - k_{22})u_3 - k_{23}u_1 - k_{13}u_2\right]}{n_2 + \theta_1^2(u_{1;1} + k_{11}u_3 - k_{13}u_2) + \theta_2^2(u_{2;2} + k_{22}u_3 + k_{23}u_1) + \theta_1\theta_2(u_{1;2} + u_{2;1} - k_{23}u_2 + k_{13}u_1)}$$

$$(25)$$

where

$$n_1 = (2 + \theta_3)\left[u_{1;2} - u_{2;1} - \theta_1(u_{3;2} - k_{22}u_2) + \theta_2(u_{3;1} - k_{11}u_1) - k_{13}u_1 - k_{23}u_2\right]$$

$$n_2 = (2 + \theta_3)[\theta_1(u_{3;1} - k_{11}u_1) + \theta_2(u_{3;2} - k_{22}u_2) - u_{1;1} - u_{2;2} - 2 - \theta_3$$

$$- k_{23}u_1 - (k_{22} + k_{11})u_3 + k_{13}u_2]$$

$$(26)$$

It is now clear that once the functions u_1, u_2, u_3, θ_1 and θ_2 are known, the entire deformation is determined. Because of this, one should expect that a variational formulation would yield only five equilibrium equations – *not six*.

For small displacement and small strain, one can obtain ϕ_3 as

$$\phi_3 = \frac{(A_2u_2)_{,1} - (A_1u_1)_{,2}}{2A_1A_2}$$

$$(27)$$

which is the angle of rotation about B_3, the same as obtained in [23].

Although one can now find exact expressions for ϵ_{11}, $2\epsilon_{12}$, ϵ_{22}, $2\gamma_{13}$ and $2\gamma_{23}$ which are independent of ϕ_3, such expressions are rather lengthy and are not given here. Alternatively, one could leave ϕ_3 in the equations and regard Eq. (25) as a constraint. This would allow the construction of a shell finite element which would be compatible with beam elements which have three rotational degrees of freedom at the nodes.

Expressions for the curvatures can be found in terms of C as

$$\widetilde{K_\alpha} = -C_{;\alpha}C^T + C\widetilde{k_\alpha}C^T \tag{28}$$

where

$$K_\alpha = \lfloor -k_{\alpha 2} \quad k_{\alpha 1} \quad k_{\alpha 3} \rfloor^T + \lfloor -\kappa_{\alpha 2} \quad \kappa_{\alpha 1} \quad \kappa_{\alpha 3} \rfloor^T \tag{29}$$

Following [24], the curvature vector can also be found using Rodrigues parameters

$$K_\alpha = \frac{I - \frac{\tilde{\rho}}{2}}{1 + \frac{\rho^T \rho}{4}} \rho_{;\alpha} + C k_\alpha \tag{30}$$

Using the form of C from Eqs. (23), the curvatures become

$$\kappa_{\alpha 1} = \theta_{1;\alpha} \cos \phi_3 + \theta_{2;\alpha} \sin \varphi_3 - \frac{\theta_{3;\alpha}(\theta_1 \cos \phi_3 + \theta_2 \sin \phi_3)}{2 + \theta_3} + \hat{k}_{\alpha 1} - k_{\alpha 1}$$

$$\kappa_{\alpha 2} = -\theta_{1;\alpha} \sin \phi_3 + \theta_{2;\alpha} \cos \phi_3 + \frac{\theta_{3;\alpha}(\theta_1 \sin \phi_3 - \theta_2 \cos \phi_3)}{2 + \theta_3} + \hat{k}_{\alpha 2} - k_{\alpha 2}$$

$$\kappa_{\alpha 3} = \phi_{3;\alpha} + \frac{\theta_{1;\alpha}\theta_2 - \theta_1 \theta_{2;\alpha}}{2 + \theta_3} + \hat{k}_{\alpha 3} \tag{31}$$

where

$$\hat{k}_{\alpha 1} = (k_{\alpha 3} - \frac{k_{\alpha 2}\theta_1}{2 + \theta_3} + \frac{k_{\alpha 1}\theta_2}{2 + \theta_3})(\theta_1 \sin \phi_3 - \theta_2 \cos \phi_3) + k_{\alpha 2} \sin \phi_3 + k_{\alpha 1} \cos \phi_3$$

$$\hat{k}_{\alpha 2} = (k_{\alpha 3} - \frac{k_{\alpha 2}\theta_1}{2 + \theta_3} + \frac{k_{\alpha 1}\theta_2}{2 + \theta_3})(\theta_1 \cos \phi_3 + \theta_2 \sin \phi_3) + k_{\alpha 2} \cos \phi_3 - k_{\alpha 1} \sin \phi_3$$

$$\hat{k}_{\alpha 3} = -k_{\alpha 2}\theta_1 + k_{\alpha 1}\theta_2 + k_{\alpha 3}\theta_3 \tag{32}$$

As before, ϕ_3 can be eliminated from these expressions, so that all six curvatures can be expressed in terms of five independent quantities. Note that $\kappa_{\alpha 3}$ are not independent 2-D generalized strains. They will, however, appear in the equilibrium equations because of their appearance in the virtual strain-displacement relations derived later.

2-D Constitutive Law

To complete the analysis for an elastic shell, a 2-D constitutive law is required to relate 2-D generalized stresses and strains. As mentioned before the constitutive law can not be exact, however, one should try to avoid introducing any unnecessary approximation in addition to the already-approximate 3-D constitutive relations.

Among many approaches that have been proposed to deal with dimensional reduction, the approach in [17] stands out for its accuracy and simplicity. In that work, a simple Reissner-Mindlin type energy model is constructed that is as close as possible to being asymptotically correct. Moreover, the original 3-D results can be recovered accurately. The resulting model can be expressed as

$$2\Pi = \epsilon^T A \epsilon + \gamma^T G \gamma + 2\epsilon^T F \tag{33}$$

where $\epsilon = \lfloor \epsilon_{11}\ 2\epsilon_{12}\ \epsilon_{22}\ \kappa_{11}\ \kappa_{12}+\kappa_{21}\ \kappa_{22} \rfloor^T$ and $\gamma = \lfloor 2\gamma_{13}\ 2\gamma_{23} \rfloor^T$. It is noticed that there is only one in-plane shear strain ϵ_{12} in Eq. (33). This is possible only after one uses the constraints in Eq. (9). Moreover, the strain energy is independent of $\kappa_{\alpha 3}$ so that the rotation about the normal only appears algebraically, making it possible for it to be eliminated.

This simple constitutive model is rigorously reduced from the original 3-D model for multilayer shells, each layer of which is made with an anisotropic material with monoclinic symmetry. The variational asymptotic method [16] is used to guarantee the resulting 2-D shell model to yield the best approximation to the energy stored in the original 3-D structure by discarding all the insignificant contribution to the energy higher than the order of $(h/l)^2$ and h/R. The stiffness matrices A and G obtained through this process carry all the material and geometry information through the thickness (see Eqs. (63) and (73) in Ref. [17] for detailed expressions). The term containing the column matrix F is produced by body forces in the shell structure and tractions on the top and bottom surfaces, and it is very important for the recovery of the original 3-D results. Interested readers can refer to Ref. [17] for details of constructing the model in Eq. (33) for multilayered composite shells.

Having obtained the 2-D constitutive law from 3-D elasticity, one can derive all the other relations over the reference surface of the shell, a 2-D continuum.

Virtual Strain Displacement Relations

In order to derive intrinsic equilibrium equations from the 2-D energy, it is necessary to express the variations of generalized strain measures in terms of virtual displacements and virtual rotations.

The variation of the energy expressed in Eq. (33) can be written as

$$\delta\Pi = \frac{\partial\Pi}{\partial\epsilon_{11}}\delta\epsilon_{11} + \frac{\partial\Pi}{\partial\epsilon_{12}}\delta\epsilon_{12} + \frac{\partial\Pi}{\partial\epsilon_{22}}\delta\epsilon_{22} + \frac{\partial\Pi}{\partial\gamma_{13}}\delta\gamma_{13}$$
$$+ \frac{\partial\Pi}{\partial\gamma_{23}}\delta\gamma_{23} + \frac{\partial\Pi}{\partial\kappa_{11}}\delta\kappa_{11} + \frac{\partial\Pi}{\partial\omega}\delta\omega + \frac{\partial\Pi}{\partial\kappa_{22}}\delta\kappa_{22} \tag{34}$$

It is now obvious that one must express $\delta\epsilon_{11}, \ldots, \delta\kappa_{22}$, in terms of virtual displacements and rotations in order to obtain the final Euler-Lagrange equations of the energy functional in their intrinsic form. Following Ref. [24], we introduce measures of virtual displacement and rotation that are "compatible" with the intrinsic strain measures. For the virtual displacement, we note the form of Eq. (18) and choose

$$\overline{\delta q} = C\delta u \tag{35}$$

Similarly, for the virtual rotation, we note the form of Eq. (28) and write

$$\widetilde{\overline{\delta\psi}} = -\delta C C^T \tag{36}$$

where $\overline{\delta\psi}$ is a column matrix arranged similarly as the curvature column matrix in Eq. (4) $\overline{\delta\psi} = \lfloor -\overline{\delta\psi}_2 \ \overline{\delta\psi}_1 \ \overline{\delta\psi}_3 \rfloor^T$. The bars indicate that these quantities are not necessarily the variations of functions. Using these relations it is clear that

$$\delta u = C^T\overline{\delta q} \tag{37}$$

and

$$\delta C = -\widetilde{\overline{\delta\psi}}C \tag{38}$$

Let us begin with the generalized strain-displacement relationship, Eq. (18). A particular in-plane strain element can be written as

$$\epsilon_{\alpha\beta} = e_\beta^T\left[C(e_\alpha + u_{;\alpha} + \widetilde{k_\alpha}u) - e_\alpha\right] \tag{39}$$

Taking a straightforward variation, one obtains

$$\delta\epsilon_{\alpha\beta} = e_\beta^T\left[\delta C(e_\alpha + u_{;\alpha} + \widetilde{k_\alpha}u) + C(\delta u_{;\alpha} + \widetilde{k_\alpha}\delta u)\right] \tag{40}$$

The right hand side contains $u_{;\alpha}$ and $\delta u_{;\alpha}$, which must be eliminated in order to obtain variations of the strain that are independent of displacements. These are needed to derive intrinsic equilibrium equations.

Premultiplying both sides of Eq. (18) by C^T, making use of Eq. (36), and finally using a

property of the tilde operator that, for arbitrary column matrices Y and Z, $\widetilde{Y}Z = -\widetilde{Z}Y$, one can make the first term in brackets on the righthand side independent of $u_{;\alpha}$. After all this, one obtains

$$\delta C(e_\alpha + u_{;\alpha} + \widetilde{k_\alpha}u) = \delta C C^T(e_\alpha + \gamma_\alpha) = -\widetilde{\overline{\delta\psi}}(e_\alpha + \gamma_\alpha) = (\widetilde{e}_\alpha + \widetilde{\gamma_\alpha})\overline{\delta\psi} \qquad (41)$$

An expression for the second term in brackets on the right hand side of Eq. (40) can now be obtained by differentiating Eq. (37) with respect to x_α and premultiplying by C. This yields

$$C(\delta u_{;\alpha} + \widetilde{k_\alpha}\delta u) = C(C^T\overline{\delta q})_{;\alpha} + C\widetilde{k_\alpha}\delta u = \overline{\delta q}_{;\alpha} + \widetilde{K_\alpha}\overline{\delta q} \qquad (42)$$

Substituting Eqs. (41) and (42) into Eq. (40), one obtains an intrinsic expression for the variation of the in-plane strain components as

$$\delta\epsilon_{\alpha\beta} = e_\beta^T\left[\overline{\delta q}_{;\alpha} + \widetilde{K_\alpha}\overline{\delta q} + (\widetilde{e}_\alpha + \widetilde{\gamma_\alpha})\overline{\delta\psi}\right] \qquad (43)$$

where $e_\beta^T\widetilde{e}_\alpha$ vanishes when $\alpha = \beta$. This matrix equation can be written explicitly as four scalar equations

$$\delta\epsilon_{11} = \overline{\delta q}_{1;1} - K_{13}\overline{\delta q}_2 + K_{11}\overline{\delta q}_3 - 2\gamma_{13}\overline{\delta\psi}_1 + \epsilon_{12}\overline{\delta\psi}_3$$
$$\delta\epsilon_{12} = \overline{\delta q}_{2;1} + K_{13}\overline{\delta q}_1 + \kappa_{12}\overline{\delta q}_3 - 2\gamma_{13}\overline{\delta\psi}_2 - (1 + \epsilon_{11})\overline{\delta\psi}_3$$
$$\delta\epsilon_{21} = \overline{\delta q}_{1;2} - K_{23}\overline{\delta q}_2 + \kappa_{21}\overline{\delta q}_3 - 2\gamma_{23}\overline{\delta\psi}_1 + (1 + \epsilon_{22})\overline{\delta\psi}_3$$
$$\delta\epsilon_{22} = \overline{\delta q}_{2;2} + K_{23}\overline{\delta q}_1 + K_{22}\overline{\delta q}_3 - 2\gamma_{23}\overline{\delta\psi}_2 - \epsilon_{12}\overline{\delta\psi}_3 \qquad (44)$$

The variations $\delta\epsilon_{12}$ and $\delta\epsilon_{21}$ should be equal due to Eq. (9); hence, one can solve for the virtual rotation component about $\mathbf{B}_3$ as

$$\overline{\delta\psi}_3 = \frac{\overline{\delta q}_{2;1} - \overline{\delta q}_{1;2} + K_{13}\overline{\delta q}_1 + K_{23}\overline{\delta q}_2 + (\kappa_{12} - \kappa_{21})\overline{\delta q}_3 - 2\gamma_{13}\overline{\delta\psi}_2 + 2\gamma_{23}\overline{\delta\psi}_1}{2 + \epsilon_{11} + \epsilon_{22}} \qquad (45)$$

It is now possible to write the variations of all strain measures in terms of three virtual displacement and two virtual rotation components as

$$\delta\epsilon_{11} = \overline{\delta q}_{1;1} - K_{13}\overline{\delta q}_2 + K_{11}\overline{\delta q}_3 - 2\gamma_{13}\overline{\delta\psi}_1 + \epsilon_{12}\overline{\delta\psi}_3$$
$$\delta\epsilon_{22} = \overline{\delta q}_{2;2} + K_{23}\overline{\delta q}_1 + K_{22}\overline{\delta q}_3 - 2\gamma_{23}\overline{\delta\psi}_2 - \epsilon_{12}\overline{\delta\psi}_3$$
$$2\delta\epsilon_{12} = \overline{\delta q}_{2;1} + \overline{\delta q}_{1;2} + K_{13}\overline{\delta q}_1 - K_{23}\overline{\delta q}_2 + 2\omega\overline{\delta q}_3$$
$$- 2\gamma_{13}\overline{\delta\psi}_2 - 2\gamma_{23}\overline{\delta\psi}_1 + (\epsilon_{22} - \epsilon_{11})\overline{\delta\psi}_3 \qquad (46)$$

with $\overline{\delta\psi}_3$ taken from Eq. (45).

Let us now consider the transverse shear strains

$$2\gamma_{\alpha3} = e_3^T \left[C(e_\alpha + u_{;\alpha} + \widetilde{k_\alpha}u) - e_\alpha \right] \tag{47}$$

Following a procedure similar to the above, one can obtain the virtual strain-displacement equation for transverse shear strains as

$$2\delta\gamma_{\alpha3} = e_3^T \left[\overline{\delta q}_{;\alpha} + \widetilde{K_\alpha}\overline{\delta q} + (\widetilde{e_\alpha} + \widetilde{\gamma_\alpha})\overline{\delta\psi} \right] \tag{48}$$

Explicit expressions for the variations of the shear strain components are now easily written as

$$2\delta\gamma_{\alpha3} = \overline{\delta q}_{3;\alpha} + \overline{\delta\psi}_\alpha + \epsilon_{\alpha\beta}\overline{\delta\psi}_\beta - K_{\alpha3}\overline{\delta q}_\beta \tag{49}$$

Finally, variations of the curvatures are found. First, taking the straightforward variation of Eq. (28), one obtains

$$\delta\widetilde{\kappa_\alpha} = -\frac{\delta C_{,\alpha}C^T}{A_\alpha} - \frac{C_{,\alpha}\delta C^T}{A_\alpha} + \delta C\widetilde{k_\alpha}C^T + C\widetilde{k_\alpha}\delta C^T \tag{50}$$

In order to eliminate $\delta C_{,\alpha}$, we differentiate Eq. (36) with respect to x_α

$$\widetilde{\overline{\delta\psi}}_{,\alpha} = -\delta C_{,\alpha}C^T - \delta C C_{,\alpha}^T \tag{51}$$

In order to eliminate δC, we can use Eq. (38). Then, Eq. (50) becomes

$$\delta\widetilde{\kappa_\alpha} = \widetilde{\overline{\delta\psi}}_{;\alpha} + \widetilde{K_\alpha}\widetilde{\overline{\delta\psi}} - \widetilde{\overline{\delta\psi}}\widetilde{K_\alpha} \tag{52}$$

Using another tilde identity $(\widetilde{\widetilde{Y}Z} = \widetilde{Y}\widetilde{Z} - \widetilde{Z}\widetilde{Y})$ one can find the virtual strain-displacement relation as

$$\delta\kappa_\alpha = \overline{\delta\psi}_{;\alpha} + \widetilde{K_\alpha}\overline{\delta\psi} \tag{53}$$

In explicit form

$$\delta\kappa_{11} = \frac{\overline{\delta\psi}_{1,1}}{A_1} - K_{13}\overline{\delta\psi}_2 + \kappa_{12}\overline{\delta\psi}_3$$

$$\delta\kappa_{22} = \frac{\overline{\delta\psi}_{2,2}}{A_2} + K_{23}\overline{\delta\psi}_1 - \kappa_{21}\overline{\delta\psi}_3$$

$$2\delta\omega = \frac{\overline{\delta\psi}_{1,2}}{A_2} + \frac{\overline{\delta\psi}_{2,1}}{A_1} + K_{13}\overline{\delta\psi}_1 - K_{23}\overline{\delta\psi}_2 + (K_{22} - K_{11})\overline{\delta\psi}_3 \tag{54}$$

where $\overline{\delta\psi}_3$ can again be eliminated by using Eq. (45).

Intrinsic Equilibrium Equations

In this section, we will make use of the virtual strain-displacement relations in the variation of the internal strain energy in order to derive the intrinsic equilibrium equations. Here we define the generalized forces as

$$\frac{\partial \Pi}{\partial \epsilon_{11}} = N_{11} \qquad \frac{\partial \Pi}{\partial \epsilon_{22}} = N_{22} \qquad \frac{1}{2}\frac{\partial \Pi}{\partial \epsilon_{12}} = N_{12}$$

$$\frac{\partial \Pi}{\partial \kappa_{11}} = M_{11} \qquad \frac{\partial \Pi}{\partial \kappa_{22}} = M_{22} \qquad \frac{1}{2}\frac{\partial \Pi}{\partial \omega} = M_{12}$$

$$\frac{1}{2}\frac{\partial \Pi}{\partial \gamma_{13}} = Q_1 \qquad \frac{1}{2}\frac{\partial \Pi}{\partial \gamma_{23}} = Q_2 \tag{55}$$

To use the principle of virtual work to derive the equilibrium equations, one needs to know the applied loads. In addition to the applied loads used in the modeling process, $\tau_i \mathbf{B}_i$ at the top surface, $\beta_i \mathbf{B}_i$ at the bottom surface and body force $\phi_i \mathbf{B}_i$ [17], one can also specify appropriate combinations of displacements, rotations (geometrical boundary conditions), running forces and moments (natural boundary conditions) along the boundary around the reference surface. It is trivial to apply the geometrical boundary conditions. Although it is possible in most cases that natural boundary conditions can be derived from Newton's law, the procedure is tedious and not easily applied here because the physical meanings for some of the generalized forces are not clear. Thus, natural boundary conditions are best derived from the principle of virtual work.

Suppose on boundary Γ (see Fig. 2), we specify a force resultant $\hat{N}_{\nu\nu}$ and moment resultant $\hat{M}_{\nu\nu}$ along the outward normal of the boundary curve tangent to the reference surface ν, $\hat{N}_{\nu\tau}$ and $\hat{M}_{\nu\tau}$ along the tangent of the boundary curve τ, $\hat{N}_{\nu 3}$ along the normal of the reference surface. Then the principle of virtual work (strictly speaking, the principle of virtual displacements) can be stated as:

$$\int\int_s (\delta\Pi - \overline{\delta q_i}f_i - \overline{\delta\psi_\alpha}m_\alpha)A_1 A_2 \mathrm{d}x_1 \mathrm{d}x_2 -$$

$$\int_\Gamma (\hat{N}_{\nu\nu}\overline{\delta q_\nu} + \hat{N}_{\nu\tau}\overline{\delta q_\tau} + \hat{N}_{\nu 3}\overline{\delta q_3} + \hat{M}_{\nu\nu}\overline{\delta\psi_\nu} + \hat{M}_{\nu\tau}\overline{\delta\psi_\tau})\mathrm{d}\Gamma = 0 \tag{56}$$

where f_i and m_α are taken directly from [17].

It is now possible to obtain intrinsic equilibrium equations and consistent edge conditions by use of the principle of virtual work and the virtual strain-displacement relations derived in the

previous section. The equilibrium equations are

$$\frac{(A_2 N_{11})_{,1}}{A_1 A_2} + \frac{[A_1(N_{12} + \mathcal{N})]_{,2}}{A_1 A_2} - K_{13}(N_{12} - \mathcal{N}) - K_{23} N_{22} + Q_1 K_{11} + Q_2 \kappa_{21} + f_1 = 0$$

$$\frac{(A_1 N_{22})_{,2}}{A_1 A_2} + \frac{[A_2(N_{12} - \mathcal{N})]_{,1}}{A_1 A_2} + K_{23}(N_{12} + \mathcal{N}) + K_{13} N_{11} + Q_1 \kappa_{12} + Q_2 K_{22} + f_2 = 0$$

$$\frac{(A_2 Q_1)_{,1}}{A_1 A_2} + \frac{(A_1 Q_2)_{,2}}{A_1 A_2} - K_{11} N_{11} - K_{22} N_{22} - 2\omega N_{12} + (\kappa_{12} - \kappa_{21})\mathcal{N} + f_3 = 0$$

$$\frac{(A_2 M_{11})_{,1}}{A_1 A_2} + \frac{(A_1 M_{12})_{,2}}{A_1 A_2} - Q_1(1 + \epsilon_{11})$$

$$\qquad - Q_2 \epsilon_{12} + 2\gamma_{13} N_{11} + 2\gamma_{23}(N_{12} + \mathcal{N}) - M_{12} K_{13} - M_{22} K_{23} + m_1 = 0$$

$$\frac{(A_2 M_{12})_{,1}}{A_1 A_2} + \frac{(A_1 M_{22})_{,2}}{A_1 A_2} - Q_2(1 + \epsilon_{22})$$

$$\qquad - Q_1 \epsilon_{12} + 2\gamma_{13}(N_{12} - \mathcal{N}) + 2\gamma_{23} N_{22} + M_{11} K_{13} + M_{12} K_{23} + m_2 = 0 \qquad (57)$$

where

$$\mathcal{N} = \frac{(N_{22} - N_{11})\epsilon_{12} + N_{12}(\epsilon_{11} - \epsilon_{22}) + M_{22}\kappa_{21} - M_{11}\kappa_{12} + M_{12}(K_{11} - K_{22})}{2 + \epsilon_{11} + \epsilon_{22}} \qquad (58)$$

The associated natural boundary conditions on Γ are

$$\hat{N}_{\nu\nu} = n_1^2 N_{11} + 2n_1 n_2 N_{12} + n_2^2 N_{22}$$

$$\hat{N}_{\nu\tau} = n_1 n_2 (N_{22} - N_{11}) + (n_1^2 - n_2^2) N_{12} - \mathcal{N}$$

$$\hat{N}_{\nu\nu} = n_1^2 N_{11} + 2n_1 n_2 N_{12} + n_2^2 N_{22}$$

$$\hat{N}_{\nu 3} = n_1 Q_1 + n_2 Q_2$$

$$\hat{M}_{\nu\nu} = n_1^2 M_{11} + 2n_1 n_2 M_{12} + n_2^2 M_{22}$$

$$\hat{M}_{\nu\tau} = n_1 n_2 (M_{22} - M_{11}) + (n_1^2 - n_2^2) M_{12} \qquad (59)$$

where $n_1 = \cos\phi$, $n_2 = \sin\phi$, and ϕ is the angle between the outward normal of the boundary and x_1 direction as shown in Fig. 2. The terms containing $\mathcal{N}$ stem from consistent inclusion of the finite rotation from undeformed triad to deformed triad although the *nonzero* rotation about $\mathbf{B}_3$ is expressed in terms of other kinematical quantities. Similar terms are found in the shell equations derived by Berdichevsky [16] where only five equilibrium equations are derived.

In a mixed formulation, $\mathcal{N}$ can be shown to be the Lagrange multiplier that enforces Eq. (45). To further understand the nature of $\mathcal{N}$ one can undertake the following exercise: Setting $P_i = 0$ and $\epsilon_{12} = \epsilon_{21}$ for the equilibrium equations given in [13], $\frac{N_{21} - N_{12}}{2}$ can be solved from Reissner's sixth equilibrium equation. This shows that Reissner's $\frac{N_{21} - N_{12}}{2}$ is the same as our $\mathcal{N}$, and Reiss-

ner's $\frac{N_{21}+N_{12}}{2}$ is the same as our N_{12}. Finally, substitution of this sixth equation into the other five yields the five equilibrium equations given here in Eqs. (57). It is noted that Reissner's equilibrium equations are derived based on the basis of Newton's law of motion without consideration of either constitutive law or strain-displacement relations. However, the present derivation is purely displacement-based. The reproduction of those equilibrium equations by the present derivation illustrates that, as long as the formulation is geometrically exact, one can derive exact equilibrium equations.

A few investigators have noted an apparent conflict between the symmetry of the stress resultants and the satisfaction of moment equilibrium about the normal. In reality there is no conflict, but one must be careful. We have shown herein that the triad $\mathbf{B}_i$ can always be chosen so that $\epsilon_{12} = \epsilon_{21}$. If this relation is enforced strongly, there is only one in-plane shear stress resultant, N_{12}, that can be derived from the energy. In that case the physical quantity associated with the antisymmetric part of Reissner's in-plane stress resultants, while it is not available from the constitutive law, is nevertheless available as a reactive quantity from the moment equilibrium equation about the normal. However, it must be stressed that the moment equilibrium equation about the normal is not available from a conventional energy approach, in which the virtual displacements and rotations must be independent.

In a somewhat similar vein, not being able to obtain the antisymmetric part of the moment stress resultants from derivatives of the 2-D strain energy is a result of the approximate dimensional reduction process in which it was determined, based on asymptotic considerations and *geometrically nonlinear* 3-D elasticity, that the antisymmetric term $\kappa_{12} - \kappa_{21}$ does not appear as an independent generalized strain measure in the 2-D constitutive law with correction only to the order of h/R. However, if a more refined theory with respect to h/R is required, then $\kappa_{12} - \kappa_{21}$ would appear as a generalized strain in the 2-D constitutive law and a new generalized moment would be defined based on the constitutive law.

For practical computational schemes, equilibrium equations and boundary conditions need to use the constitutive law to relate with the generalized 2-D strains. Finally a set of kinematical equations is needed. Depending on how this part is done, the analysis can be completed in either of two fundamentally different ways: a purely intrinsic form, relying on compatibility equations, and a mixed form relying on explicit strain-displacement relations.

In the intrinsic form we have five equilibrium equations, Eqs. (57); six compatibility equations, Eqs. (12) – (14); and the eight constitutive equations – a total of 19 equations. The 19 unknowns are the eight stress resultants, N_{11}, N_{12}, N_{22}, Q_1, Q_2, M_{11}, M_{12}, and M_{22}; and the 11 strain measures ϵ_{11}, $2\epsilon_{12}$, ϵ_{22}, $2\gamma_{13}$, $2\gamma_{23}$, κ_{11}, $2\omega_{12}$, and κ_{22}, along with κ_{13}, κ_{23}, and $\kappa_{12} - \kappa_{21}$. The last three strain measures appear in the equilibrium equations but not in the constitutive law.

In a mixed formulation one would use the same five equilibrium equations and eight con-

stitutive equations. One would also need a set of strain-displacement relations among the 11 generalized strain measures ϵ_{11}, $2\epsilon_{12}$, ϵ_{22}, $2\gamma_{13}$, $2\gamma_{23}$, κ_{11}, 2ω, and κ_{22}, along with κ_{13}, κ_{23}, and $\kappa_{12} - \kappa_{21}$, and the five global displacement and rotational variables u_1, u_2, u_3, θ_1, and θ_2. One possible set of such equations is as follows: use five of Eqs. (24), using either ϵ_{12} or ϵ_{21}; use the six Eqs. (31). There are also the two other rotational variables θ_3 and ϕ_3, which are governed by Eqs. (22) and (25), respectively. This way there are 26 equations and 26 unknowns. This mixed formulation is capable of handling boundary conditions on 2-D stress resultants and displacement/rotation variables. At least in principle, one could recover a displacement formulation by eliminating all the unknowns except the displacement and rotation variables.

Eqs. (57) and (58) contain terms that could be disregarded because of the original assumption of small strain. We will not undertake this simplification here, because it is out of the scope of the present study to actually implement the 2-D nonlinear theory. Therefore, our equilibrium equations and kinematical equations are geometrically exact; all approximations stem from the dimensional reduction process used to obtain the 2-D constitutive law.

The present work is a direct extension of [18] to treat shells. If one sets $k_{ij} = 0$ and $A_\alpha = 1$, all the formulas developed here will reduce to those in [18], which indirectly verifies that derivation.

Conclusions

A nonlinear shear-deformable shell theory has been developed to be completely compatible with the modeling process in [17]. The compatibility equations, kinematical relations and equilibrium equations are derived for arbitrarily large displacements and rotations under the restriction that the strain must be small. The resulting formulae are compared with others in the literature. The following conclusions can be drawn from the present work:

1. The variational asymptotic method can be used to decouple the original 3-D elasticity problem of a shell into a 1-D, through-the-thickness analysis [17] and a 2-D, shell analysis. The through-the-thickness analysis provides both an accurate 2-D constitutive law for the nonlinear shell theory and accurate through-the-thickness recovery relations for 3-D displacement, strain, and stress. This way, an intimate relation between the shell theory and 3-D elasticity is established.

2. A full finite rotation must be applied to fully specify the displacement field. However, since the strain energy on which the formulation is based is independent of $\kappa_{\alpha 3}$, the rotation about the normal is not independent and can be expressed in terms of other quantities. Thus, it can be chosen so that the two-dimensional, in-plane shear strain measures are equal. This way all the strain measures can be expressed in terms of five independent quantities: three displacement and two rotation measures, and only one stress resultant for in-plane shear can be derived from the 2-D energy.

3. Only five equilibrium equations are obtainable in a displacement-based variational formulation. Moment equilibrium about the normal is satisfied implicitly. If one does not include the full finite rotation, but rather sets the rotation about the normal equal to zero, the correct equilibrium equations cannot be obtained. This should shed some light on the nature of "drilling" degrees of freedom.

References

[1] W. Yu. *Variational Asymptotic Modeling of Composite Dimensionally Reducible Structures.* PhD thesis, Aerospace Engineering, Georgia Institute of Technology, May 2002.

[2] A. Campbell. On vibration galvanometer with unifilar torsional control. *Proceedings of the Physical Society*, 25:203 – 205, April 1913.

[3] H. Pealing. On an anomalous variation of the rigidity of phosphor bronze. *Philosophical Magazine*, 25(147):418 – 427, March 1913.

[4] J. C. Buckley. The bifilar property of twisted strips. *Philosophical Magazine*, 28:778 – 785, 1914.

[5] H. Wagner. Torsion and buckling of open sections. *NACA TM 807*, 1936.

[6] A. E. H. Love. *Mathematical Theory of Elasticity.* Dover Publications, New York, New York, 4th edition, 1944.

[7] B. Cosserat and F. Cosserat. *Théorie des Corps Deformables.* Hermann, Paris, 1909.

[8] P. M. Naghdi. The theory of shells and plates. *Handbuch der Pyhsik*, 6 a/2:425–640, 1972. Springer-Verlag, Berlin.

[9] J.C. Simo and D. D. Fox. On a stress resultant geometrically exact shell model. part i: Formulation and optimal parametrization. *Computer Methods in Applied Mechanics and Engineering*, 72:267–304, 1989.

[10] J.C. Simo and D. D. Fox. On a stress resultant geometrically exact shell model. part ii: The linear theory; computational aspects. *Computer Methods in Applied Mechanics and Engineering*, 73:53–92, 1989.

[11] A. Ibrahimbegovic. Stress resultant geometrically nonlinear shell theory with drilling rotations-part i. a consistent formulation. *Computer Methods in Applied Mechanics and Engineering*, 118:265–284, 1994.

[12] W. B. Kratzig. 'best' transverse shearing and stretching shell theory for nonlinear finite element simulations. *Computer Methods in Applied Mechanics and Engineering*, 103(1-2):135–160, 1993.

[13] E. Reissner. Linear and nonlinear theory of shells. In Y. C. Fung and E. E. Sechler, editors, *Thin Shell Structures*, pages 29 – 44. Prentice Hall, 1974.

[14] J. N. Reddy. *Mechanics of Laminated Composite Plates: Theory and Analysis.* CRC Press, Boca Raton, Florida, 1997.

[15] A. Libai and J. G. Simmonds. *The Nonlinear Theory of Elastic Shells.* Cambridge University Press, 2nd edition, 1998.

[16] V. L. Berdichevsky. Variational-asymptotic method of constructing a theory of shells. *PMM,* 43(4):664 – 687, 1979.

[17] Wenbin Yu, Dewey H. Hodges, and Vitali V. Volovoi. Asymptotic generalization of reissner-mindlin theory: Accurate three-dimensional recovery for composite shells. *Computer Methods in Applied Mechanics and Engineering,* 191(44):4971–5112, 2002.

[18] D. H. Hodges, A. R. Atilgan, and D. A. Danielson. A geometrically nonlinear theory of elastic plates. *Journal of Applied Mechanics,* 60(1):109 – 116, March 1993.

[19] J. G. Simmonds and Donald A. Danielson. Nonlinear shell theory with finite rotation and stress-function vectors. *Journal of Applied Mechanics,* pages 1085–1090, December 1972.

[20] Thomas R. Kane, Peter W. Likins, and David A. Levinson. *Spacecraft Dynamics.* McGraw-Hill Book Company, New York, New York, 1983.

[21] D. H. Hodges. Finite rotation and nonlinear beam kinematics. *Vertica,* 11(1/2):297 – 307, 1987.

[22] E. Reissner. On finite deflections of anisotropic laminated elastic plates. *International Journal of Solids and Structures,* 22(10):1107 – 1115, 1986.

[23] E. L. Axelrad. *Theory of Flexible Shells.* Elsevier Science Publishers, North-Holland, 1986.

[24] D. H. Hodges. A mixed variational formulation based on exact intrinsic equations for dynamics of moving beams. *International Journal of Solids and Structures,* 26(11):1253 – 1273, 1990.

List of Figures

Undeformed State

$\mathbf{b}_3(x_1,x_2)$

$\mathbf{b}_2(x_1,x_2)$

$\mathbf{b}_1(x_1,x_2)$

Deformed State

$\mathbf{B}_3(x_1,x_2)$

$\mathbf{B}_2(x_1,x_2)$

$\mathbf{u}(x_1,x_2)$

$\mathbf{B}_1(x_1,x_2)$

$\mathbf{r}(x_1,x_2)$

$\mathbf{R}(x_1,x_2)$

O

Figure 1:   Schematic of shell deformation
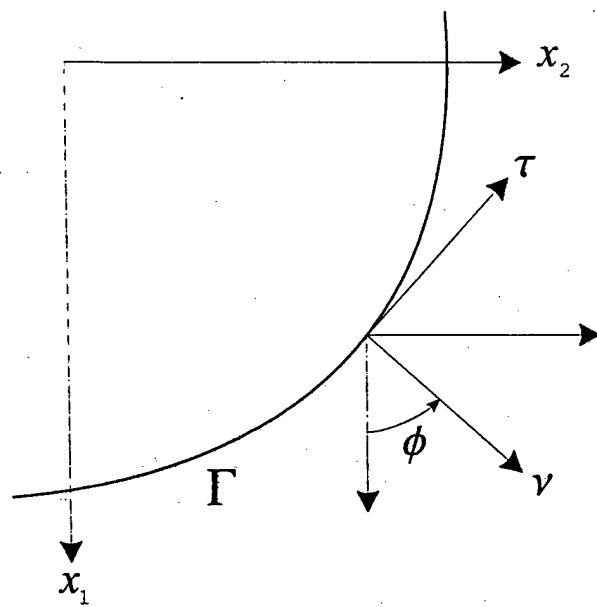
Figure 2: **Schematic of an arbitrary boundary**

An Asymptotic Approach for Thermoelastic Analysis of Laminated Composite Plates

Wenbin Yu[*] and Dewey H. Hodges[†]

Georgia Institute of Technology, Atlanta, Georgia 30332-0150

A thermoelastic model for analyzing laminated composite plates under both mechanical and thermal loadings is constructed by the variational asymptotic method. The original three-dimensional nonlinear thermoelasticity problem is formulated based on a set of intrinsic variables defined on the reference plane and for arbitrary deformation of the normal line. Then the variational asymptotic method is used to rigorously split the three-dimensional problem into two problems: a nonlinear, two-dimensional, plate analysis over the reference plane to obtain the global deformation and a linear analysis through the thickness to provide the two-dimensional generalized constitutive law and the recovering relations to approximate the original three-dimensional results. The nonuniqueness of asymptotic theory correct up to a certain order is used to cast the obtained asymptotically correct second-order free energy into a Reissner-Mindlin type model to account for transverse shear deformation. The present theory is implemented into the computer program, Variational Asymptotic Plate and Shell Analysis (VAPAS). Results from VAPAS for several cases have been compared with the exact thermoelasticity solutions, classical lamination theory and first-order shear-deformation theory to demonstrate the accuracy and power of the proposed theory.

Keywords: Asymptotic series, anisotropic plates, finite element method, strain distribution, stress distribution, thermoelasticity

Introduction

Composite materials have found increasing applications in engineering practices due to their superior engineering properties and improving manufacturing technology. However, the heterogeneity and anisotropy of such materials make the traditional analysis method used for designing homogeneous and isotropic structures obsolete. Moreover, structures made

---

[*]Post Doctoral Fellow, School of Aerospace Engineering. Presently, Assistant Professor, Department of Mechanical and Aerospace Engineering, Utah State University, Logan Utah 84322-4130.

[†]Professor, School of Aerospace Engineering.

with composite materials are more sensitive and vulnerable to temperature change than their isotropic counterpart. The reason is that the thermal expansion coefficients of different constituents of the material are usually dramatically different from each other resulting in high stresses due to sudden temperature change. The analysis including thermal effects is much more involved than that for isothermal conditions.

Many engineering structures made with composite materials have one dimension much smaller than the other two and can be modeled as plates. Only a few exact solutions exist for very idealized cases (see Savoia and Reddy (1995) and the references cited there). Researchers are trying to develop simplified models to provide an approximate representation for more general cases. Within the last few decades, a tremendous research effort has been invested in this area, and various approximate models have been proposed (Wu and Tauchert (1980); Noor and Burton (1992); Reddy (1997); Noor and Malik (2000); Rohwer *et al.* (2001)). Generally speaking, these models are derived from three-dimensional (3-D) thermoelasticity theory, making use of the fact that the plate is thin in some sense. Although it is plausible to consider the smallness of the thickness of plate structures, construction of an accurate two-dimensional (2-D) model for a 3-D body still introduces a lot of challenges. Almost all the proposed models in the literature can give a good prediction of the global behavior of the plate. However, they have serious difficulties in providing accurate distributions of the 3-D displacements, strains, and stresses through the thickness. Part of the reason is that most models adopt *ad hoc* assumptions (such as having displacement or stress components vary through the thickness according to a certain function) which violate the exact solutions. For example, most high order theories (except for some layerwise theories such as Cho and Averill (2000)) assume a C^∞ continuity for the 3-D displacement field through the thickness which in reality they are piecewise continuous. In the case of thermal loading, the prediction of these *ad hoc* models become even worse, if not wrong, and the results should be examined more cautiously.

It must be understood that all plate theories, no matter how involved they may appear, are inherently approximate. The approximation lies in the 2-D constitutive law relating 2-D strains and stress resultants, which is a direct consequence of eliminating the thickness coordinate from the independent variables of the governing equations of the boundary-value problem for a plate. This sort of approximation is inevitable if one wants to take advantage of the smallness of the thickness to simplify the analysis. It is interesting to note that the 3-D constitutive relations are essentially approximate and determined by experiments. However, this cannot be used as an excuse to introduce unnecessary assumptions. For example, for small-strain analysis of plates, it is reasonable to assume that the thickness, h, is small compared to the wavelength of deformation of the reference surface, l. However, it is not at

all reasonable to assume a priori some *ad hoc* displacement field, although that is the way most plate theories are constructed.

In this paper, we first cast the original 3-D thermoelasticity problem in an intrinsic form so that the theory is applicable for arbitrarily large displacement and global rotation, subject only to the strain's being small; see Hodges *et al.* (1993). Then, the Variational Asymptotic Method (VAM), introduced by Berdichevsky (1979), is used to split the original nonlinear 3-D elasticity problem into a linear, one-dimensional (1-D), through-the-thickness analysis and a nonlinear, 2-D, plate analysis. The through-the-thickness analysis produces the 2-D constitutive law and non-mechanical stress resultants to be used in the 2-D plate analysis, along with recovering relations that yield the 3-D displacement, strain and stress fields through the thickness using results obtained from the solution of the 2-D problem. The present work extends a simple yet accurate model developed recently for composite plates and shells, namely Variational Asymptotic Plate and Shell Analysis (VAPAS) by Yu *et al.* (2002a,b, 2003) so that thermoelastic effects can be treated in the same framework.

Since the procedure is quite similar, the authors have chosen to repeat some formulae and text from their previous publications in order to make the present paper more self-contained. The present theory has been implemented into the computer program VAPAS. The hygro effects due to moisture can be treated in a similar manner as thermal effects. Thus, for simplicity of presentation, the hygro effect is not included in the formulation. It has, however, also been implemented in VAPAS. Now, one can use VAPAS along some 2-D plate solver (say, some finite element program such as DYMORE, Bauchau (1998)) to carry out an accurate and efficient hygrothermoelastic analysis for composite plates.

3-D Formulation

A point in the plate can be described by its Cartesian coordinates x_i (see Fig. 1), where x_α are two orthogonal lines in the reference plane and x_3 is the normal coordinate. (Here and throughout the paper, Greek indices assume values 1 and 2 while Latin indices assume 1, 2, and 3. Repeated indices are summed over their range except where explicitly indicated.) Letting b_i denote the unit vector along x_i for the undeformed plate, one can then describe the position of any material point in the undeformed configuration by its position vector $\hat{r}$ from a fixed point O, such that

$$\hat{r}(x_1, x_2, x_3) = r(x_1, x_2) + x_3 b_3 \tag{1}$$

where r is the position vector from O to the point located by x_α on the reference surface. When the reference surface of the undeformed plate coincides with its middle surface, it

naturally follows that

$$\langle \hat{\mathbf{r}}(x_1, x_2, x_3) \rangle = \mathbf{r}(x_1, x_2) \tag{2}$$

where the angle-brackets denote the definite integral through the thickness of the plate and will be used throughout the paper.

When the plate deforms, the particle that had position vector $\hat{\mathbf{r}}$ in the undeformed state now has position vector $\hat{\mathbf{R}}$ in the deformed plate. The latter can be uniquely determined by the deformation of the 3-D body. Similarly, another triad $\mathbf{B}_i$ is introduced for the deformed configuration. The relation between $\mathbf{B}_i$ and $\mathbf{b}_i$ can be specified by an arbitrarily large rotation specified in terms of the matrix of direction cosines $C(x_1, x_2)$ so that

$$\mathbf{B}_i = C_{ij}\mathbf{b}_j \qquad C_{ij} = \mathbf{B}_i \cdot \mathbf{b}_j \tag{3}$$

subject to the requirement that $\mathbf{B}_i$ is coincident with $\mathbf{b}_i$ when the structure is undeformed. Now the position vector $\hat{\mathbf{R}}$ can be represented as

$$\hat{\mathbf{R}}(x_1, x_2, x_3) = \mathbf{R}(x_1, x_2) + x_3\mathbf{B}_3(x_1, x_2) + w_i(x_1, x_2, x_3)\mathbf{B}_i(x_1, x_2) \tag{4}$$

where w_i is the warping of the normal-line element. In the present work, the form of the warping w_i is not assumed, as in most plate theories. Rather, these quantities are treated as unknown 3-D functions and will be solved for later. Eq. (4) is six times redundant because of the way warping introduced. Six constraints are needed to make the formulation unique. The redundancy can be removed by choosing appropriate definitions of $\mathbf{R}$ and $\mathbf{B}_i$. One can define $\mathbf{R}$ similarly as Eq. (2) to be the average position through the thickness, from which it follows that the warping functions must satisfy the three constraints

$$\langle w_i(x_1, x_2, x_3) \rangle = 0 \tag{5}$$

Another two constraints can be specified by taking $\mathbf{B}_3$ as the normal to the reference surface of the deformed plate. It should be noted that this choice has nothing to do with the famous Kirchhoff hypothesis. Indeed, it is only for convenience in the derivation. In the Kirchhoff assumption, no local deformation of the transverse normal is allowed. On the other hand, according to the present scheme we allow all possible deformation, classifying all deformation other than that of classical lamination theory (CLT) as warping, which is assumed to be small. This assumption is valid if the strain is small and if the order of the local rotation (*i.e.* the rotation of the normal line due to warping) is of the order of the strain or smaller; see Danielson (1991).

Based on the concept of decomposition of rotation tensor, Danielson and Hodges (1987)

and Danielson (1991), the Jauman-Biot-Cauchy strain components for small local rotation are given by

$$\Gamma_{ij} = \frac{1}{2}(F_{ij} + F_{ji}) - \delta_{ij} \tag{6}$$

where F_{ij} is the mixed-basis component of the deformation gradient tensor such that

$$F_{ij} = \mathbf{B}_i \cdot \mathbf{G}_k \mathbf{g}^k \cdot \mathbf{b}_j \tag{7}$$

Here $\mathbf{G}_k = \frac{\partial \hat{\mathbf{R}}}{\partial x_k}$ is the covariant basis vector of the deformed configuration and $\mathbf{g}^k$ the contravariant base vector of the undeformed configuration and $\mathbf{g}^k = \mathbf{g}_k = \mathbf{b}_k$. One can obtain $\mathbf{G}_k$ with the help of the definition of so-called generalized 2-D strains similarly as Hodges et $al.$ (1993), given by

$$\mathbf{R}_{,\alpha} = \mathbf{B}_\alpha + \varepsilon_{\alpha\beta}\mathbf{B}_\beta$$
$$\mathbf{B}_{i,\alpha} = (-K_{\alpha\beta}\mathbf{B}_\beta \times \mathbf{B}_3 + K_{\alpha3}\mathbf{B}_3) \times \mathbf{B}_i \tag{8}$$

where $\varepsilon_{\alpha\beta}$ and $K_{\alpha\beta}$ are the 2-D generalized strains and $( )_{,\alpha} = \frac{\partial ()}{\partial x_\alpha}$. Here one is free to set $\varepsilon_{12} = \varepsilon_{21}$, $i.e.$

$$\mathbf{B}_1 \cdot \mathbf{R}_{,2} = \mathbf{B}_2 \cdot \mathbf{R}_{,1} \tag{9}$$

which can serve as another constraint to specify the deformed configuration.

With the assumption that the strain is small compared to unity, which has the effect of removing all the terms that are products of the warping and the generalized strains, one can express the 3-D strain field as

$$\Gamma = \Gamma_h w + \Gamma_\epsilon \epsilon + \Gamma_{l_1} w_{,1} + \Gamma_{l_2} w_{,2} \tag{10}$$

where

$$\Gamma = \lfloor \Gamma_{11} \ 2\Gamma_{12} \ \Gamma_{22} \ 2\Gamma_{13} \ 2\Gamma_{23} \ \Gamma_{33} \rfloor^T \tag{11}$$

$$w = \lfloor w_1 \ w_2 \ w_3 \rfloor^T \tag{12}$$

$$\epsilon = \lfloor \varepsilon_{11} \ 2\varepsilon_{12} \ \varepsilon_{22} \ K_{11} \ K_{12} + K_{21} \ K_{22} \rfloor^T \tag{13}$$

and all the operators are defined as:

$$
\Gamma_h =
\begin{bmatrix}
0 & 0 & 0 \\
0 & 0 & 0 \\
0 & 0 & 0 \\
\frac{\partial}{\partial x_3} & 0 & 0 \\
0 & \frac{\partial}{\partial x_3} & 0 \\
0 & 0 & \frac{\partial}{\partial x_3}
\end{bmatrix}
\qquad
\Gamma_{l_1} =
\begin{bmatrix}
1 & 0 & 0 \\
0 & 1 & 0 \\
0 & 0 & 0 \\
0 & 0 & 1 \\
0 & 0 & 0 \\
0 & 0 & 0
\end{bmatrix}
$$

$$
\Gamma_\epsilon =
\begin{bmatrix}
1 & 0 & 0 & x_3 & 0 & 0 \\
0 & 1 & 0 & 0 & x_3 & 0 \\
0 & 0 & 1 & 0 & 0 & x_3 \\
0 & 0 & 0 & 0 & 0 & 0 \\
0 & 0 & 0 & 0 & 0 & 0 \\
0 & 0 & 0 & 0 & 0 & 0
\end{bmatrix}
\qquad
\Gamma_{l_2} =
\begin{bmatrix}
0 & 0 & 0 \\
1 & 0 & 0 \\
0 & 1 & 0 \\
0 & 0 & 0 \\
0 & 0 & 1 \\
0 & 0 & 0
\end{bmatrix}
\tag{14}
$$

In the present work, we only consider one-way thermomechanical coupling and temperature change due to the deformation of the plate is negligible. Then we can use the Helmholtz free-energy functional (Reddy (1997)) without quadratic terms involving temperature only to carry out the analysis. The free energy per unit area (which is the same as the free energy of the normal-line element) can be written as

$$
U = \left\langle \frac{1}{2} \Gamma^T D \, \Gamma - \Gamma^T D \alpha \, T \right\rangle
\tag{15}
$$

where T is the difference of temperature inside the structure with respect to the reference temperature when the plate is stress free, and D is the 3-D 6×6 material matrix, which consists of elements of the elasticity tensor expressed in the global coordinate system x_i. α is a 6×1 column matrix representing the 3-D thermal expansion coefficients. These matrices are in general fully populated. However, if it is desired to model laminated composite plates in which each lamina exhibits a monoclinic symmetry about its own mid-plane and is rotated about the local normal to be a layer in the composite laminated plate, then as shown in Yu *et al.* (2002a), some parts of these matrices will always vanish no matter what the layup angle is.

To deal with applied mechanical loads as well with thermal loads, we will at first leave open the existence of a potential energy and develop instead the virtual work of the applied mechanical loads. The virtual displacement is taken as the Lagrangean variation of the

displacement field, such that

$$\delta\hat{\mathbf{R}} = \overline{\delta q}_{Bi}\mathbf{B}_i + x_3\overline{\delta\psi}_{Bi}\mathbf{B}_i \times \mathbf{B}_3 + \delta w_i\mathbf{B}_i + \overline{\delta\psi}_{Bi}\mathbf{B}_i \times w_j\mathbf{B}_j \qquad (16)$$

where the virtual displacement of the reference surface is given by

$$\overline{\delta q}_{Bi} = \delta\mathbf{u}\cdot\mathbf{B}_i \qquad (17)$$

and the virtual rotation of the reference surface is defined such that

$$\delta\mathbf{B}_i = \overline{\delta\psi}_{Bj}\mathbf{B}_j \times \mathbf{B}_i \qquad (18)$$

Since the strain is small, one may safely ignore products of the warping and the loading in the virtual rotation term. Then, the work done through a virtual displacement due to the applied loads $\tau_i\mathbf{B}_i$ at the top surface and $\beta_i\mathbf{B}_i$ at the bottom surface and body force $\phi_i\mathbf{B}_i$ through the thickness is

$$\overline{\delta W} = (\tau_i + \beta_i + \langle\phi_i\rangle)\overline{\delta q}_{Bi} + \overline{\delta\psi}_{B\alpha}\left[\frac{h}{2}(\tau_\alpha - \beta_\alpha) + \langle x_3\phi_\alpha\rangle\right] + \delta\left(\tau_i w_i^+ + \beta_i w_i^- + \langle\phi_i w_i\rangle\right) \quad (19)$$

where τ_i, β_i, and ϕ_i are taken to be independent of the deformation, $(\ )^+ = (\ )|_{x_3=\frac{h}{2}}$, and $(\ )^- = (\ )|_{x_3=-\frac{h}{2}}$. By introducing column matrices $\overline{\delta q}$, $\overline{\delta\psi}$, τ, β, and ϕ, which are formed by stacking the three elements associated with indexed symbols of the same names, and using Eqs. (1), (3), and (4), one may write the virtual work in matrix form, so that

$$\overline{\delta W} = \overline{\delta q}^T f + \overline{\delta\psi}^T m + \delta\left(\tau^T w^+ + \beta^T w^- + \langle\phi^T w\rangle\right) \qquad (20)$$

where

$$f = \tau + \beta + \langle\phi\rangle$$

$$m = \left\{\begin{array}{c} \frac{h}{2}(\tau_1 - \beta_1) + \langle x_3\phi_1\rangle \\ \frac{h}{2}(\tau_2 - \beta_2) + \langle x_3\phi_2\rangle \\ 0 \end{array}\right\} \qquad (21)$$

The complete statement of the problem can now be presented in terms of the principle of virtual work, such that

$$\delta U - \overline{\delta W} = 0 \qquad (22)$$

In spite of the possibility of accounting for nonconservative forces in the above, the problem that governs the warping is conservative. Thus, one can pose the problem that governs the

warping as the minimization of a total potential functional

$$\Pi = U + W \tag{23}$$

so that

$$\delta\Pi = 0 \tag{24}$$

in which only the warping displacement is varied, subject to the constraints Eq. (5). This implies that the potential of the applied mechanical loads for the functional governing warping is given by

$$W = -\tau^T w^+ - \beta^T w^- - \left\langle \phi^T w \right\rangle \tag{25}$$

Below, for simplicity of terminology, we will refer to Π as the total potential energy, or the total energy.

By principle of minimum total potential energy, one can solve for the unknown warping functions by minimizing the functional in Eq. (23) subject to the constraints of Eq. (5). Up to this point, this is simply an alternative formulation of the original 3-D elasticity problem. If we attempt to solve this problem directly, we will meet the same difficulty as solving any full 3-D elasticity problem. Fortunately, as shown in Yu *et al.* (2002a,b, 2003), the VAM can be used to calculate the 3-D warping functions asymptotically. The through-the-thickness analysis is one dimensional and can be solved analytically. However, finite element discretization is preferred to solve the minimization problem for the sake of dealing with multiple layers and arbitrary monoclinic material. A 5-noded isoparametric element is used because we need the second-order warping functions, which are piecewise, fourth-degree polynomials. Discretizing the transverse normal line into 1-D finite elements, one can express the warping field as

$$w(x_i) = S(x_3)V(x_1, x_2) \tag{26}$$

where S is the shape function and V is the nodal value of warping field along the transverse normal. Substituting Eq. (26) into Eq. (23), one can express the total energy in discretized form as

$$
\begin{aligned}
2\Pi = & V^T E V + 2V^T(D_{h\epsilon}\epsilon + D_{hl_1}V_{,1} + D_{hl_2}V_{,2}) \\
& + \epsilon^T D_{\epsilon\epsilon}\epsilon + V_{,1}^T D_{l_1l_1}V_{,1} + V_{,2}^T D_{l_2l_2}V_{,2} \\
& + 2(V_{,1}^T D_{l_1\epsilon}\epsilon + V_{,2}^T D_{l_2\epsilon}\epsilon + V_{,1}^T D_{l_1l_2}V_{,2}) \\
& - 2V^T\alpha_h - 2\epsilon^T\alpha_\epsilon - 2V_{,1}^T\alpha_{l_1} - 2V_{,2}^T\alpha_{l_2} + 2V^T L
\end{aligned}
\tag{27}
$$

where L contains the load related terms such that

$$L = -S^{+T}\tau - S^{-T}\beta - \langle S^T \phi \rangle \qquad (28)$$

The new matrix variables carry the properties of both the geometry and material:

$$E = \langle [\Gamma_h S]^T D [\Gamma_h S] \rangle \qquad\qquad D_{h\epsilon} = \langle [\Gamma_h S]^T D \Gamma_\epsilon \rangle$$
$$D_{hl_1} = \langle [\Gamma_h S]^T D [\Gamma_{l_1} S] \rangle \qquad\qquad D_{hl_2} = \langle [\Gamma_h S]^T D [\Gamma_{l_2} S] \rangle$$
$$D_{\epsilon\epsilon} = \langle \Gamma_\epsilon^T D \Gamma_\epsilon \rangle \qquad\qquad D_{l_1 l_1} = \langle [\Gamma_{l_1} S]^T D [\Gamma_{l_1} S] \rangle$$
$$D_{l_1 l_2} = \langle [\Gamma_{l_1} S]^T D [\Gamma_{l_2} S] \rangle \qquad\qquad D_{l_2 l_2} = \langle [\Gamma_{l_2} S]^T D [\Gamma_{l_2} S] \rangle$$
$$D_{l_1\epsilon} = \langle [\Gamma_{l_1} S]^T D \Gamma_\epsilon \rangle \qquad\qquad D_{l_2\epsilon} = \langle [\Gamma_{l_2} S]^T D \Gamma_\epsilon \rangle$$
$$\alpha_h = \langle [\Gamma_h S]^T D\alpha\, T \rangle \qquad\qquad \alpha_\epsilon = \langle \Gamma_\epsilon^T D\alpha\, T \rangle$$
$$\alpha_{l_1} = \langle [\Gamma_{l_1} S]^T D\alpha\, T \rangle \qquad\qquad \alpha_{l_2} = \langle [\Gamma_{l_2} S]^T D\alpha\, T \rangle \qquad (29)$$

Although the theory itself allows for an analytical representation for arbitrary temperature distribution through the thickness, here a fourth-degree polynomial is used to approximate the temperature distribution for each normal-line element. The discretized form of Eq. (5) is

$$V^T H \psi = 0 \qquad (30)$$

where $H = \langle S^T S \rangle$ and ψ is the normalized kernel matrix of E such that $\psi^T H \psi = I$. Now our problem is transformed to minimize Eq. (27) numerically, subject to the constraints in Eq. (30).

Dimensional Reduction

To rigorously reduce the original 3-D problem to a 2-D plate problem, one must attempt to reproduce the energy stored in the 3-D structure in a 2-D formulation. This dimensional reduction can only be done approximately, and one way to do it is by taking advantage of the smallness of h/l. The small parameter ε, representing the order of the generalized 2-D strains ϵ has already been taken advantage of when we derive Eq. (10). To reduce the number of small parameters in the asymptotic analysis, it is reasonable to assume that the order of strains due to thermal loading is of the order ε. Thus, the quantities of interest assume the following orders:

$$\epsilon_{\alpha\beta} \sim h\kappa_{\alpha\beta} \sim \varepsilon \quad \alpha T \sim \varepsilon \quad f_3 \sim \mu(h/l)^2 \varepsilon \quad f_\alpha \sim \mu(h/l)\varepsilon \quad m_\alpha \sim \mu h(h/l)\varepsilon \qquad (31)$$

where μ is the order of the material constants (all of which are assumed to be of the same order). It is noted that $m_3 = 0$.

Having assessed the orders of all the interested quantities, the VAM can be used to mathematically perform a dimensional reduction of the 3-D problem to a series of 2-D models, similarly as what have been done in Yu *et al.* (2002a,b, 2003).

The VAM requires one to find the leading terms of the functional according to the different orders. Since only the warping is varied, the leading terms needed are all of those terms associated with warping. For the zeroth-order approximation, these leading terms of Eq. (27) are

$$2\Pi_0^* = V^T E V + 2V^T D_{h\epsilon}\epsilon - 2V^T \alpha_h \tag{32}$$

The Euler-Lagrange equation for functional Eq. (32) subject to constraints Eq. (30) can be obtained by usual procedure of calculus of variation with the aid of a Lagrange multiplier as follows:

$$EV + D_{h\epsilon}\epsilon - \alpha_h = H\psi\Lambda \tag{33}$$

Considering the properties of the kernel matrix ψ, one calculates the Lagrange multiplier Λ as

$$\Lambda = \psi^T (D_{h\epsilon}\epsilon - \alpha_h) \tag{34}$$

Substituting Eq. (34) back into Eq. (33), we obtain

$$EV = (H\psi\psi^T - I)(D_{h\epsilon}\epsilon - \alpha_h) \tag{35}$$

There is a unique solution of zeroth-order warping functions and can be written as:

$$V = \hat{V}_0\epsilon + V_T = V_0 \tag{36}$$

Substituting Eq. (36) back into Eq. (27), one can obtain the total energy asymptotically correct up to the order of $\mu\varepsilon^2$ as

$$2\Pi_0 = \epsilon^T (\hat{V}_0^T D_{h\epsilon} + D_{\epsilon\epsilon})\epsilon + \epsilon^T (D_{h\epsilon}^T V_T - \hat{V}_0^T \alpha_h - 2\alpha_\epsilon) \tag{37}$$

Note the quadratic terms associated with temperature $-V_T^T \alpha_h$ is dropped due to the same reason for Eq. (15). This 2-D free energy, Eq. (37), is the same as what is used in CLT for thermoelastic analysis:

$$2\Pi_0 = \epsilon^T A \epsilon - 2\epsilon^T N_T \tag{38}$$

with

$$A = (\hat{V}_0^T D_{h\epsilon} + D_{\epsilon\epsilon}) \quad N_T = \alpha_\epsilon + \frac{1}{2}(\hat{V}_0^T \alpha_h - D_{h\epsilon}^T V_T) \qquad (39)$$

Although the energy of this approximation coincides with CLT, we have not used any *ad hoc* kinematic assumptions such as the Kirchhoff assumption to obtain this result. Moreover, the transverse normal strain from our zeroth-order approximation is not zero.

It is understood that our zeroth-order approximation will give the same stress results as what is obtained from CLT, *i.e.*, all the transverse stress components which are very important for analyzing the failure of composite plates cannot be predicted. One must carry out the next approximation so that those quantities can be approximately predicted. To obtain the first-order approximation, we simply perturb the zeroth-order result, resulting in warping functions of the form

$$V = V_0 + V_1 \qquad (40)$$

Substituting Eq. (40) back into Eq. (10) and then into Eq. (27), one can obtain the leading terms for the first-order approximation as

$$2\Pi_1^* = V_1^T E V_1 + 2V_1^T D_1 \epsilon_{,1} + 2V_2^T D_2 \epsilon_{,2} + 2V^T L_T + 2V_1^T L \qquad (41)$$

with

$$
\begin{aligned}
D_1 &= (D_{hl_1} - D_{hl_1}^T)\hat{V}_0 - D_{l_1\epsilon} \\
D_2 &= (D_{hl_2} - D_{hl_2}^T)\hat{V}_0 - D_{l_2\epsilon} \\
L_T &= (D_{hl_1} - D_{hl_1}^T)V_{T,1} + (D_{hl_2} - D_{hl_2}^T)V_{T,2} + \alpha_{l_1,1} + \alpha_{l_2,2}
\end{aligned}
\qquad (42)
$$

Integration by parts with respect to the in-plane coordinates is used here and hereafter whenever it is convenient for the derivation, because the present goal is to obtain an interior solution for the plate without consideration of boundary layer effects.

Similarly as in the zeroth-order approximation, one can solve the first-order warping field as

$$V_1 = V_{11}\epsilon_{,1} + V_{12}\epsilon_{,2} + V_{1T} + V_{1L} \qquad (43)$$

and obtain a total energy that is asymptotically correct up to the order of $\mu(h/l)^2\varepsilon$, given by

$$2\Pi_1 = \epsilon^T A\epsilon + \epsilon_{,1}^T B\epsilon_{,1} + 2\epsilon_{,1}^T C\epsilon_{,2} + \epsilon_{,2}^T \mathcal{D}\epsilon_{,2} + 2\epsilon^T F - 2\epsilon^T F_T \qquad (44)$$

where

$$B = \hat{V}_0^T D_{l_1 l_1} \hat{V}_0 + V_{11}^T D_1 \qquad C = \hat{V}_0^T D_{l_1 l_2} \hat{V}_0 + \frac{1}{2}(V_{11}^T D_2 + D_1^T V_{11})$$

$$\mathcal{D} = \hat{V}_0^T D_{l_2 l_2} \hat{V}_0 + V_{12}^T D_2 \qquad F = \hat{V}_0^T L - \frac{1}{2}(D_1^T V_{1L,1} + V_{11}^T L_{,1} + D_2^T V_{1L,2} + V_{12}^T L_{,2}) \qquad (45)$$

with the non-mechanical load due to temperature

$$\begin{aligned}
F_T =& N_T + \hat{V}_0^T D_{l_1 l_1} V_{T,11} + \hat{V}_0^T D_{l_2 l_2} V_{T,22} + \hat{V}_0^T (D_{l_1 l_2} + D_{l_1 l_2}^T) V_{T,12} \\
& + \frac{1}{2}(V_{11}^T L_{T,1} + V_{12}^T L_{T2} + D_1^T V_{1T,1} + D_2^T V_{1T,2})
\end{aligned} \qquad (46)$$

Here the monoclinic symmetry has already been taken advantage of to obtain the asymptotically correct energy in Eq. (44). The applied mechanical loads and temperature distribution should not vary rapidly over the plate surface; otherwise the structure, although plate-like, can not be analyzed with enough accuracy using a reduced plate model.

Transforming Into Reissner-Mindlin Model

Although Eq. (44) is asymptotically correct through the second order and straightforward use of this free energy expression is possible, it involves more complicated boundary conditions than necessary since it contains derivatives of the generalized strain measures. To obtain an energy functional that is of practical use, one can transform the present approximation into a Reissner-Mindlin type model. We would like to state that fitting the asymptotic energy into such model is just a choice, and the possibility of fitting the same energy into other more sophisticated plate models is under investigation.

In a Reissner-Mindlin model, there are two additional degrees of freedom, which are the transverse shear strains. These are incorporated into the rotation of transverse normal. If we introduce another triad $\mathbf{B}_i^*$ for the deformed Reissner-Mindlin plate, the definition of 2-D strains becomes

$$\mathbf{R}_{,\alpha} = \mathbf{B}_\alpha^* + \varepsilon_{\alpha\beta}^* \mathbf{B}_\beta^* + 2\gamma_{\alpha 3}\mathbf{B}_3^*$$
$$\mathbf{B}_{i,\alpha}^* = (-K_{\alpha\beta}^* \mathbf{B}_\beta^* \times \mathbf{B}_3^* + K_{\alpha 3}^* \mathbf{B}_3^*) \times \mathbf{B}_i^* \qquad (47)$$

where the transverse shear strains are $\gamma = \lfloor 2\gamma_{13} \quad 2\gamma_{23} \rfloor^T$. From the definitions in Eqs. (8) and (47), one can obtain the Rodrigues parameters corresponding to the rotation relating $\mathbf{B}_i$ and $\mathbf{B}_i^*$. Using the procedures listed in Hodges (1987), one can express the classical strain measures ϵ in terms of the strain measures of the Reissner-Mindlin plate model (see

Yu (2002) for the details of the derivation):

$$\epsilon = \mathcal{R} - \mathcal{D}_\alpha \gamma_{,\alpha} \tag{48}$$

where

$$\mathcal{D}_1 = \begin{bmatrix} 0 & 0 & 0 & 1 & 0 & 0 \\ 0 & 0 & 0 & 0 & 1 & 0 \end{bmatrix}^T$$

$$\mathcal{D}_2 = \begin{bmatrix} 0 & 0 & 0 & 0 & 1 & 0 \\ 0 & 0 & 0 & 0 & 0 & 1 \end{bmatrix}^T$$

$$\mathcal{R} = \lfloor \varepsilon_{11}^* \quad 2\varepsilon_{12}^* \quad \varepsilon_{22}^* \quad K_{11}^* \quad K_{12}^* + K_{21}^* \quad K_{22}^* \rfloor^T \tag{49}$$

Now one can express the energy, Eq. (44), correct to second order, in terms of strains of the Reissner-Mindlin model as

$$2\Pi_1 = \mathcal{R}^T A \mathcal{R} - 2\mathcal{R}^T A \mathcal{D}_\alpha \gamma_{,\alpha} + \mathcal{R}_{,1}^T B \mathcal{R}_{,1} + 2\mathcal{R}_{,1}^T C \mathcal{R}_{,2} + \mathcal{R}_{,2}^T D \mathcal{R}_{,2}$$
$$+ 2\mathcal{R}^T F - 2R^T F_T + 2\gamma_{,\alpha}^T D_\alpha N_T \tag{50}$$

The generalized Reissner-Mindlin model used in the 2-D thermoelastic analyses is of the form

$$2\Pi_\mathcal{R} = \mathcal{R}^T A \mathcal{R} + \gamma^T G \gamma + 2\mathcal{R}^T F_\mathcal{R} + 2\gamma^T F_\gamma + 2\mathcal{R}^T F_{T\mathcal{R}} + 2\gamma^T F_{T\gamma} \tag{51}$$

To find an equivalent Reissner model Eq. (51) for Eq. (50), one has to eliminate all partial derivatives of the classical 2-D strain measures. The equilibrium equations are used to achieve this purpose. From the two equilibrium equations balancing bending moments with applied moments m_α which is calculated from Eq. (21), one can obtain the following formula

$$G\gamma + F_\gamma + F_{T\gamma} = \mathcal{D}_\alpha^T (A\mathcal{R}_{,\alpha} + F_{\mathcal{R},\alpha} + F_{T\mathcal{R},\alpha}) + \begin{Bmatrix} m_1 \\ m_2 \end{Bmatrix} \tag{52}$$

Using Eq. (52), one can rewrite Eq. (50) as

$$2\Pi_1 = \mathcal{R}^T A \mathcal{R} + \gamma^T G \gamma + 2\mathcal{R}^T F - 2\mathcal{R}^T F_T - 2\gamma^T \mathcal{D}_\alpha N_{T,\alpha} + U^* \tag{53}$$

where

$$U^* = \mathcal{R}_{,1}^T \overline{B} \mathcal{R}_{,1} + 2\mathcal{R}_{,1}^T \overline{C} \mathcal{R}_{,2} + \mathcal{R}_{,2}^T \overline{D} \mathcal{R}_{,2} \tag{54}$$

and

$$\overline{B} = B + A\mathcal{D}_1 G^{-1} \mathcal{D}_1^T A$$
$$\overline{C} = C + A\mathcal{D}_1 G^{-1} \mathcal{D}_2^T A$$
$$\overline{D} = D + A\mathcal{D}_2 G^{-1} \mathcal{D}_2^T A \tag{55}$$

If we can drive U^* to zero for any $\mathcal{R}$, then we have found an asymptotically correct Reissner-Mindlin plate model. For generally anisotropic plates, this term will not be zero; but we can minimize the error to obtain a Reissner-Mindlin model that is as close to asymptotical correctness as possible. The accuracy of the Reissner-Mindlin model depends on how close to zero one can drive this term of the energy.

One could proceed with the optimization at this point, but the problem will require a least squares solution for 3 unknowns (the shear stiffness matrix G) from a linear system of 78 equations (12×12 and symmetric). This optimization problem is too rigid. The solution will be better if we can bring more unknowns into the problem. As stated in Sutyrin and Hodges (1996), there is no unique plate theory of a given order. One can relax the constraints in Eq. (5) to be $\langle w_i \rangle =$ const and still obtain an asymptotically correct strain energy. Since the zeroth-order approximation gives us an asymptotic model corresponding to classical plate theory, we only relax the constraints for the first-order approximation. This relaxation will modify the warping field to be

$$\overline{V}_1 = V_{11}\epsilon_{,1} + V_{12}\epsilon_{,2} + V_{1L} + V_{1T} + L_1\epsilon_{,1} + L_2\epsilon_{,2} \tag{56}$$

where L_1, L_2 consist of 24 constants. The remaining energy U^* will also be modified to be

$$U^* = \mathcal{R}_{,1}^T \hat{B} \mathcal{R}_{,1} + 2\mathcal{R}_{,1}^T \hat{C} \mathcal{R}_{,2} + \mathcal{R}_{,2}^T \hat{D} \mathcal{R}_{,2} \tag{57}$$

and

$$\hat{B} = \overline{B} + 2L_1^T D_1 \quad \hat{C} = \overline{C} + (L_1^T D_2 + D_1^T L_2) \quad \hat{D} = \overline{D} + 2L_2^T D_2 \tag{58}$$

Since now we have 27 unknowns, the optimization is much more flexible. It can give us a more optimal solution for the shear stiffness matrix G to fit the second-order, asymptotically correct energy into a Reissner-Mindlin model. In other words, here we have found the Reissner-Mindlin model that describes as closely as possible the 2-D energy that is asymptotically correct through the second order in h/l. However, the asymptotical correctness of the warping field to that same order can only be ascertained after obtaining another higher-order approximation, which will be discussed in the next section.

And after minimizing U^*, the "best" total energy to be used for the 2-D plate Reissner-Mindlin model can be expressed as:

$$2\Pi_\mathcal{R} = \mathcal{R}^T A \mathcal{R} + \gamma^T G \gamma + 2\mathcal{R}^T F - 2\mathcal{R}^T F_T - 2\gamma^T \mathcal{D}_\alpha N_{T,\alpha} \tag{59}$$

Recovering Relations

From the above, we have obtained a Reissner-Mindlin plate model which is as close as possible to being asymptotically correct in the sense of matching the total energy. The stiffness matrices A, G, load-related terms, and non-mechanical stress resultants can be used as input for a plate theory derived from the total energy obtained here. The geometrically nonlinear theory presented in Hodges *et al.* (1993) is an appropriate choice, but some straightforward modification of the loading terms is required.

However, while it is necessary to accurately calculate the 2-D displacement field of composite plates, this is not sufficient in many applications. Ultimately, *the fidelity of a reduced-order model such as this depends on how well it can predict the 3-D results in the original 3-D problem.* Hence, recovering relations should be provided to complete the reduced-order model. By recovering relations, we mean expressions for 3-D displacement, strain, and stress fields in terms of 2-D quantities and x_3. For validation, results obtained for the 3-D field variables from the reduced-order model must be compared with those of the original 3-D model.

For an energy that is asymptotically correct through the second order, we can recover the 3-D displacement, strain and stress fields only through the first order in the strict sense of asymptotical correctness. Using Eqs. (1), (3), and (4), one can recover the 3-D displacement field through the first order as

$$U_{3d} = u_{2d} + x_3 \begin{bmatrix} C_{31} \\ C_{32} \\ C_{33} - 1 \end{bmatrix} + SV_0 + S\overline{V}_1 \tag{60}$$

where U_{3d} is the column matrix of 3-D displacements and u_{2d} is the plate displacements. C_{ij} are the components of global rotation tensor from Eq. (3). And from Eq. (10), one can recover the 3-D strain field through the first order as

$$\Gamma = \Gamma_h S(V_0 + \overline{V}_1) + \Gamma_\epsilon \epsilon + \Gamma_{l_1} SV_{0,1} + \Gamma_{l_2} SV_{0,2} \tag{61}$$

Then, one can use the inverse of 3-D Duhamel-Neumann law

$$\sigma = D\Gamma - D\alpha\, T \tag{62}$$

to obtain 3-D stresses σ_{ij}.

Since we have obtained an optimum shear stiffness matrix G, some of the recovered 3-D results through the first order are better than classical theory and conventional first-order deformation theory. However, for the transverse normal component of strain and stress (*i.e.* Γ_{33} and σ_{33}), the agreement is not satisfactory at all. Let us recall, that the Reissner-Mindlin theory that has been constructed only ensures a good fit with the asymptotically correct 3-D displacement field of the first order (while energy is approximated to the second order). Thus, in order to obtain recovering relations that are valid to the same order as the energy, the VAM iteration needs to be applied one more time.

Using the same procedure listed in previous section, the second-order warping can be obtained and expressed symbolically as

$$V_2 = V_{21}\epsilon_{,11} + V_{22}\epsilon_{,12} + V_{23}\epsilon_{,22} + V_{2L} + V_{2T} \tag{63}$$

Eq. (63) is obtained by taking the original first-order warping V_1 to be the result of the first-order approximation. It is clear that V_2 is one order higher than V_1 which confirms that V_1 is the first-order approximation. One might be tempted to use V_1 in the recovering relations. However, the VAM has split the original 3-D problem into two sets of problems. As far as recovering relations concerned, it is observed that the normal-line analysis can at best give us an approximate shape of the distribution of 3-D results. The 2-D plate analysis will govern the global behavior of the structure. Since $\overline{V}_1$ is the warping that yields a Reissner-Mindlin plate model that is as close as possible to being asymptotically correct, we should still use $\overline{V}_1$ in the recovering relations instead of V_1. By doing this, we choose to be more consistent with Reissner-Mindlin plate model while compromising somewhat on the asymptotical correctness of the shape of the distribution. It has been verified by numerical examples that this is a good choice.

Hence, we write the 3-D recovering relations for displacement through the second order as

$$U_{3d} = u_{2d} + x_3 \begin{Bmatrix} C_{31} \\ C_{32} \\ C_{33} - 1 \end{Bmatrix} + S(V_0 + \overline{V}_1 + V_2) \tag{64}$$

and the strain field through the second order is

$$\Gamma = \Gamma_h S(V_0 + \overline{V}_1 + V_2) + \Gamma_\epsilon \epsilon + \Gamma_{l_1} S(V_{0,1} + \overline{V}_{1,1}) + \Gamma_{l_2} S(V_{0,2} + \overline{V}_{1,2}) \qquad (65)$$

Again the stresses through the second order can be obtained from use of the 3-D constitutive law, Eq. (62).

Numerical Examples

The computer program VAPAS has been extended to implement the present theory. Several numerical examples are given here to validate the proposed theory and code against the 3-D thermoelasticity solutions.

First to assess the asymptotical correctness of the proposed theory, we study a cylindrical bending type problem for an isotropic plate with E as the Young's modulus, ν Poisson's ratio and α thermal expansion coefficient. The plate is simply supported with width L along x_1 axis (the "lateral" direction) and infinitely long along the x_2 axis (the "longitudinal" direction) under the following temperature changes:

$$T = T_0(x_3) \sin\left(\frac{\pi x_1}{L}\right) \qquad (66)$$

Let us assume the thickness of the plate is h, and the normalized thickness coordinate $\zeta = x_3/h$, then the small parameter used in our theory is:

$$\delta = \frac{h}{l} = \frac{\pi h}{L} \qquad (67)$$

When there is a uniform temperature T_c change through the thickness, the nontrivial displacements and stresses are listed in Table 1. The exact solutions are obtained based on Savoia and Reddy (1995) and expanded into a series in terms of δ with $o(*)$ denoting terms asymptotically smaller than the order of $*$. The present theory can predict the correct results up to the second order of δ with respect to the leading terms for each 3-D quantities, which clearly demonstrate that our theory is asymptotically correct up to the second order for this particular problem. We admit that the prediction of transverse components for this problem is out of the power of our theory. However, this should not mislead the reader to assume that the present theory is asymptotically correct up to the second order for general cases. The authors are aware that the proposed theory can be at best asymptotically correct up to the second order for particular cases. For general cases, however, the theory can only be interpreted as a Reissner-Mindlin type theory which is closest to being asymptotically correct. To illustrate the above statement, we provide the results for the same isotropic plate

under a linearly distributed temperature through the thickness, assuming $T_0 = \zeta T_1$. Here only nontrivial displacement results are listed in Table 2 which is sufficient for the aforementioned purpose. One can observe from Table 2 that there is a slight difference for the second order prediction between the present theory and exact solution. It is interesting to note that if one sets ν equal to zero the difference disappears. Evidently some information belonging to second order and indeed included in the asymptotically correct energy cannot be captured in a Reissner-Mindlin type model. When we transform the asymptotically correct model into a Reissner-Mindlin model, this information is lost.

The present theory is formulated with sufficient generality to carry out a thermoelastic analysis for arbitrary composite laminated plates made with monoclinic material with a computational cost equivalent to that of first-order shear-deformation theory (FOSDT). Hence, before overemphasizing the loss of information in the repackaging of the model one should determine if this loss is exhibited in numerical results. To investigate this, we will present some numerical results for composite plates to demonstrate the advantages of our theory relative to CLT and FOSDT. The plate we are going to study has material properties given by

$$
\begin{aligned}
E_L &= 172.4 \text{ GPa } (25 \times 10^6 \text{ psi}) & E_T &= 6.895 \text{ GPa } (10^6 \text{ psi}) \\
G_{LT} &= 3.447 \text{ GPa } (0.5 \times 10^6 \text{ psi}) & G_{TT} &= 1.379 \text{ GPa } (0.2 \times 10^6 \text{ psi}) \\
\nu_{LT} &= 0.25 & \nu_{TT} &= 0.25 \\
\alpha_L &= 0.139 \times 10^{-6}/\,^0C & \alpha_T &= 9 \times 10^{-6}/\,^0C
\end{aligned}
\tag{68}
$$

For the purpose of comparing with the exact solution, we still consider cylindrical bending type problem. In lieu of our definition of small parameter Eq. (67), even if our theory is asymptotically correct up to the second order, we require $\delta^3 \ll 1$. If we assume the thickness is 25.4 mm and $L = 254$ mm, δ will be approximately 0.314 which can be considered small in our theory. Two different cases are investigated:

- case 1: nearly cross ply, $[-0.5^\circ/89.5^\circ]$ under $T_0 = T_c + \zeta T_c$

- case 2: nearly cross ply, $[90.5^\circ/0.5^\circ/90.5^\circ/0.5^\circ]$ under $T_0 = T_c + \zeta T_c + \zeta^2 T_c + \zeta^3 T_c + \zeta^4 T_c$, $\tau_3 = \beta_3 = \frac{p_0}{2}\sin\left(\frac{\pi x_1}{L}\right)$, $\tau_\alpha = \beta_\alpha = 0$, and $p_0 = E_T \alpha_T T_c/9$.

Because thermal stresses due to temperature change are the most interesting quantities, we only present stress results here with mentioning that the accuracy of displacements and strains is similar to that of stresses. For case 1, results from VAPAS (dots in the plots), are compared with those from CLT (dash-dotted line), FOSDT (dashed line) and the exact solution (solid line) in Figs. 2 – 7. Note that, because the 2-D variables are either sine

functions or cosine functions, $\sigma_{\alpha3}$ and σ_{33} are plotted at $x_1 = L/2$ and $\sigma_{\alpha3}$ at $x_1 = L$. The results presented here are normalized as follows:

$$\bar{\sigma}_{ij} = \frac{9\sigma_{ij}}{E_T \alpha_T T_c} \tag{69}$$

As one can observe from the plots, for $\sigma_{\alpha3}$ VAPAS results are much closer to the exact solutions than CLT and FOSDT. VAPAS also does a fairly good job for predicting the transverse stress components which for the isotropic plate under uniform temperature change we concluded was out of the power of VAPAS because these terms are asymptotically smaller than the second order. One can infer that due to the special layup scheme (cross-ply) the dominant terms of transverse stress components could now be asymptotically equal or larger than the second order. Considering the smallness of σ_{33} in comparison to the in-plane components, we expect the slight shift of VAPAS results for this quantity to be tolerable for most engineering applications.

Finally, to demonstrate that VAPAS can handle the temperature change through the thickness exactly up to a fourth-degree polynomial and both mechanical loads and thermal load can be treated simultaneously, we present the results for case 2 in Figs. 8 – 13. Except for a small shift for transverse normal stress, all the other results from VAPAS are almost on top of the exact solutions. Careful readers may even find there is a small discontinuity for σ_{33} which should not be the case in reality. The reason is due to that the stress results obtained by VAPAS are calculated directly using 3-D constitutive law from the approximate strain field. The approximation in the strain field may cause the discontinuity for the transverse stress components. It is worthy to emphasize that integration of the 3-D equilibrium equations through the thickness is not used here to obtain results for the transverse stresses presented herein, in contrast to what is usually done in CLT and FOSDT.

Mathematically, the accuracy of the present theory should be comparable to that of a reduced layer-wise plate theory with assumed in-plane displacements as layer-wise cubic polynomials of the thickness direction and transverse displacement as a layer-wise fourth-degree polynomial. However, the present theory is still an equivalent single-layer theory, and the computational requirement is much less than that for layer-wise theories.

Conclusion

A Reissner-Mindlin type plate model capable of performing a thermoelastic stress analysis of laminated composite plates has been constructed by the variational-asymptotic method. A general 2-D constitutive law being as close to asymptotical correctness as possible has been obtained by solving the 1-D through-the-thickness analysis. The original 3-D results have

been reproduced as accurate as possible from a Reissner-Mindlin type plate analysis. The resulting theory is as simple and efficient as a first-order shear deformation theory (FOSDT) while it also has an accuracy comparable to higher-order layerwise theories.

The present study distinguishes from previous work reported in the literature at least in the following four aspects:

1. The present formulation is in an intrinsic form which is suitable for geometrically nonlinear plate theory as well as linear theory.

2. The dimensional reduction from 3-D to 2-D is carried out systematically by using variational asymptotic method, which is completely different from models that rely on the introduction of *ad hoc* kinematic assumptions to reduce the dimensionality.

3. To create a smooth interface with well-established 2-D solvers, the degrees of freedom of the present model are chosen to be essentially the same as those of traditional Reissner-Mindlin type plate theory. However, the present model is *not* a FOSDT. The present theory differs from FOSDT by representing all the deformations that are purposely eliminated in the development of FOSDT. This is accomplished through allowing all possible deformation in the 3-D warping functions, which are solved in turn by the variational-asymptotic method.

4. The present study has treated both mechanical and thermal loading. The temperature distribution through the thickness can be arbitrary and is approximated in VAPAS by a layerwise fourth-degree polynomial. This is more realistic and accurate than most published models, in which the temperature is assumed to be distributed linearly through the thickness of the whole plate (single-layer theories) or a layer (for layerwise theories).

The hygro effect due to moisture to composite plates can also be handled in exactly the same procedure except one has to replace the thermal expansion coefficients with hygroscopic expansion coefficients and temperature with moisture. The computer program VAPAS can now be used along with a 2-D solver to perform an efficient yet accurate and detailed analysis for hygrothermoelastic behavior for laminated composite plates under severe environments.

Acknowledgements

References

Bauchau, O. (1998). Computational schemes for flexible, nonlinear multi-body systems. *Multibody System Dynamics* 2, 169–225.

Berdichevsky, V. L. (1979). Variational-asymptotic method of constructing a theory of shells. *PMM* 43, 664 – 687.

Cho, Y. B. and Averill, R. C. (2000). First-order zig-zag sublaminate plate theory and finite element model for laminated composite and sandwich panels. *Composite Structures* 50, 1 – 15.

Danielson, D. A. (1991). Finite rotation with small strain in beams and plates. In Proceedings of the 2nd Pan American Congress of Applied Mechanics. Valparaiso, Chile. Valparaiso Chile.

Danielson, D. A. and Hodges, D. H. (1987). Nonlinear beam kinematics by decomposition of the rotation tensor. *Journal of Applied Mechanics* 54, 258 – 262.

Hodges, D. H. (1987). Finite rotation and nonlinear beam kinematics. *Vertica* 11, 297 – 307.

Hodges, D. H., Atılgan, A. R. and Danielson, D. A. (1993). A geometrically nonlinear theory of elastic plates. *Journal of Applied Mechanics* 60, 109 – 116.

Noor, A. K. and Burton, S. W. (1992). Computational models for high-temperature multi-layered composite plates and shells. *Applied Mechanics Reviews* 45, 419–446.

Noor, A. K. and Malik, M. (2000). An assessment of five modeling approaches for thermo-mechanical stress analysis of laminated composite panels. *Computational Mechanics* 25, 43–58.

Reddy, J. N. (1997). Mechanics of Laminated Composite Plates: Theory and Analysis. CRC Press, Boca Raton, Florida.

Rohwer, K., Rolfes, R. and Sparr, H. (2001). Higher-order theories for thermal stresses in layered plates. *International Journal of Solids and Structures* 38, 3673–3687.

Savoia, M. and Reddy, J. N. (1995). Three-dimensional thermal analysis of laminated composite plates. *International Journal of Solids and Structures* 32, 593–608.

Sutyrin, V. G. and Hodges, D. H. (1996). On asymptotically correct linear laminated plate theory. *International Journal of Solids and Structures* 33, 3649 – 3671.

Wu. C. and Tauchert, T. (1980). Thermoelastic analysis of laminated plates. part I: symmetric specially orthotropic laminates. *Journal of Thermal Stresses* 3, 247–259.

Yu. W. (2002). Variational asymptotic modeling of composite dimensionally reducible structures. Ph.D. thesis, Aerospace Engineering, Georgia Institute of Technology.

Yu, W., Hodges, D. H. and Volovoi, V. V. (2002a). Asymptotic construction of Reissner-like models for composite plates with accurate strain recovery. *International Journal of Solids and Structures* 39, 5185 – 5203.

Yu. W., Hodges, D. H. and Volovoi, V. V. (2002b). Asymptotic generalization of Reissner-Mindlin theory: accurate three-dimensional recovery for composite shells. *Computer Methods in Applied Mechanics and Engineering* 191, 5087 – 5109.

Yu. W., Hodges, D. H. and Volovoi, V. V. (2003). Asymptotically accurate 3-d recovery from Reissner-like composite plate finite elements. *Computers and Structures* 81, 439 – 454.

List of Tables

Table 1: 3-D displacements and stresses under uniform temperature change through the thickness

	Normalized lateral displacement $\left(\frac{u}{hT_c\alpha}\right)$
Exact	$-\frac{(\nu+1)}{\pi}\delta^{-1} - \frac{\pi(12\zeta^2-1)(\nu+1)}{24}\delta + \frac{\pi^3[120\zeta^2(1-2\zeta^2)(\nu^2-\nu-2)+\nu^2+15\nu+14]}{5760(\nu-1)}\delta^3 + o(\delta^4)$
Present	$-\frac{(\nu+1)}{\pi}\delta^{-1} - \frac{\pi(12\zeta^2-1)(\nu+1)}{24}\delta + o(\delta)$

	Normalized transverse displacement $\left(\frac{w}{hT_c\alpha}\right)$
Exact	$(\nu+1)\zeta + \frac{\pi^2\zeta(4\zeta^2-1)\nu(\nu+1)}{24(\nu-1)}\delta^2 + \frac{\pi^4\zeta[8\zeta^2(6\zeta^2-5)(\nu+1)^2-\nu^2+14\nu+15]}{5760(\nu-1)\delta^4} + o(\delta^4)$
Present	$(\nu+1)\zeta + \frac{\pi^2\zeta(4\zeta^2-1)\nu(\nu+1)}{24(\nu-1)}\delta^2 + o(\delta^2)$

	Normalized lateral in-plane stress $\left(\frac{\sigma_{11}}{ET_c\alpha}\right)$
Exact	$-\frac{\pi^2(12\zeta^2-1)}{24(\nu-1)}\delta^2 - \frac{\pi^4(240\zeta^4-120\zeta^2+7)}{2880(\nu-1)}\delta^4 + o(\delta^4)$
Present	$-\frac{\pi^2(12\zeta^2-1)}{24(\nu-1)}\delta^2 + o(\delta^2)$

	Normalized longitudinal in-plane stress $\left(\frac{\sigma_{22}}{ET_c\alpha}\right)$
Exact	$-1 - \frac{\pi^2(12\zeta^2-1)\nu}{24(\nu-1)}\delta^2 + \frac{\pi^4(-240\zeta^4+120\zeta^2+1)\nu}{5760(\nu-1)}\delta^4 + o(\delta^4)$
Present	$-1 - \frac{\pi^2(12\zeta^2-1)\nu}{24(\nu-1)}\delta^2 + o(\delta^2)$

	Normalized lateral transverse shear stress $\left(\frac{\sigma_{13}}{ET_c\alpha}\right)$
Exact	$\frac{\pi^3\zeta(4\zeta^2-1)}{24(\nu-1)}\delta^3 + o(\delta^4)$
Present	Not available

	Normalized transverse normal stress $\left(\frac{\sigma_{33}}{ET_c\alpha}\right)$
Exact	$\frac{\pi^4(4\zeta^2-1)^2}{384(\nu-1)}\delta^4 + o(\delta^4)$
Present	Not available

Table 2: **3-D displacements under linearly distributed temperature change through the thickness**

	Normalized lateral displacement $\left(\frac{u}{hT_1\alpha}\right)$
Exact	$-\frac{\zeta(\nu+1)}{\pi}\delta^{-1} - \frac{\pi\zeta(20\zeta^2-3)(\nu+1)}{120}\delta + o(\delta)$
Present	$-\frac{\zeta(\nu+1)}{\pi}\delta^{-1} - \frac{\pi\zeta(20\zeta^2-3)(\nu+1)}{120}\delta + \frac{\pi\zeta\nu(11\nu^4+2\nu^3+8\nu^2+14\nu-3)}{30(11\nu^4-12\nu^3+34\nu^2-12\nu+11)}\delta + o(\delta)$
	Normalized transverse displacement $\left(\frac{w}{hT_1\alpha}\right)$
Exact	$\frac{\nu+1}{\pi^2}\delta^{-2} + \frac{1}{40}(20\zeta^2-1)(\nu+1) + o(\delta^0)$
Present	$\frac{\nu+1}{\pi^2}\delta^{-2} + \frac{1}{40}(20\zeta^2-1)(\nu+1) - \frac{\nu(11\nu^4+2\nu^3+8\nu^2+14\nu-3)}{30(11\nu^4-12\nu^3+34\nu^2-12\nu+11)} + o(\delta^0)$

List of Figures

Undeformed State

Deformed State

$w_i(x_1,x_2,x_3)\mathbf{B}_i(x_1,x_2)$

$\mathbf{b}_3$

$\mathbf{b}_2$

$\mathbf{b}_1$

$\mathbf{B}_3(x_1,x_2)$

$\mathbf{B}_2(x_1,x_2)$

$\mathbf{u}(x_1,x_2)$

$\mathbf{B}_1(x_1,x_2)$

$\hat{\mathbf{r}}(x_1,x_2,x_3)$

$\mathbf{r}(x_1,x_2)$

$\hat{\mathbf{R}}(x_1,x_2,x_3)$

$\mathbf{R}(x_1,x_2)$

O

Figure 1:   Schematic of plate deformation

Figure 2: Distribution of the 3-D stress σ_{11} vs the thickness coordinate (case 1)
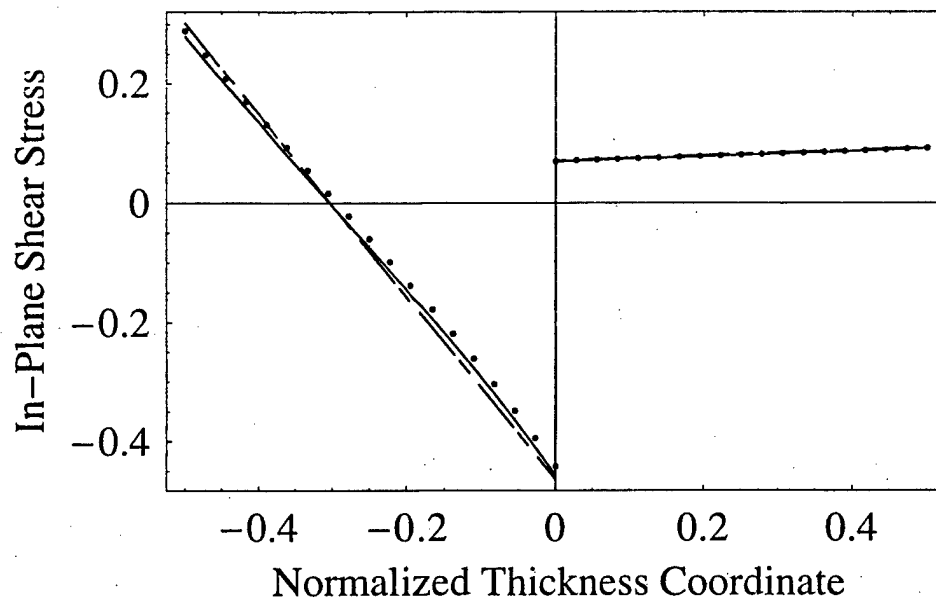
Figure 3: Distribution of the 3-D stress σ_{12} vs the thickness coordinate (case 1)
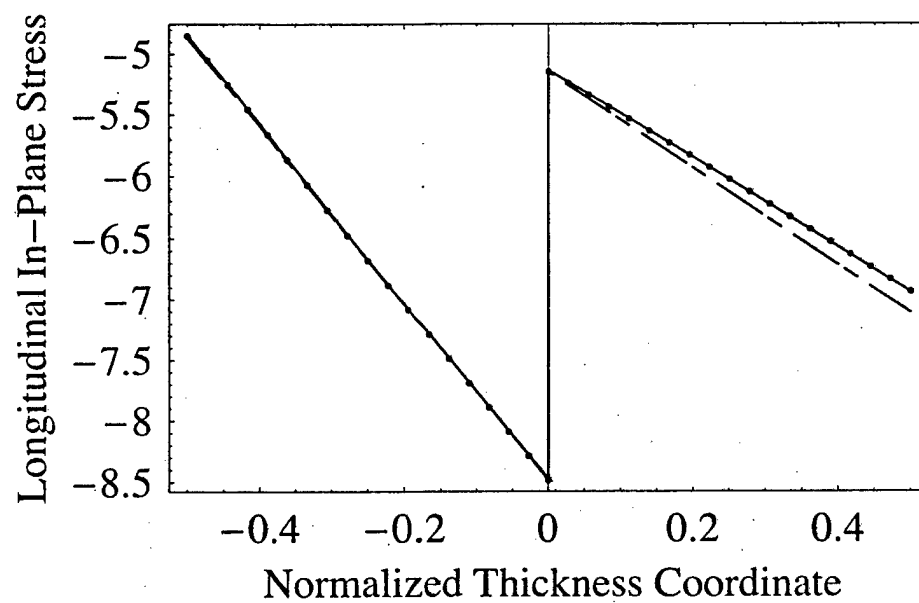
Figure 4: Distribution of the 3-D stress σ_{22} vs the thickness coordinate (case 1)
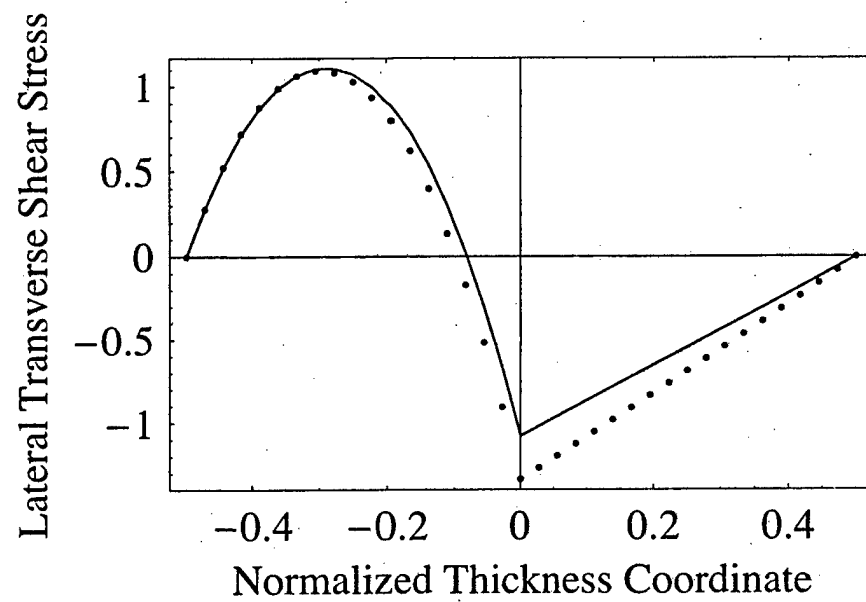
Figure 5:   Distribution of the 3-D stress σ_{13} vs the thickness coordinate (case 1)
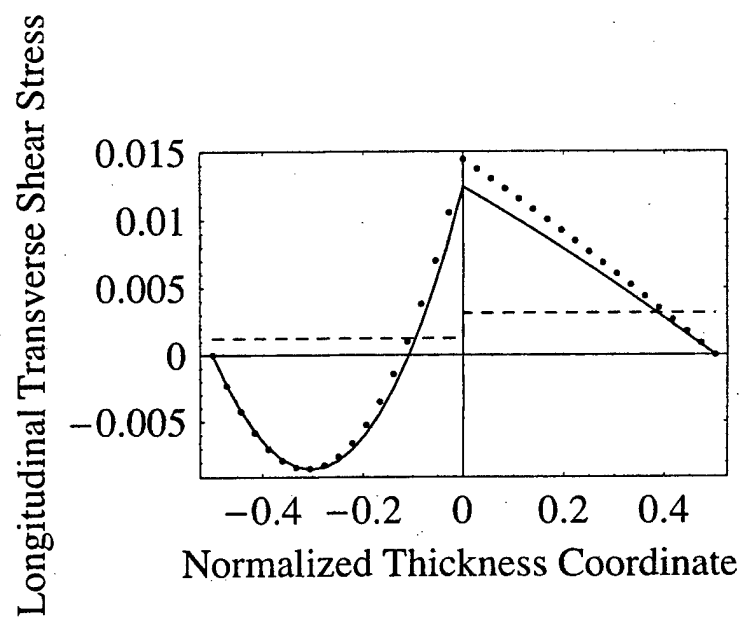
Figure 6:   Distribution of the 3-D stress σ_{23} vs the thickness coordinate (case 1)
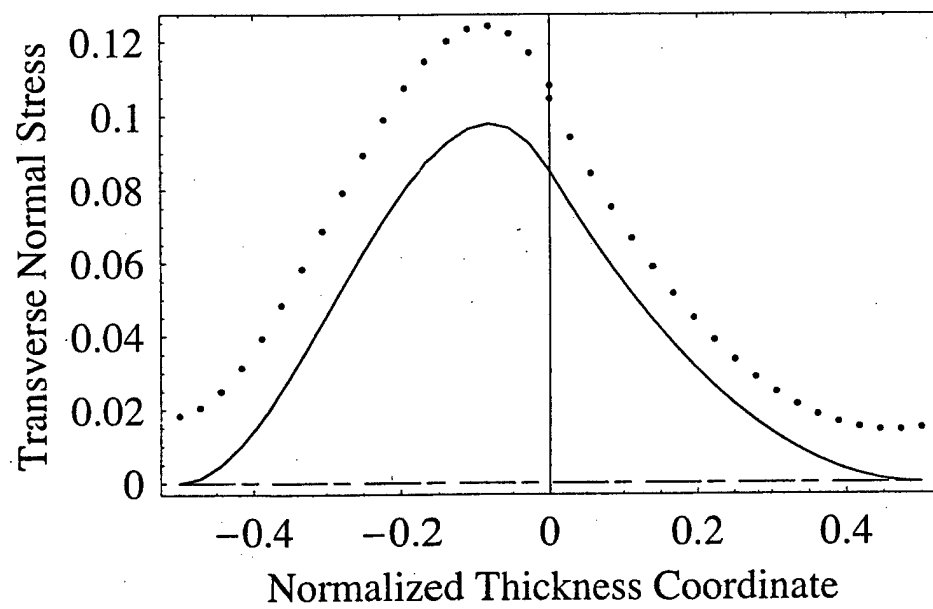
Figure 7: Distribution of the 3-D stress σ_{33} vs the thickness coordinate (case 1)
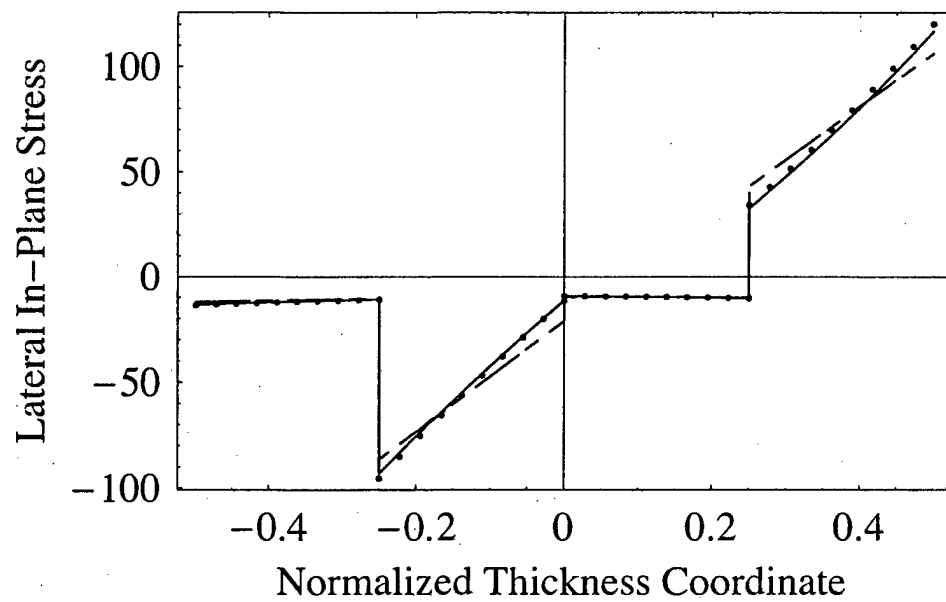
Figure 8: Distribution of the 3-D stress σ_{11} vs the thickness coordinate (case 2)
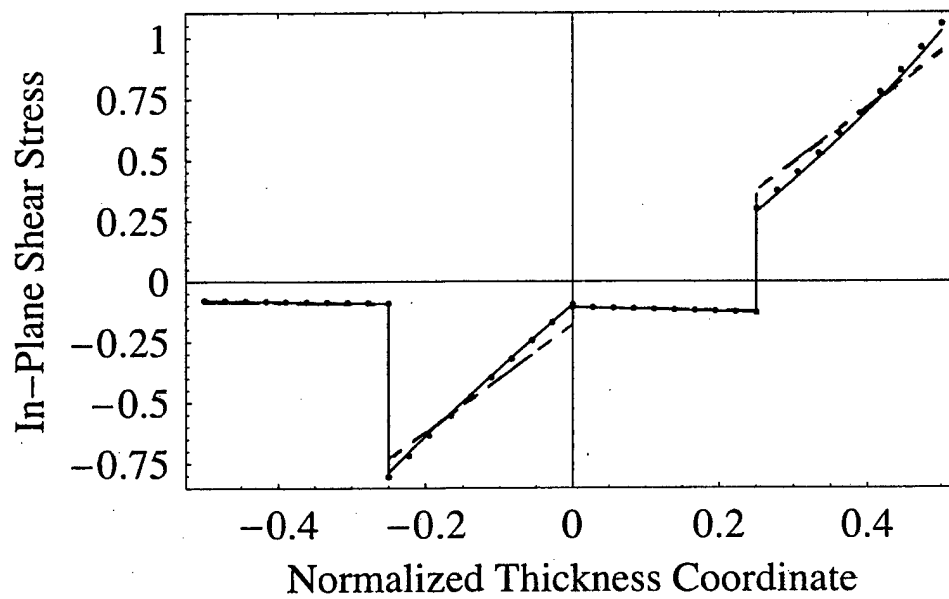
Figure 9: Distribution of the 3-D stress σ_{12} vs the thickness coordinate (case 2)
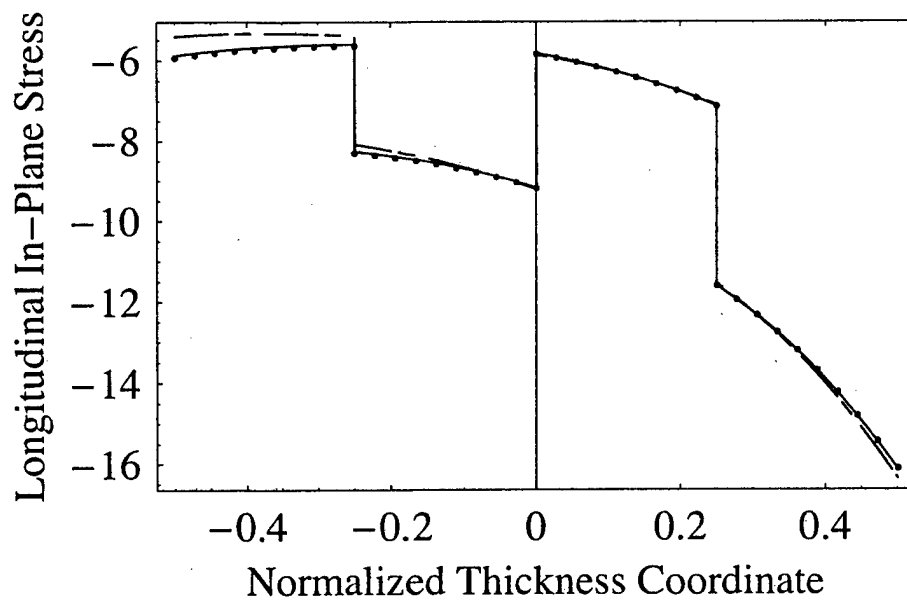
Figure 10: Distribution of the 3-D stress σ_{22} vs the thickness coordinate (case 2)
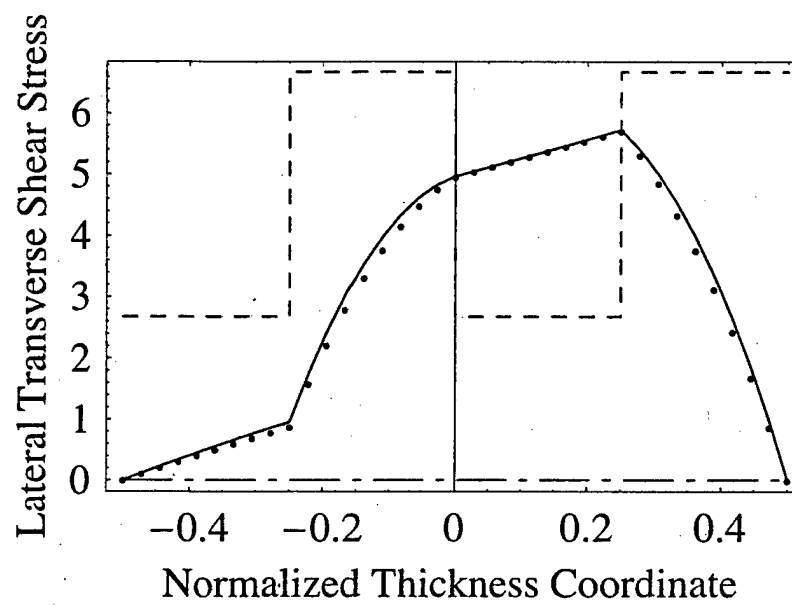
Figure 11:   Distribution of the 3-D stress σ_{13} vs the thickness coordinate (case 2)
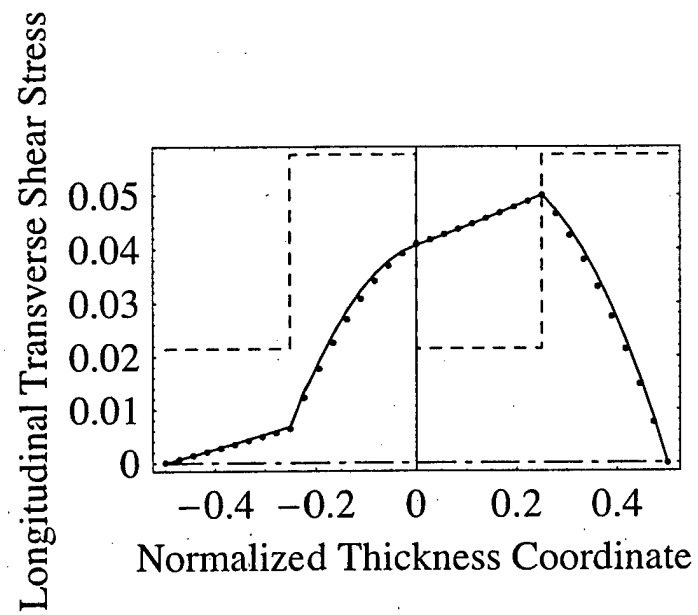
Figure 12: Distribution of the 3-D stress σ_{23} vs the thickness coordinate (case 2)
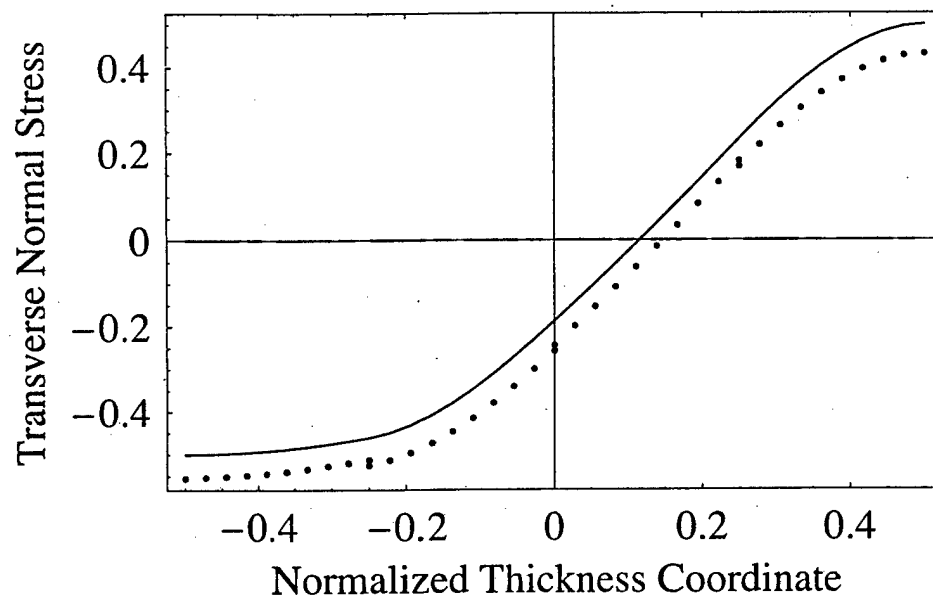
Figure 13: Distribution of the 3-D stress σ_{33} vs the thickness coordinate (case 2)

A Simple Thermopiezoelastic Model for Composite Plates with Accurate Stress Recovery†

Wenbin Yu ‡ and Dewey H. Hodges§

Georgia Institute of Technology, Atlanta, Georgia 30332-0150

E-mail: dewey.hodges@ae.gatech.edu

Abstract. A Reissner-Mindlin type model for analyzing laminated composite plates including piezoelectric layers under mechanical, thermal and electric loads has been constructed by the variational asymptotic method. The present work formulates the original nonlinear, three-dimensional, one-way coupled, thermopiezoelasticity problem allowing for arbitrary deformation of the normal line and using a set of intrinsic variables defined on the reference plane. The variational asymptotic method is used to rigorously split the three-dimensional problem into two problems: a nonlinear, two-dimensional, plate analysis over the reference plane to obtain the global deformation, and a linear analysis through the thickness to provide both the two-dimensional generalized constitutive model and recovering relations to approximate the original three-dimensional results. The obtained asymptotically correct second-order free energy is cast into the form of the commonly-used Reissner-Mindlin type model to account for transverse shear deformation. The present theory is implemented into the computer program VAPAS (Variational Asymptotic Plate and Shell Analysis). Results for several cases obtained from VAPAS are compared with the exact thermopiezoelasticity solutions, classical lamination theory and first-order shear-deformation theory for the purpose of demonstrating advantages and limitations of the proposed theory. The proposed theory can achieve an accuracy comparable to higher-order layerwise theories at the cost of a first-order shear deformation theory.

1. Introduction

Research on smart structures has received enormous attention in recent years [1, 2, 3, 4, 5]. Smart structures are capable of sensing and reacting to external disturbances and thus create the possibility of building structures that are self-monitorable and self-controllable. Such smart structures are promising candidates to meet the demanding requirements of high-strength, high-stiffness, and light-weight structures for modern engineering, especially aerospace applications. Among many possible candidates for actuators and sensors,

† Presented at the 44th Structures, Structural Dynamics and Materials Conference, Norfolk, Virginia, April 7 – 10, 2003.
‡ Post Doctoral Fellow, School of Aerospace Engineering.
§ Professor, School of Aerospace Engineering. Fellow, AIAA.

piezoelectric materials receive the most attention. One reason for this preference is that piezoelectric materials can directly relate electrical signals to strains in the material and vice versa. Thus, they can be used both as actuators and sensors. Moreover, in most cases, piezoelectric materials are used along with tailored anisotropic materials to maximize the intelligence of a smart structure. While most research has been focused on the behavior of piezoelectric structures under isothermal conditions, an increasing effort has been directed to address thermal-piezoelectric-mechanical response [6, 7, 8].

Many engineering smart structures have one dimension much smaller than the other two and can be modeled as plates if there are no initial curvatures associated with the plane formed by the two large dimensions. The present capability of analyzing thermopiezoelastic behavior of smart plates is limited. The mathematical models are generally derived from three-dimensional (3-D) elasticity theory, making use of the fact that the thickness is small in some sense. Most analyses prevailing in the literature are so-called *ad hoc* theories, which can be generally classified as Classical Lamination Theory (CLT) [9], First-Order Shear Deformation Theory (FOSDT) [10], Higher-Order Theory [8] and Layerwise Theory [11]. Layerwise theory can produce reasonable results at the cost of complex models and expensive computation. All the other *ad hoc* approaches are doomed to fail, especially for stress prediction through the thickness, even for shells of moderate thickness. The reason is that these theories assume the displacements to be C^∞ functions, while in fact the displacement field of a layered plate may have discontinuous derivatives through the thickness.

From a mathematical point of view, the approximation in the analysis stems from elimination of the thickness coordinate from the independent variables of the governing equations of motion for the plate structure. This sort of approximation is inevitable if one wants to take advantage of the smallness of the thickness to simplify the analysis. However, other approximations that are not absolutely necessary should be avoided. For example, for small-strain analysis of plates, it is reasonable to assume that the thickness, h, is small compared to the wavelength of deformation of the reference plane, l. However, it is not at all reasonable to assume *a priori* some *ad hoc* displacement field, although that is the way most existing plate theories have been constructed.

A simple and accurate model of composite plates and shells, namely, Variational Asymptotic Plate and Shell Analysis (VAPAS) [12, 13, 14, 15], was developed recently. VAPAS starts with formulation of the 3-D anisotropic elasticity problem in which the deformation of the reference plane is expressed in terms of intrinsic two-dimensional (2-D) variables. The intrinsic formulation allows the body to undergo arbitrarily large displacements and global rotations subject only to the restriction that the generalized 2-D strains are small. The Variational Asymptotic Method (VAM) [16] is then used to systematically reduce the dimensionality of the problem by taking advantage of the small parameters inherent in the problem. The original nonlinear 3-D problem is thus mathematically split into a linear one-dimensional (1-D) through-the-thickness analysis and a nonlinear 2-D plate/shell analysis accounting for transverse shear deformation. The through-the-thickness analysis is solved by finite element method and provides a constitutive model between the generalized, 2-D strains and stress resultants as well as recovery relations to accurately approximate the 3-D

displacement, strain and stress fields in terms of 2-D variables calculated in the 2-D plate/shell analysis. Numerical examples presented in previous works [12, 13, 14, 15] have demonstrated for mechanical and thermal loading that although the resulting theory is as simple as a single-layer FOSDT, the recovered 3-D displacement, strain and stress results have an accuracy comparable to that of higher-order, layer-wise theories with many more degrees of freedom.

The present work extends VAPAS so that the thermopiezoelastic effects of smart plates can be treated in the same framework. Because the procedure is quite similar, the authors have chosen to repeat some formulae and text from their previous publications in order to make the present paper more self-contained. The present theory has been implemented into the computer program VAPAS and now one can use this program along with some 2-D plate solver (e.g., a standard plate finite element in commercial finite element software or in a flexible multi-body code such as DYMORE [17]) to carry out an accurate and efficient thermopiezoelastic analysis for smart composite plates made with piezoelectric material.

2. 3-D Formulation

A point in the plate can be described by its Cartesian coordinates x_i (see Figure 1), where x_α are two orthogonal lines in the reference plane and x_3 is the normal coordinate. (Here and throughout the paper, Greek indices assume values 1 and 2 while Latin indices assume 1, 2, and 3. Repeated indices are summed over their range except where explicitly indicated.) Letting b_i denote the unit vector along x_i for the undeformed plate, one can then describe the position of any material point in the undeformed configuration by its position vector $\hat{r}$ from a fixed point O, such that

$$\hat{r}(x_1, x_2, x_3) = r(x_1, x_2) + x_3 b_3 \tag{1}$$

where r is the position vector from O to the point located by x_α on the reference plane. When the reference plane of the undeformed plate coincides with its middle plane, it naturally follows that

$$\langle \hat{r}(x_1, x_2, x_3) \rangle = r(x_1, x_2) \tag{2}$$

where the angle-brackets denote the definite integral through the thickness of the plate and will be used throughout the rest of the development.

When the plate deforms, the particle that had position vector $\hat{r}$ in the undeformed state now has position vector $\hat{R}$ in the deformed plate. The latter can be uniquely determined by the deformation of the 3-D body. Analogous to b_i for the undeformed state, another triad B_i is introduced for the deformed configuration. The relation between B_i and b_i can be specified by an arbitrarily large rotation specified in terms of the matrix of direction cosines $C(x_1, x_2)$ so that

$$B_i = C_{ij} b_j \qquad C_{ij} = B_i \cdot b_j \tag{3}$$

subject to the requirement that B_i is coincident with b_i when the structure is undeformed. Now the position vector $\hat{R}$ can be re presented as

$$\hat{R}(x_1, x_2, x_3) = R(x_1, x_2) + x_3 B_3(x_1, x_2) + w_i(x_1, x_2, x_3) B_i(x_1, x_2) \tag{4}$$

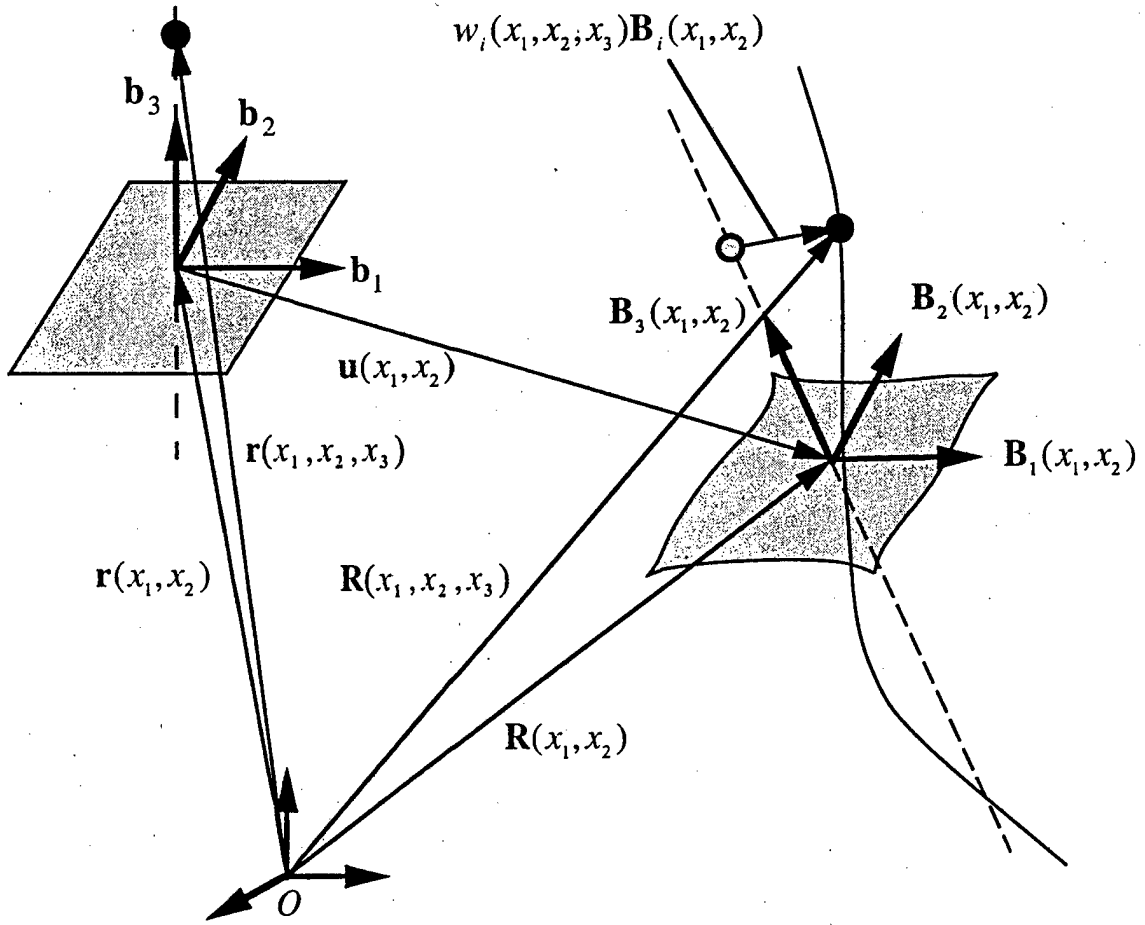Undeformed State   Deformed State

Figure 1. Schematic of plate deformation

where w_i is the warping of the normal-line element. In the present work, the form of the warping w_i is not assumed, as in most plate theories. Rather, these quantities are treated as unknown 3-D functions and will be solved for later. Equation (4) is six times redundant because of the way warping introduced. Six constraints are needed to make the formulation unique. The redundancy can be removed by choosing appropriate definitions of R and B_i. One can define R similarly as Equation (2) to be the average position through the thickness, from which it follows that the warping functions must satisfy the three constraints

$$\langle w_i(x_1, x_2, x_3) \rangle = 0 \tag{5}$$

Another two constraints can be specified by taking B_3 as the normal to the reference plane of the deformed plate. It should be noted that this choice has nothing to do with the Kirchhoff hypothesis. Indeed, it is only for convenience in the derivation. In the Kirchhoff assumption, no local deformation of the transverse normal is allowed. However, according to the present scheme we allow all possible deformation, classifying all deformation other than that of classical lamination theory (CLT) as warping, which is assumed to be small. This assumption

is valid if the strain is small and if the local rotation (*i.e.* the rotation of the normal line caused by warping) is no larger than the order of the strain [18].

Based on the concept of decomposition of rotation tensor [19, 18], the Jauman-Biot-Cauchy strain components for small local rotation are given by

$$\Gamma_{ij} = \frac{1}{2}(F_{ij} + F_{ji}) - \delta_{ij} \tag{6}$$

where F_{ij} is the mixed-basis component of the deformation gradient tensor such that

$$F_{ij} = \mathbf{B}_i \cdot \mathbf{G}_k \mathbf{g}^k \cdot \mathbf{b}_j \tag{7}$$

Here

$$\mathbf{G}_k = \frac{\partial \hat{\mathbf{R}}}{\partial x_k}$$

is the covariant basis vector of the deformed configuration and $\mathbf{g}^k$ the contravariant base vector of the undeformed configuration and $\mathbf{g}^k = \mathbf{g}_k = \mathbf{b}_k$. One can obtain $\mathbf{G}_k$ with the help of the definition of so-called generalized 2-D strains similarly as [20], given by

$$\mathbf{R}_{,\alpha} = \mathbf{B}_\alpha + \varepsilon_{\alpha 3} \mathbf{B}_3 \tag{8}$$

$$\mathbf{B}_{i,\alpha} = (-K_{\alpha 3} \mathbf{B}_3 \times \mathbf{B}_3 + K_{\alpha 3} \mathbf{B}_3) \times \mathbf{B}_i \tag{9}$$

where $\varepsilon_{\alpha 3}$ and $K_{\alpha 3}$ are the 2-D generalized strains and comma denotes the differentiation with respect to the coordinates. Here one is free to set $\varepsilon_{12} = \varepsilon_{21}$, *i.e.*

$$\mathbf{B}_1 \cdot \mathbf{R}_{,2} = \mathbf{B}_2 \cdot \mathbf{R}_{,1} \tag{10}$$

which can serve as another constraint to specify the deformed configuration.

With the assumption that the strain is small compared to unity, which has the effect of removing all the terms that are products of the warping and the generalized strains, one can express the 3-D strain field as

$$\Gamma = \Gamma_h w + \Gamma_\epsilon \epsilon + \Gamma_{l_1} w_{,1} + \Gamma_{l_2} w_{,2} \tag{11}$$

where

$$\Gamma = \lfloor \Gamma_{11} \; 2\Gamma_{12} \; \Gamma_{22} \; 2\Gamma_{13} \; 2\Gamma_{23} \; \Gamma_{33} \rfloor^T \tag{12}$$

$$w = \lfloor w_1 \; w_2 \; w_3 \rfloor^T \tag{13}$$

$$\epsilon = \lfloor \varepsilon_{11} \; 2\varepsilon_{12} \; \varepsilon_{22} \; K_{11} \; K_{12} + K_{21} \; K_{22} \rfloor^T \tag{14}$$

and all the operators are defined as:

$$\Gamma_h = \begin{bmatrix} 0 & 0 & 0 \\ 0 & 0 & 0 \\ 0 & 0 & 0 \\ \frac{\partial}{\partial x_3} & 0 & 0 \\ 0 & \frac{\partial}{\partial x_3} & 0 \\ 0 & 0 & \frac{\partial}{\partial x_3} \end{bmatrix} \qquad \Gamma_{l_1} = \begin{bmatrix} 1 & 0 & 0 \\ 0 & 1 & 0 \\ 0 & 0 & 0 \\ 0 & 0 & 1 \\ 0 & 0 & 0 \\ 0 & 0 & 0 \end{bmatrix} \tag{15}$$

$$\Gamma_\epsilon = \begin{bmatrix} 1 & 0 & 0 & x_3 & 0 & 0 \\ 0 & 1 & 0 & 0 & x_3 & 0 \\ 0 & 0 & 1 & 0 & 0 & x_3 \\ 0 & 0 & 0 & 0 & 0 & 0 \\ 0 & 0 & 0 & 0 & 0 & 0 \\ 0 & 0 & 0 & 0 & 0 & 0 \end{bmatrix} \qquad \Gamma_{l_2} = \begin{bmatrix} 0 & 0 & 0 \\ 1 & 0 & 0 \\ 0 & 1 & 0 \\ 0 & 0 & 0 \\ 0 & 0 & 1 \\ 0 & 0 & 0 \end{bmatrix} \qquad (16)$$

In the present work, we only study the actuated effect caused by applied thermal or electrical loads, which means there is only one-way thermopiezoelastic coupling. The changes of temperature and electrical fields caused by deformation of the plate are negligible, and the interactions between temperature and electric field are not considered either. Then we can use the Gibbs free-energy function [21] without the quadratic terms involving temperature and/or electric field to carry out the analysis. The free energy per unit area (which is the same as the free energy of the normal-line element) can be written as

$$U = \left\langle \frac{1}{2} \Gamma^T D \Gamma - \Gamma^T D \alpha \, T - \Gamma^T D d \, \mathcal{E} \right\rangle \qquad (17)$$

where T is the difference of temperature inside the structure with respect to the reference temperature when the plate is stress free; $\mathcal{E}$ is the electric field vector; D is the 3-D $6{\times}6$ material matrix, which consists of elements of the elasticity tensor expressed in the global coordinate system x_i; α is a $6{\times}1$ column matrix representing the 3-D thermal expansion coefficients; and d is a $6{\times}3$ matrix representing the 3-D strain-piezoelectric coefficients. These matrices are in general fully populated. However, if it is desired to model laminated composite plates in which each lamina exhibits a monoclinic symmetry about its own midplane and is rotated about the local normal to be a layer in the composite laminated plate, some parts of D will always vanish [12] no matter what the layup angle is, and α and d will assume the following forms:

$$\alpha = \lfloor \alpha_{11} \; 2\alpha_{12} \; \alpha_{22} \; 0 \; 0 \; \alpha_{33} \rfloor^T \qquad (18)$$

$$d = \begin{bmatrix} 0 & 0 & d_{113} \\ 0 & 0 & 2d_{123} \\ 0 & 0 & d_{223} \\ 2d_{131} & 2d_{132} & 0 \\ 2d_{231} & 2d_{232} & 0 \\ 0 & 0 & d_{333} \end{bmatrix} \qquad (19)$$

To deal with applied mechanical loads, we will at first leave open the existence of a potential energy and develop instead the virtual work of the applied mechanical loads. The virtual displacement is taken as the Lagrangean variation of the displacement field, such that

$$\delta\hat{\mathbf{R}} = \overline{\delta q}_{Bi}\mathbf{B}_i + x_3\overline{\delta\psi}_{Bi}\mathbf{B}_i \times \mathbf{B}_3 + \delta w_i\mathbf{B}_i + \overline{\delta\psi}_{Bi}\mathbf{B}_i \times w_j\mathbf{B}_j \qquad (20)$$

where the virtual displacement of the reference plane is given by

$$\overline{\delta q}_{Bi} = \delta\mathbf{u} \cdot \mathbf{B}_i \qquad (21)$$

and the virtual rotation of the reference plane is defined such that

$$\delta\mathbf{B}_i = \overline{\delta\psi}_{Bj}\mathbf{B}_j \times \mathbf{B}_i \qquad (22)$$

Since the strain is small, one may safely ignore products of the warping and the loading in the virtual rotation term. Then, the work done through a virtual displacement by the applied loads $\tau_i \mathbf{B}_i$ at the top surface and $\beta_i \mathbf{B}_i$ at the bottom surface and by the body force $\phi_i \mathbf{B}_i$ through the thickness is

$$\overline{\delta W} = (\tau_i + \beta_i + \langle \phi_i \rangle)\overline{\delta q}_{Bi} + \overline{\delta \psi}_{B\alpha}\left[\frac{h}{2}(\tau_\alpha - \beta_\alpha) + \langle x_3 \phi_\alpha \rangle\right] + \delta\left(\tau_i w_i^+ + \beta_i w_i^- + \langle \phi_i w_i \rangle\right) \quad (23)$$

where τ_i, β_i, and ϕ_i are taken to be independent of the deformation, $()^+ = ()|_{x_3=\frac{h}{2}}$, and $()^- = ()|_{x_3=-\frac{h}{2}}$. By introducing column matrices $\overline{\delta q}$, $\overline{\delta \psi}$, τ, β, and ϕ, which are formed by stacking the three elements associated with indexed symbols of the same names, and using Equations (1), (3), and (4), one may write the virtual work in matrix form, so that

$$\overline{\delta W} = \overline{\delta q}^T f + \overline{\delta \psi}^T m + \delta\left(\tau^T w^+ + \beta^T w^- + \langle \phi^T w \rangle\right) \quad (24)$$

where

$$f = \tau + \beta + \langle \phi \rangle$$
$$m = \left\{ \begin{array}{c} \frac{h}{2}(\tau_1 - \beta_1) + \langle x_3 \phi_1 \rangle \\ \frac{h}{2}(\tau_2 - \beta_2) + \langle x_3 \phi_2 \rangle \\ 0 \end{array} \right\} \quad (25)$$

The complete statement of the problem can now be presented in terms of the principle of virtual work, such that

$$\delta U - \overline{\delta W} = 0 \quad (26)$$

In spite of the possibility of accounting for nonconservative forces in the above, the problem that governs the warping is conservative when τ_i, β_i, and ϕ_i are taken to be independent of the deformation. Thus, one can pose the problem that governs the warping as the minimization of a total potential functional

$$\Pi = U + W \quad (27)$$

so that

$$\delta \Pi = 0 \quad (28)$$

in which only the warping displacement is varied, subject to the constraints Equation (5). This implies that the potential of the applied mechanical loads for the functional governing warping is given by

$$W = -\tau^T w^+ - \beta^T w^- - \langle \phi^T w \rangle \quad (29)$$

By the principle of minimum total potential energy, one can solve for the unknown warping functions by minimizing the functional in Equation (27) subject to the constraints of Equation (5). Up to this point, this is simply an alternative formulation of the original 3-D elasticity problem. If we attempt to solve this problem directly, we will meet the same difficulty as solving any full 3-D elasticity problem. Fortunately, the VAM can be used to calculate the 3-D warping functions asymptotically. Although through-the-thickness analysis is one dimensional and can be solved analytically [12], we prefer to use finite element discretization

to solve the minimization problem for the sake of dealing with multiple layers and arbitrary monoclinic material, and connecting with any 2-D standard plate solver which is normally implemented using finite element method. A 5-noded isoparametric element is used because we need the second-order warping functions for the purpose of recovering the original 3-D fields up to the second order of h/l. These second-order warping functions are piecewise, fourth-degree polynomials as shown in [12]. Discretizing the transverse normal line into 1-D finite elements, one can express the warping field as

$$w(x_i) = S(x_3)V(x_1, x_2) \tag{30}$$

where S is the shape function and V is the nodal value of warping field along the transverse normal. Substituting Equation (30) into Equation (27), one can express the total energy in discretized form as

$$
\begin{aligned}
2\Pi = {}& V^T E V + 2V^T(D_{h\epsilon}\epsilon + D_{hl_1}V_{,1} + D_{hl_2}V_{,2}) \\
& + \epsilon^T D_{\epsilon\epsilon}\epsilon + V_{,1}^T D_{l_1 l_1}V_{,1} + V_{,2}^T D_{l_2 l_2}V_{,2} \\
& + 2(V_{,1}^T D_{l_1\epsilon}\epsilon + V_{,2}^T D_{l_2\epsilon}\epsilon + V_{,1}^T D_{l_1 l_2}V_{,2}) \\
& - 2V^T\alpha_h - 2\epsilon^T\alpha_\epsilon - 2V_{,1}^T\alpha_{l_1} - 2V_{,2}^T\alpha_{l_2} \\
& - 2V^T\mathcal{E}_h - 2\epsilon^T\mathcal{E}_\epsilon - 2V_{,1}^T\mathcal{E}_{l_1} - 2V_{,2}^T\mathcal{E}_{l_2} + 2V^T L
\end{aligned} \tag{31}
$$

where L contains the load related terms such that

$$L = -S^{+T}\tau - S^{-T}\beta - \left\langle S^T\phi \right\rangle \tag{32}$$

The new matrix variables carry the properties of both the geometry and material:

$$
\begin{array}{ll}
E = \left\langle [\Gamma_h S]^T D[\Gamma_h S] \right\rangle & D_{h\epsilon} = \left\langle [\Gamma_h S]^T D\Gamma_\epsilon \right\rangle \\[2mm]
D_{hl_1} = \left\langle [\Gamma_h S]^T D[\Gamma_{l_1} S] \right\rangle & D_{hl_2} = \left\langle [\Gamma_h S]^T D[\Gamma_{l_2} S] \right\rangle \\[2mm]
D_{\epsilon\epsilon} = \left\langle \Gamma_\epsilon^T D\Gamma_\epsilon \right\rangle & D_{l_1 l_1} = \left\langle [\Gamma_{l_1} S]^T D[\Gamma_{l_1} S] \right\rangle \\[2mm]
D_{l_1 l_2} = \left\langle [\Gamma_{l_1} S]^T D[\Gamma_{l_2} S] \right\rangle & D_{l_2 l_2} = \left\langle [\Gamma_{l_2} S]^T D[\Gamma_{l_2} S] \right\rangle \\[2mm]
D_{l_1\epsilon} = \left\langle [\Gamma_{l_1} S]^T D\Gamma_\epsilon \right\rangle & D_{l_2\epsilon} = \left\langle [\Gamma_{l_2} S]^T D\Gamma_\epsilon \right\rangle \\[2mm]
\alpha_h = \left\langle [\Gamma_h S]^T D\alpha\, T \right\rangle & \alpha_\epsilon = \left\langle \Gamma_\epsilon^T D\alpha\, T \right\rangle \\[2mm]
\alpha_{l_1} = \left\langle [\Gamma_{l_1} S]^T D\alpha\, T \right\rangle & \alpha_{l_2} = \left\langle [\Gamma_{l_2} S]^T D\alpha\, T \right\rangle \\[2mm]
\mathcal{E}_h = \left\langle [\Gamma_h S]^T D\, d\, \mathcal{E} \right\rangle & \mathcal{E}_\epsilon = \left\langle \Gamma_\epsilon^T D\, d\, \mathcal{E} \right\rangle \\[2mm]
\mathcal{E}_{l_1} = \left\langle [\Gamma_{l_1} S]^T D\, d\, \mathcal{E} \right\rangle & \mathcal{E}_{l_2} = \left\langle [\Gamma_{l_2} S]^T D\, d\, \mathcal{E} \right\rangle
\end{array} \tag{33}
$$

Although the theory itself allows for an exact representation for arbitrary temperature and electric field distribution through the thickness, here fourth-degree polynomials are used to approximate both distributions for each normal-line element. The discretized form of Equation (5) is

$$V^T H\psi = 0 \tag{34}$$

where $H = \left\langle S^T S \right\rangle$ and ψ is the normalized kernel matrix of E such that $\psi^T H\psi = I$. Now our problem is transformed to minimize Equation (31) numerically, subject to the constraints in Equation (34).

3. Dimensional Reduction

To rigorously reduce the original 3-D problem to a 2-D plate problem, one must attempt to reproduce the energy stored in the 3-D structure in a 2-D formulation. This dimensional reduction can only be done approximately, and one way to do it is by taking advantage of the smallness of h/l. The small parameter ε, representing the order of the generalized 2-D strains ϵ has already been taken advantage of when we derive Equation (11). To reduce the number of small parameters in the asymptotic analysis, it is reasonable to assume that the strains caused by temperature and electricity are of the order ε. Thus, the quantities of interest assume the following orders:

$$\epsilon_{\alpha\beta} \sim h\kappa_{\alpha\beta} \sim \varepsilon \quad f_3 \sim \mu(h/l)^2\varepsilon \quad f_\alpha \sim \mu(h/l)\varepsilon$$
$$m_\alpha \sim \mu h(h/l)\varepsilon \quad \alpha T \sim \varepsilon \quad d\mathcal{E} \sim \varepsilon \tag{35}$$

where μ is the order of the elastic constants (all of which are assumed to be of the same order).

Having assessed the orders of all the interested quantities, the VAM can be used to mathematically perform a dimensional reduction of the 3-D problem to a series of 2-D models. This method requires one to find the leading terms of the functional according to the different orders. Since only the warping is varied, the leading terms needed are all of those terms associated with warping. For the zeroth-order approximation, these leading terms of Equation (31) are

$$2\Pi_0^* = V^T E V + 2V^T D_{h\epsilon}\epsilon - 2V^T\alpha_h - 2V^T\mathcal{E}_h \tag{36}$$

The zeroth-order warping functions which minimize the above functional subject to constraints Equation (34) can be obtained by usual procedure of calculus of variation as:

$$V = \hat{V}_0\epsilon + V_T + V_\mathcal{E} = V_0 \tag{37}$$

Substituting Equation (37) back into Equation (31), one can obtain the total energy asymptotically correct up to the order of $\mu\varepsilon^2$ as

$$2\Pi_0 = \epsilon^T A\epsilon - 2\epsilon^T N_T - 2\epsilon^T N_\mathcal{E} \tag{38}$$

with

$$A = (\hat{V}_0^T D_{h\epsilon} + D_{\epsilon\epsilon})$$
$$N_T = \alpha_\epsilon + \frac{1}{2}(\hat{V}_0^T\alpha_h - D_{h\epsilon}^T V_T)$$
$$N_\mathcal{E} = \mathcal{E}_\epsilon + \frac{1}{2}(\hat{V}_0^T\mathcal{E}_h - D_{h\epsilon}^T V_\mathcal{E}) \tag{39}$$

Although the energy of this approximation coincides with the classical plate theories for thermopiezoelastic analysis, we have not used any *ad hoc* kinematic assumptions such as the Kirchhoff assumption to obtain this result. Moreover, the transverse normal strain from our zeroth-order approximation is not zero.

It is understood that our zeroth-order approximation will give the same stress results as what is obtained from CLT, *i.e.*, all the transverse stress components which are very important for analyzing the failure of composite plates cannot be predicted. One must carry out the

next approximation so that those quantities can be approximately predicted. To obtain the first-order approximation, we simply perturb the zeroth-order result, such that

$$V = V_0 + V_1 \qquad (40)$$

Substituting Equation (40) back into Equation (11) and then into Equation (31), one can obtain the leading terms for the first-order approximation as

$$2\Pi_1^* = V_1^T E V_1 + 2V_1^T D_1 \epsilon_{,1} + 2V_2^T D_2 \epsilon_{,2} + 2V^T L_T + 2V_1^T L_{\mathcal{E}} + 2V_1^T L \qquad (41)$$

with

$$
\begin{aligned}
L_T &= (D_{hl_1} - D_{hl_1}^T)V_{T,1} + (D_{hl_2} - D_{hl_2}^T)V_{T,2} + \alpha_{l_1,1} + \alpha_{l_2,2} \\
L_{\mathcal{E}} &= (D_{hl_1} - D_{hl_1}^T)V_{\mathcal{E},1} + (D_{hl_2} - D_{hl_2}^T)V_{\mathcal{E},2} + \mathcal{E}_{l_1,1} + \mathcal{E}_{l_2,2} \\
D_1 &= (D_{hl_1} - D_{hl_1}^T)\hat{V}_0 - D_{l_1\epsilon} \\
D_2 &= (D_{hl_2} - D_{hl_2}^T)\hat{V}_0 - D_{l_2\epsilon}
\end{aligned}
\qquad (42)
$$

Integration by parts with respect to the in-plane coordinates is used here and hereafter whenever it is convenient for the derivation, because the present goal is to obtain an interior solution for the plate without consideration of edge effects. Note that the treatment of edge effects is itself a very important problem to tackle, but it is outside the scope of the present work.

Similarly as in the zeroth-order approximation, one can solve the first-order warping field as

$$V_1 = V_{11}\epsilon_{,1} + V_{12}\epsilon_{,2} + V_{1T} + V_{1\mathcal{E}} + V_{1L} \qquad (43)$$

and obtain a total energy that is asymptotically correct up to the order of $\mu(h/l)^2 \varepsilon$, given by

$$2\Pi_1 = \epsilon^T A \epsilon + \epsilon_{,1}^T B \epsilon_{,1} + 2\epsilon_{,1}^T C \epsilon_{,2} + \epsilon_{,2}^T \mathcal{D} \epsilon_{,2} - 2\epsilon^T F - 2\epsilon^T F_T - 2\epsilon^T F_{\mathcal{E}} \qquad (44)$$

where

$$
\begin{aligned}
B &= \hat{V}_0^T D_{l_1 l_1} \hat{V}_0 + V_{11}^T D_1 \\
C &= \hat{V}_0^T D_{l_1 l_2} \hat{V}_0 + \frac{1}{2}(V_{11}^T D_2 + D_1^T V_{11}) \\
\mathcal{D} &= \hat{V}_0^T D_{l_2 l_2} \hat{V}_0 + V_{12}^T D_2 \\
F &= \hat{V}_0^T L - \frac{1}{2}(D_1^T V_{1L,1} + V_{11}^T L_{,1} + D_2^T V_{1L,2} + V_{12}^T L_{,2})
\end{aligned}
\qquad (45)
$$

with the non-mechanical load due to temperature

$$
\begin{aligned}
F_T = \ & N_T + \hat{V}_0^T D_{l_1 l_1} V_{T,11} + \hat{V}_0^T D_{l_2 l_2} V_{T,22} + \hat{V}_0^T (D_{l_1 l_2} + D_{l_1 l_2}^T)V_{T,12} \\
& + \frac{1}{2}(V_{11}^T L_{T,1} + V_{12}^T L_{T,2} + D_1^T V_{1T,1} + D_2^T V_{1T,2})
\end{aligned}
\qquad (46)
$$

and the non-mechanical load due to electric field

$$
\begin{aligned}
F_{\mathcal{E}} = \ & N_{\mathcal{E}} - \hat{V}_0^T D_{hl_1} V_{\mathcal{E},1} - \hat{V}_0^T D_{hl_2} V_{\mathcal{E},2} - D_{\epsilon l_1} V_{\mathcal{E},1} - D_{\epsilon l_2} V_{\mathcal{E},2} \\
& + \hat{V}_0^T D_{l_1 l_1} V_{\mathcal{E},11} + \hat{V}_0^T D_{l_2 l_2} V_{\mathcal{E},22} + \hat{V}_0^T (D_{l_1 l_2} + D_{l_1 l_2}^T)V_{\mathcal{E},12} \\
& + \frac{1}{2}(V_{11}^T L_{\mathcal{E},1} + V_{12}^T L_{\mathcal{E},2} + D_1^T V_{1\mathcal{E},1} + D_2^T V_{1\mathcal{E},2})
\end{aligned}
\qquad (47)
$$

Here the monoclinic symmetry has already been used to obtain the asymptotically correct energy in Equation (44). The applied mechanical loads, temperature and electric field should not vary rapidly over the plate surface, so that F, F_T and $F_{\mathcal{E}}$ will be of sufficiently high order to meet the requirement of asymptotical correctness.

4. Transforming into a Reissner-Mindlin Model

Although Equation (44) is asymptotically correct through the second order and use of this free energy expression is possible, it involves more complicated boundary conditions than necessary since it contains derivatives of the generalized strain measures. To obtain an energy functional that is of practical use, one can transform the present approximation into a Reissner-Mindlin type model. It should be noted that fitting the asymptotic energy into such model is just one possible choice, and the possibility of fitting the same energy into other more sophisticated 2-D plate models exists.

In a Reissner-Mindlin model, there are two additional degrees of freedom, which are the transverse shear strains. These are incorporated into the rotation of transverse normal. If we introduce another triad $\mathbf{B}_i^*$ for the deformed Reissner-Mindlin plate, the definition of 2-D strains becomes

$$\mathbf{R}_{,\alpha} = \mathbf{B}_\alpha^* + \varepsilon_{\alpha\beta}^* \mathbf{B}_3^* + 2\gamma_{\alpha3} \mathbf{B}_3^*$$

$$\mathbf{B}_{i,\alpha}^* = (-K_{\alpha\beta}^* \mathbf{B}_\beta^* \times \mathbf{B}_3^* + K_{\alpha3}^* \mathbf{B}_3^*) \times \mathbf{B}_i^* \tag{48}$$

where the transverse shear strains are $\gamma = \lfloor 2\gamma_{13} \ 2\gamma_{23} \rfloor^T$. One can express the classical strain measures ϵ in terms of the strain measures of the Reissner-Mindlin plate model as

$$\epsilon = \mathcal{R} - \mathcal{D}_\alpha \gamma_{,\alpha} \tag{49}$$

where

$$\mathcal{D}_1 = \begin{bmatrix} 0 & 0 & 0 & 1 & 0 & 0 \\ 0 & 0 & 0 & 0 & 1 & 0 \end{bmatrix}^T$$

$$\mathcal{D}_2 = \begin{bmatrix} 0 & 0 & 0 & 0 & 1 & 0 \\ 0 & 0 & 0 & 0 & 0 & 1 \end{bmatrix}^T$$

$$\mathcal{R} = \lfloor \varepsilon_{11}^* \ 2\varepsilon_{12}^* \ \varepsilon_{22}^* \ K_{11}^* \ K_{12}^* + K_{21}^* \ K_{22}^* \rfloor^T \tag{50}$$

Now one can express the energy, Equation (44), correct to second order, in terms of strains of the Reissner-Mindlin model as

$$\begin{aligned}
2\Pi_1 &= \mathcal{R}^T A \mathcal{R} - 2\mathcal{R}^T A \mathcal{D}_\alpha \gamma_{,\alpha} + \mathcal{R}_{,1}^T B \mathcal{R}_{,1} + 2\mathcal{R}_{,1}^T C \mathcal{R}_{,2} + \mathcal{R}_{,2}^T D \mathcal{R}_{,2} \\
&\quad - 2\mathcal{R}^T F - 2R^T F_T + 2\gamma_{,\alpha}^T D_\alpha N_T \\
&\quad - 2R^T F_{\mathcal{E}} + 2\gamma_{,\alpha}^T D_\alpha N_{\mathcal{E}}
\end{aligned} \tag{51}$$

The generalized Reissner-Mindlin model used in the 2-D thermopiezoelastic analysis is of the form

$$2\Pi_{\mathcal{R}} = \mathcal{R}^T A \mathcal{R} - 2\mathcal{R}^T (F_{\mathcal{R}} + F_{T\mathcal{R}} + F_{\mathcal{E}\mathcal{R}}) + \gamma^T G \gamma - 2\gamma^T (F_\gamma + F_{T\gamma} + F_{\mathcal{E}\gamma}) \tag{52}$$

To find an equivalent Reissner-Mindlin model Equation (52) for Equation (51), one has to eliminate all partial derivatives of the classical 2-D strain measures. The equilibrium equations are used to achieve this purpose. From the two equilibrium equations balancing bending moments with applied moments m_α which is calculated from Equation (25), one can obtain the following formula

$$\mathcal{D}_\alpha^T(A\mathcal{R}_{,\alpha} - F_{\mathcal{R},\alpha} - F_{T\mathcal{R},\alpha} - F_{\mathcal{E}\mathcal{R},\alpha}) = G\gamma - F_\gamma - F_{T\gamma} - F_{\mathcal{E}\gamma} - \begin{Bmatrix} m_1 \\ m_2 \end{Bmatrix} \quad (53)$$

Using Equation (53), one can rewrite Equation (51) as

$$2\Pi_1 = \mathcal{R}^T A\mathcal{R} + \gamma^T G\gamma - 2\mathcal{R}^T(F + F_T + F_{\mathcal{E}}) - 2\gamma^T \mathcal{D}_\alpha N_{T,\alpha} - 2\gamma^T \mathcal{D}_\alpha N_{\mathcal{E},\alpha} + U^* \quad (54)$$

where

$$U^* = \mathcal{R}_{,1}^T \overline{B}\mathcal{R}_{,1} + 2\mathcal{R}_{,1}^T \overline{C}\mathcal{R}_{,2} + \mathcal{R}_{,2}^T \overline{D}\mathcal{R}_{,2} \quad (55)$$

and

$$\begin{aligned}
\overline{B} &= B + A\mathcal{D}_1 G^{-1}\mathcal{D}_1^T A \\
\overline{C} &= C + A\mathcal{D}_1 G^{-1}\mathcal{D}_2^T A \\
\overline{D} &= D + A\mathcal{D}_2 G^{-1}\mathcal{D}_2^T A
\end{aligned} \quad (56)$$

If we can drive U^* to zero for any $\mathcal{R}$, then we have found an asymptotically correct Reissner-Mindlin plate model. For generally anisotropic plates, however, this term cannot be driven to zero; but we can minimize the error to obtain a Reissner-Mindlin model that is as close to asymptotical correctness as possible. The accuracy of the Reissner-Mindlin model depends on how close to zero one can drive this term of the energy.

One could proceed with the optimization at this point, but the problem will require a least squares solution for 3 unknowns (elements of the shear stiffness matrix G) from a linear system of 78 equations (12×12 and symmetric), a very rigid optimization problem. The solution will be better if we can bring more unknowns into the problem. There is no unique plate theory of a given order [22]. One can relax the constraints in Equation (5) to be $\langle w_i \rangle$ = constant and still obtain an asymptotically correct strain energy. Since the zeroth-order approximation gives us an asymptotic model corresponding to classical plate theory, we only relax the constraints for the first-order approximation. This relaxation will modify the warping field to be

$$\overline{V}_1 = V_{11}\epsilon_{,1} + V_{12}\epsilon_{,2} + V_{1L} + V_{1T} + V_{1\mathcal{E}} + L_1\epsilon_{,1} + L_2\epsilon_{,2} \quad (57)$$

where L_1, L_2 consist of 24 constants. The remaining energy U^* will also be modified to be

$$U^* = \mathcal{R}_{,1}^T \hat{B}\mathcal{R}_{,1} + 2\mathcal{R}_{,1}^T \hat{C}\mathcal{R}_{,2} + \mathcal{R}_{,2}^T \hat{D}\mathcal{R}_{,2} \quad (58)$$

and

$$\begin{aligned}
\hat{B} &= \overline{B} + 2L_1^T D_1 \\
\hat{C} &= \overline{C} + (L_1^T D_2 + D_1^T L_2) \\
\hat{D} &= \overline{D} + 2L_2^T D_2
\end{aligned} \quad (59)$$

Since now we have 27 unknowns, the optimization is much more flexible. It can give us a more optimal solution for the shear stiffness matrix G to fit the second-order, asymptotically-correct energy into a Reissner-Mindlin model. In other words, when one carries out the optimization as described here, one finds the Reissner-Mindlin model that describes as closely as possible the 2-D energy that is asymptotically correct through the second order in h/l. However, the asymptotical correctness of the warping field to that same order can only be ascertained after obtaining another higher-order approximation, which will be discussed in the next section.

After minimizing U^*, the "best" total energy to be used for the 2-D plate Reissner-Mindlin model for the purposes of thermopiezoelastic analysis can be expressed as:

$$2\Pi_{\mathcal{R}} = \mathcal{R}^T A \mathcal{R} - 2\mathcal{R}^T(F + F_T + F_{\mathcal{E}}) + \gamma^T G \gamma - 2\gamma^T \mathcal{D}_\alpha (N_{T,\alpha} + N_{\mathcal{E},\alpha}) \quad (60)$$

5. Recovering Relations

From the above, we have obtained a Reissner-Mindlin plate model which is as close as possible to being asymptotically correct in the sense of matching the total energy. The stiffness matrices A, G, load-related terms and non-mechanical stress resultants can be used as input for a plate theory derived from the total energy obtained here. The nonlinear theory presented in [20] is an appropriate choice, but some modification of the loading terms is required.

However, while it is necessary to accurately calculate the 2-D displacement field of the plates, this is not sufficient in many applications. Ultimately, *the fidelity of a reduced-order model such as this depends on how well it can predict the 3-D results in the original 3-D problem*. Hence, recovering relations should be provided to complete the reduced-order model. By recovering relations, we mean expressions for 3-D displacement, strain, and stress fields in terms of 2-D quantities and x_3. For validation, results obtained for the 3-D field variables from the reduced-order model must be compared with those of the original 3-D model.

For an energy that is asymptotically correct through the second order, we can recover the 3-D displacement, strain and stress fields only through the first order in a strict sense of asymptotical correctness. Using Equations (1), (3), and (4), one can recover the 3-D displacement field through the first order as

$$U_{3d} = u_{2d} + x_3 \left\{ \begin{array}{c} C_{31} \\ C_{32} \\ C_{33} - 1 \end{array} \right\} + SV_0 + S\overline{V}_1 \quad (61)$$

where U_{3d} is the column matrix of 3-D displacements and u_{2d} is the plate displacements. C_{ij} are the components of global rotation tensor from Equation (3). From Equation (11), one can recover the 3-D strain field through the first order as

$$\Gamma = \Gamma_h S(V_0 + \overline{V}_1) + \Gamma_\epsilon \epsilon + \Gamma_{l_1} SV_{0,1} + \Gamma_{l_2} SV_{0,2} \quad (62)$$

Then, one can use the 3-D constitutive relation

$$\sigma = D\Gamma - D\alpha \, T - D \, d \, \mathcal{E} \quad (63)$$

to obtain 3-D stresses σ_{ij}.

Since we have obtained an optimum shear stiffness matrix G, some of the recovered 3-D results through the first order are better than classical theory and conventional FOSDT. (Note that conventional FOSDT has no rational way to find the shear stiffness coefficients.) However, for the transverse normal component of strain and stress (*i.e.* Γ_{33} and σ_{33}), it can be shown that the agreement is not satisfactory. Let us recall that the Reissner-Mindlin theory that has been constructed only ensures a good fit with the asymptotically correct 3-D displacement field of the first order (while energy is approximated to the second order). Thus, in order to obtain recovering relations that are valid to the same order as the energy, the VAM iteration needs to be applied one more time.

Using the same procedure listed in previous section, the second-order warping can be obtained and expressed symbolically as

$$V_2 = V_{21}\epsilon_{,11} + V_{22}\epsilon_{,12} + V_{23}\epsilon_{,22} + V_{2L} + V_{2T} + V_{2\varepsilon} \tag{64}$$

Equation (64) is obtained by taking the original first-order warping V_1 to be the result of the first-order approximation. It is clear that V_2 is one order higher than V_1 which confirms that V_1 is the first-order approximation. One might be tempted to use V_1 in the recovering relations. However, the VAM has split the original 3-D problem into two sets of problems. As far as recovering relations concerned, it is observed that the normal-line analysis can at best give us an approximate shape of the distribution of 3-D results. The 2-D plate analysis will govern the global behavior of the structure. Since $\overline{V}_1$ is the warping that yields a Reissner-Mindlin plate model that is as close as possible to being asymptotically correct, we should still use $\overline{V}_1$ in the recovering relations instead of V_1. By doing this, we choose to be more consistent with Reissner-Mindlin plate model while compromising somewhat on the asymptotical correctness of the shape of the distribution. It has been verified by numerical examples that this is a good choice.

Hence, we write the 3-D recovering relations for displacement through the second order as

$$U_{3d} = u_{2d} + x_3 \left\{ \begin{array}{c} C_{31} \\ C_{32} \\ C_{33} - 1 \end{array} \right\} + S(V_0 + \overline{V}_1 + V_2) \tag{65}$$

and the strain field through the second order is

$$\Gamma = \Gamma_h S(V_0 + \overline{V}_1 + V_2) + \Gamma_\epsilon \epsilon + \Gamma_{l_1} S(V_{0,1} + \overline{V}_{1,1}) + \Gamma_{l_2} S(V_{0,2} + \overline{V}_{1,2}) \tag{66}$$

Again the stresses through the second order can be obtained from the 3-D constitutive law, Equation (63).

6. Numerical Examples

The computer program VAPAS has been extended to implement the present theory. Several numerical examples are given here to validate the proposed theory and code against the 3-D thermopiezoelasticity solutions with one-way coupling that are specialized from [23].

First to assess the asymptotical correctness of the proposed theory, we study a cylindrical bending type problem for a single-layer plate made with a piezoelectric material with isotropic

mechanical properties (E as the Young's modulus, ν Poisson's ratio) and d as the strain-piezoelectric constants in the both directions of the reference plane. The plate is simply supported with width L along x_1 axis (the "lateral" direction) and infinitely long along the x_2 axis (the "longitudinal" direction) under the following electricity applied in voltage throughout the plate:

$$\phi = \phi_0 \sin\left(\frac{\pi x_1}{L}\right) \tag{67}$$

Let us assume the thickness of the plate is h, and the normalized thickness coordinate $\zeta = x_3/h$. Then, the small parameter used in our theory is

$$\delta = \frac{h}{l} = \frac{\pi h}{L} \tag{68}$$

Table 1 lists the nontrivial displacements and stresses. The exact solutions are obtained based on [23] and expanded into a series in terms of δ with $o(*)$ denoting terms asymptotically smaller than the order of $*$. The present theory can predict the correct results up to the second order of δ with respect to the leading terms for each 3-D quantities, which clearly demonstrate that our theory is asymptotically correct up to the second order for this particular problem, although the prediction of transverse components for this problem is out of the power of our theory.

However, this should not mislead the reader to assume that the present theory is asymptotically correct up to the second order in general. The authors are aware that the proposed theory can be at best asymptotically correct up to the second order for particular cases. For the general case, however, the theory can only be interpreted as that Reissner-Mindlin model which is the closest to being asymptotically correct. To illustrate the above statement, we provide the results for the same piezoelectric plate under a transverse surface mechanical load in addition to the aforementioned electrical charge:

$$\tau_3 = \beta_3 = \frac{p_0}{2} \sin\left(\frac{\pi x_1}{L}\right) \tag{69}$$

Table 2 only lists the nontrivial displacement results. One can observe from Table 2 that there is a slight difference for the second order prediction (relative to the dominant terms) between the present theory and exact solution. It is interesting to note that if one sets ν equal to zero the difference disappears. Evidently some information belonging to second order and indeed included in the asymptotically correct energy cannot be captured in a Reissner-Mindlin type model. When we transform the asymptotically correct model into a Reissner-Mindlin model, this information is lost.

However, since the loss is small in comparison to the dominant terms, the numerical difference between the present theory and the exact solution is expected to be small. To verify this expectation, we will present some numerical results for piezoelectric plates to demonstrate the accuracy of our theory. We study a single-layer plate with h=1 mm and L=4 mm under the applied electricity as in Equation (67) with ϕ_0=100 V and mechanical load on the surfaces as in Equation (69) with p_0=1 MPa. The piezoelectric material properties are taken from [8]

$$E_L = E_T = 63\,\text{GPa}$$

Table 1. Three-dimensional displacement and stresses under uniform temperature change through the thickness

Normalized lateral displacement ($\frac{U_1}{hd\phi_0}$)

Exact	$-\frac{(\nu+1)}{\pi}\delta^{-1} - \frac{\pi(12\zeta^2-1)\nu}{24}\delta + \frac{\pi^3\nu[120\zeta^2(1-2\zeta^2)(\nu-2)+\nu+14]}{5760(\nu-1)}\delta^3 + o(\delta^4)$
Present	$-\frac{(\nu+1)}{\pi}\delta^{-1} - \frac{\pi(12\zeta^2-1)\nu}{24}\delta + o(\delta^2)$

Normalized transverse displacement ($\frac{U_3}{hd\phi_0}$)

Exact	$\nu\zeta + \frac{\pi^2\zeta(4\zeta^2-1)\nu^2}{24(\nu-1)}\delta^2 + \frac{\pi^4\zeta\nu[8\zeta^2(6\zeta^2-5)(\nu+1)-\nu+15]}{5760(\nu-1)}\delta^4 + o(\delta^4)$
Present	$\nu\zeta + \frac{\pi^2\zeta(4\zeta^2-1)\nu^2}{24(\nu-1)}\delta^2 + o(\delta^2)$

Normalized lateral in-plane stress ($\frac{\sigma_{11}}{Ed\phi_0}$)

Exact	$-\frac{\pi^2(12\zeta^2-1)\nu}{24(\nu^2-1)}\delta^2 - \frac{\pi^4(240\zeta^4-120\zeta^2+7)\nu}{2880(\nu^2-1)}\delta^4 + o(\delta^4)$
Present	$-\frac{\pi^2(12\zeta^2-1)\nu}{24(\nu^2-1)}\delta^2 + o(\delta^2)$

Normalized longitudinal in-plane stress ($\frac{\sigma_{22}}{Ed\phi_0}$)

Exact	$-1 - \frac{\pi^2(12\zeta^2-1)\nu^2}{24(\nu^2-1)}\delta^2 + \frac{\pi^4(-240\zeta^4+120\zeta^2+1)\nu^2}{5760(\nu^2-1)}\delta^4 + o(\delta^4)$
Present	$-1 - \frac{\pi^2(12\zeta^2-1)\nu^2}{24(\nu^2-1)}\delta^2 + o(\delta^2)$

Normalized lateral transverse shear stress ($\frac{\sigma_{13}}{Ed\phi_0}$)

Exact	$\frac{\pi^3\zeta(4\zeta^2-1)\nu}{24(\nu^2-1)}\delta^3 + o(\delta^4)$
Present	Not available

Normalized lateral transverse shear stress ($\frac{\sigma_{33}}{Ed\phi_0}$)

Exact	$\frac{\pi^4(4\zeta^2-1)^2\nu}{384(\nu^2-1)}\delta^4 + o(\delta^4)$
Present	Not available

Table 2. Three-dimensional displacements under linearly distributed temperature change through the thickness

Normalized lateral displacement (U_1)

Exact	$\frac{12hp_0\zeta(\nu^2-1)}{E\pi^3}\delta^{-3} + \frac{h(\nu+1)\left\{p_0\zeta\left[(20\nu-40)\zeta^2+9\nu+6\right]-10Ed\phi_0\right\}}{E\pi^3}\delta^{-1} + o(\delta^{-1})$
Present	$\frac{12hp_0\zeta(\nu^2-1)}{E\pi^3}\delta^{-3} + \left(\frac{h(\nu+1)\left\{p_0\zeta\left[(20\nu-40)\zeta^2+9\nu+6\right]-10Ed\phi_0\right\}}{E\pi^3} + \hat{U}_{\text{diff}}\right)\delta^{-1} + o(\delta^{-1})$

Normalized transverse displacement (U_3)

Exact	$\frac{12hp_0(\nu^2-1)}{E\pi^4}\delta^{-4} - \frac{3hp_0(\nu+1)\left[(20\zeta^2+3)\nu-8\right]}{10E\pi^2}\delta^{-2} + o(\delta^{-2})$
Present	$\frac{12hp_0(\nu^2-1)}{E\pi^4}\delta^{-4} - \left(\frac{3hp_0(\nu+1)\left[(20\zeta^2+3)\nu-8\right]}{10E\pi^2} + \hat{U}_{\text{diff}}\right)\delta^{-2} + o(\delta^{-2})$

$$\hat{U}_{\text{diff}} = \frac{4hp_0\zeta\nu(33\nu^5-7\nu^4+58\nu^3+58\nu^2-11\nu+29)}{5E\pi(11\nu^4-12\nu^3+34\nu^2-12\nu+11)}$$
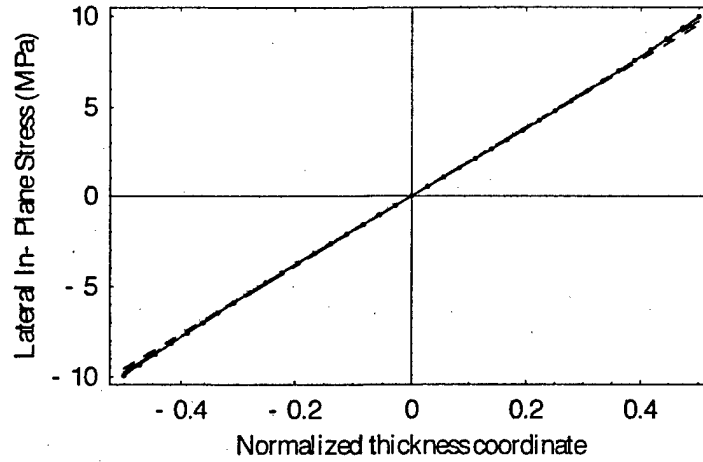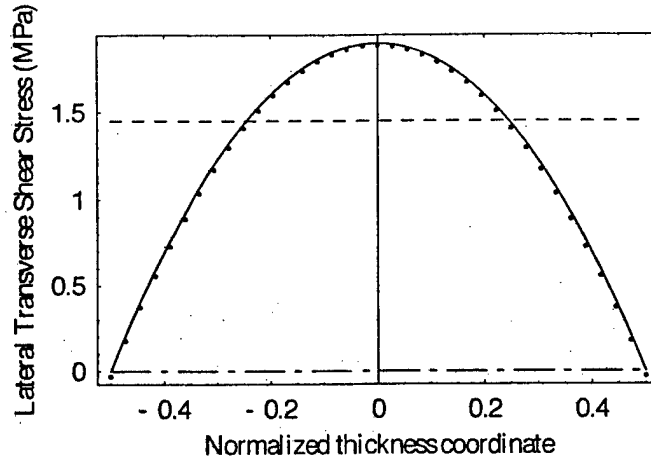
Figure 2. Distribution of the 3-D stress σ_{11} vs the thickness coordinate. Solid line: exact solution; dots: VAPAS; dashed line: FOSDT; long-dash/short-dash line: CLT.
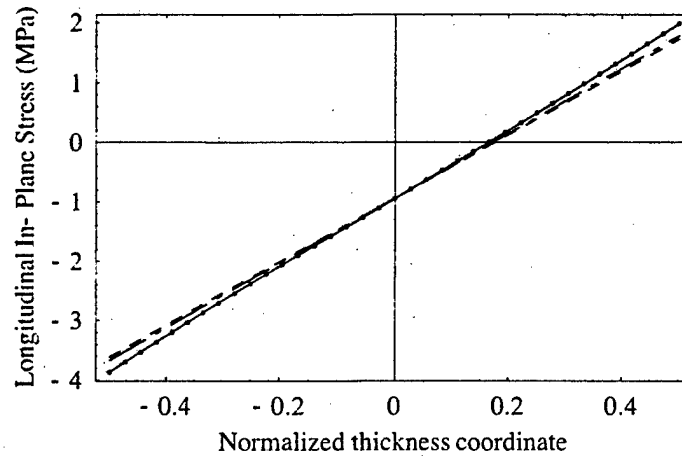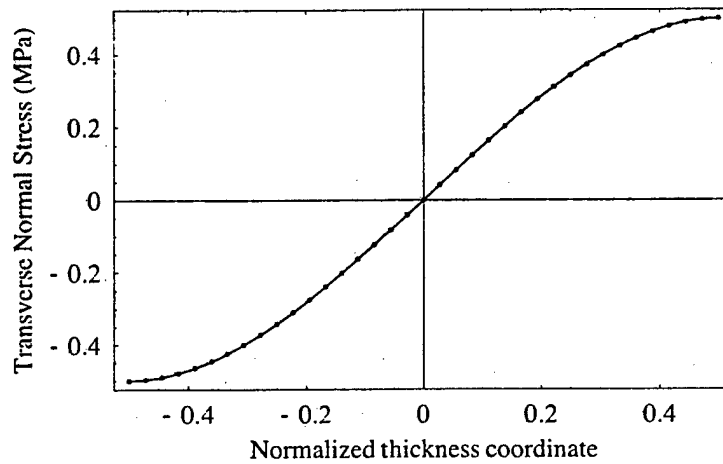

Figure 3. Distribution of the 3-D stress σ_{22} vs the thickness coordinate. Solid line: exact solution; dots: VAPAS; dashed line: FOSDT; long-dash/short-dash line: CLT.

$$G_{LT} = G_{TT} = 24.6 \, \text{GPa}$$

$$\nu_{LT} = \nu_{TT} = 0.28$$

$$d_{113} = d_{223} = 150 \times 10^{-12} \, \text{m/V} \tag{70}$$

Figures 2 – 5 plot the nontrivial components of 3-D stress distribution through the thickness. (Note that, because the 2-D variables are either sine or cosine functions of x_1, $\sigma_{\alpha\beta}$ and σ_{33} are plotted for the position $x_1 = L/2$, and $\sigma_{\alpha 3}$ are plotted for the position $x_1 = 0$ or $x_1 = L$.) One can observe that VAPAS results are almost on the top of exact solutions and much better than the results of CLT and FOSDT. The loss of information is almost negligible.

The present theory is formulated with sufficient generality to carry out a thermopiezoelastic analysis for arbitrary composite laminated piezoelectric plates made with monoclinic material with a computational cost equivalent to that of FOSDT. To demonstrate this fact, we study a more challenging and realistic problem. It is a four-layer smart plate with h=1 mm
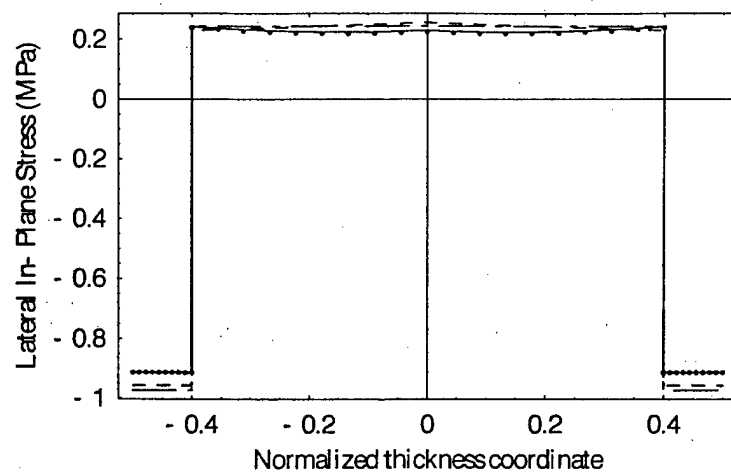
Figure 4. Distribution of the 3-D stress σ_{13} vs the thickness coordinate. Solid line: exact solution: dots: VAPAS; dashed line: FOSDT; long-dash/short-dash line: CLT.
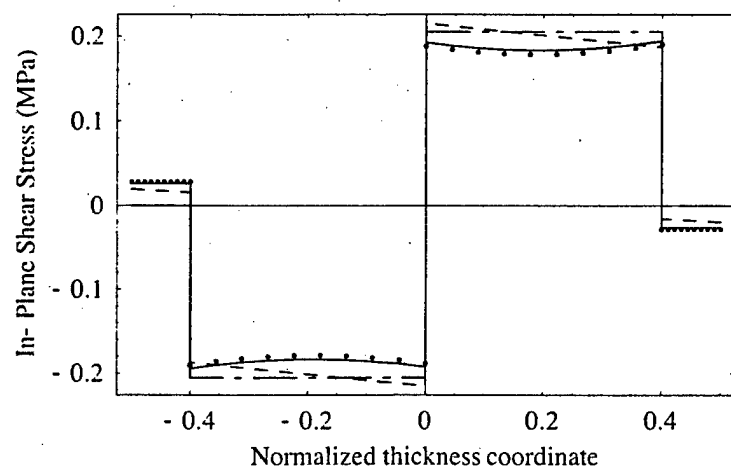

Figure 5. Distribution of the 3-D stress σ_{33} vs the thickness coordinate. Solid line: exact solution; dots: VAPAS; dashed line: FOSDT; long-dash/short-dash line: CLT.

and $L=10$ mm (see Figure 6). The two face sheets are made with piezoelectric material with properties as in Equation (70) and the inside layers are normal graphite/epoxy composites with the following properties:

$$E_L = 172\,\text{GPa} \quad E_T = 6.9\,\text{GPa}$$
$$G_{LT} = 3.4\,\text{GPa} \quad G_{TT} = 1.4\,\text{GPa}$$
$$\nu_{LT} = 0.25 \qquad \nu_{TT} = 0.25 \tag{71}$$

The piezoelectric layers are each 0.1 mm thick, and the regular composite layers are each 0.4 mm thick. The layup scheme is $[0°/-45°/45°/0°]$ from bottom to top. An electric charge according to Equation (67) with $\phi_0=10$ V is applied to both piezoelectric layers with the positive direction align with the x_3 coordinate. The recovered stresses are plotted in Figures 7 - 12. Again, there is an excellent agreement between VAPAS results and those of the exact solution except the transverse normal stress. VAPAS cannot predict a very accurate transverse
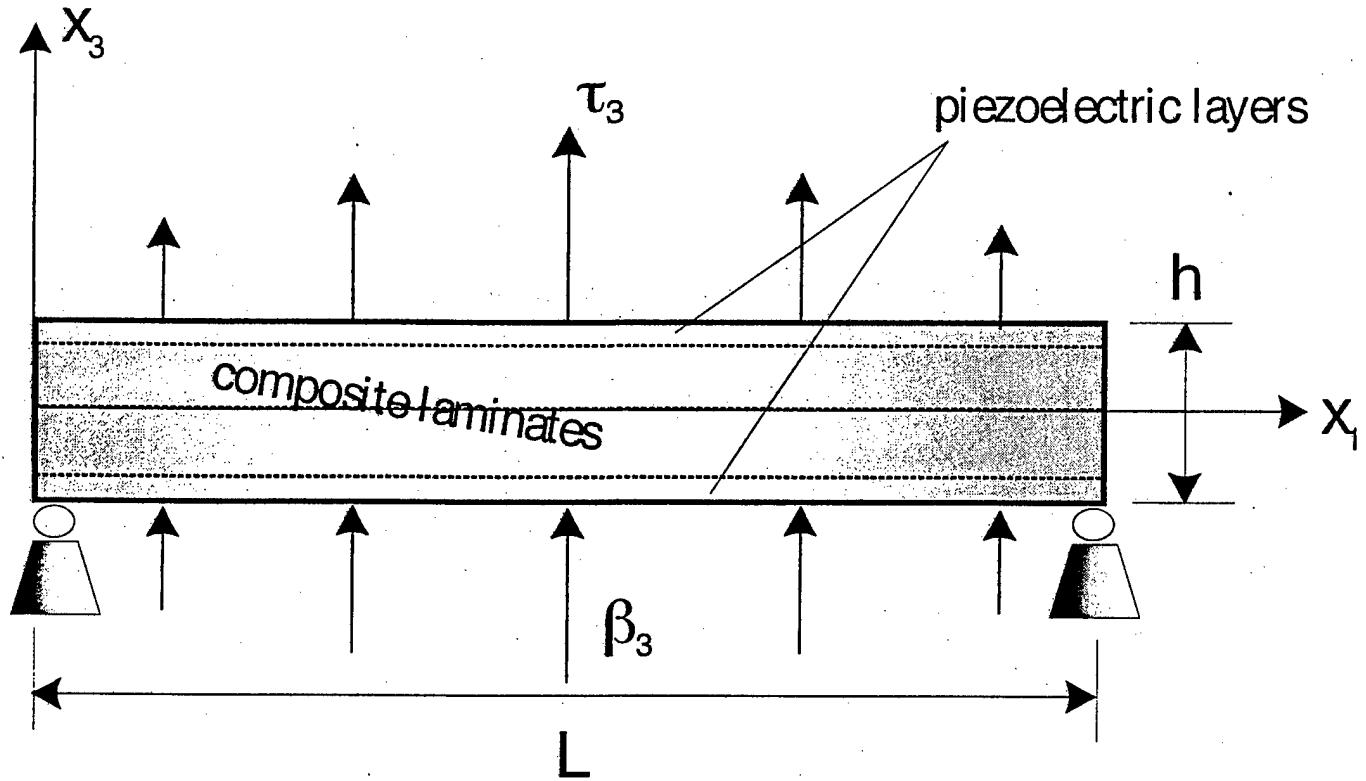
Figure 6. Sketch of a four-layer smart plate

normal stress for this case because this quantity contains significant terms with order higher than the second order which is beyond the capability of VAPAS, as we observed from Table 1. Nevertheless VAPAS qualitatively captures the shape of the distribution through the thickness. Careful readers may also find that there is an obvious discontinuity of the distribution of the transverse normal stress which should not be there. The reason for this violation is that our theory is displacement-based and at most asymptotically correct up to the second order. The approximation causes this discontinuity. However, it is comforting to notice that the actual values for this stress component are very small relative to the rest.

To investigate the behavior of a piezoelectric plate under a combination of different kinds of loads, we apply a mechanical load according to Equation (69) with $p_0 = 1$MPa onto the surfaces. All the components of the stress due to the combination of these two loads are plotted in Figures 13 – 18. This time VAPAS achieves excellent agreement with the exact solution for all six stress components, including the transverse normal stress. This happens because stresses caused by mechanical loads are of orders lower than the second order and within the power of the present theory.

The thermoelastic behavior of composite plates has been studied in [15]. The current version of VAPAS can reproduce all the results there. No additional examples will be given here for the sake of brevity.

Figure 7. Distribution of the 3-D stress σ_{11} vs the thickness coordinate. Solid line: exact solution; dots: VAPAS; dashed line: FOSDT; long-dash/short-dash line: CLT.

Figure 8. Distribution of the 3-D stress σ_{12} vs the thickness coordinate. Solid line: exact solution; dots: VAPAS; dashed line: FOSDT; long-dash/short-dash line: CLT.
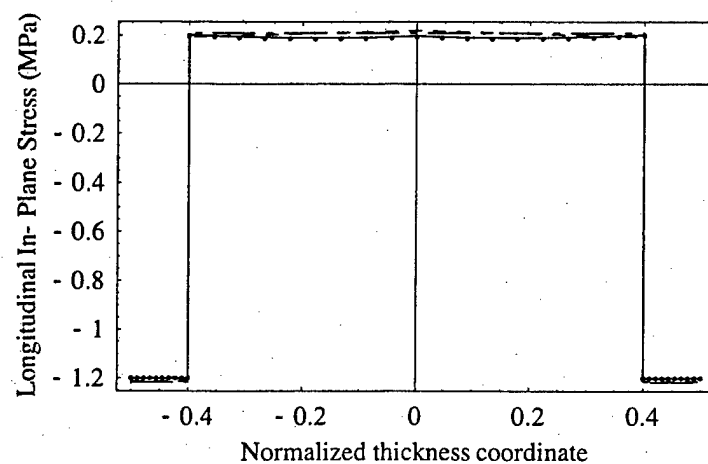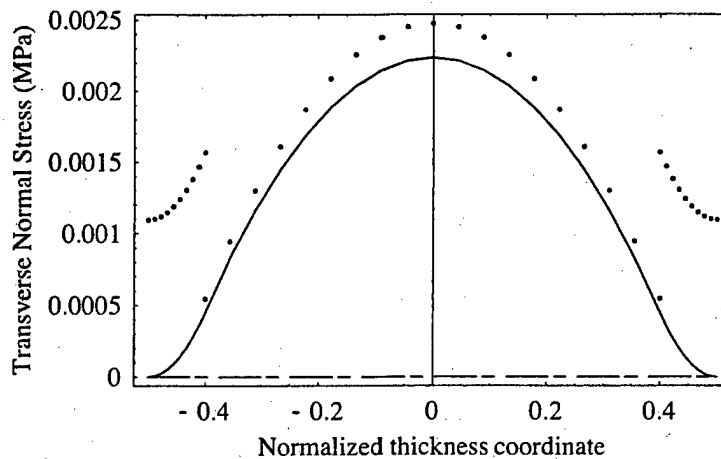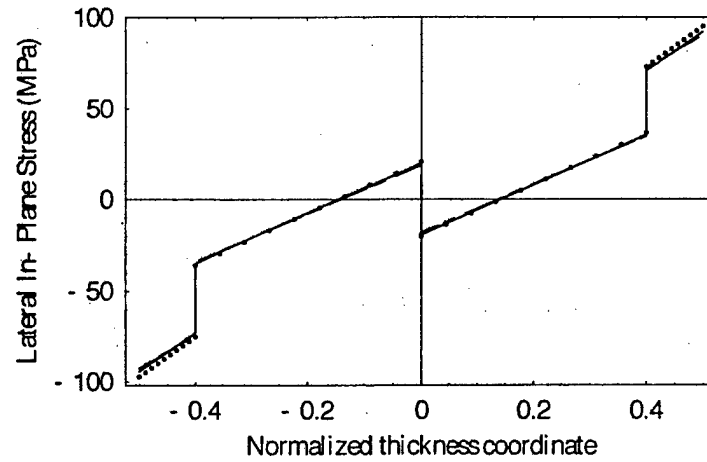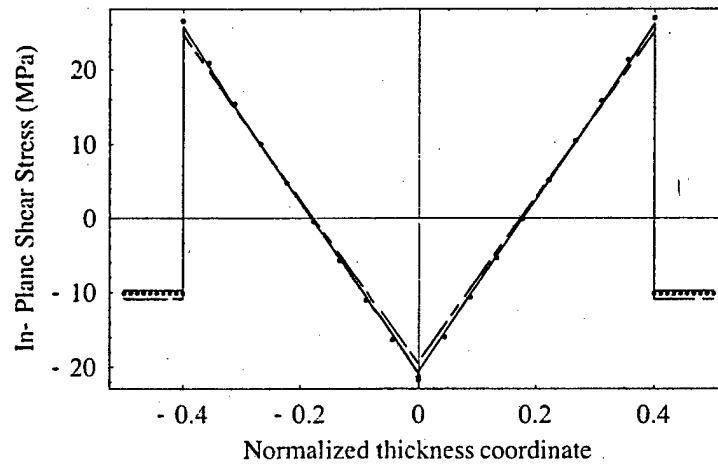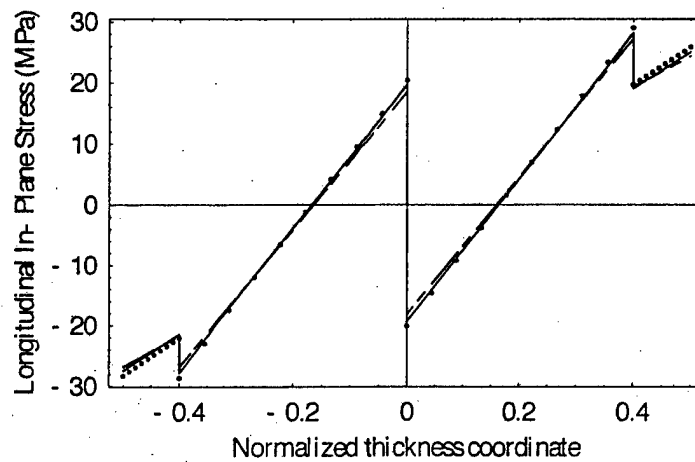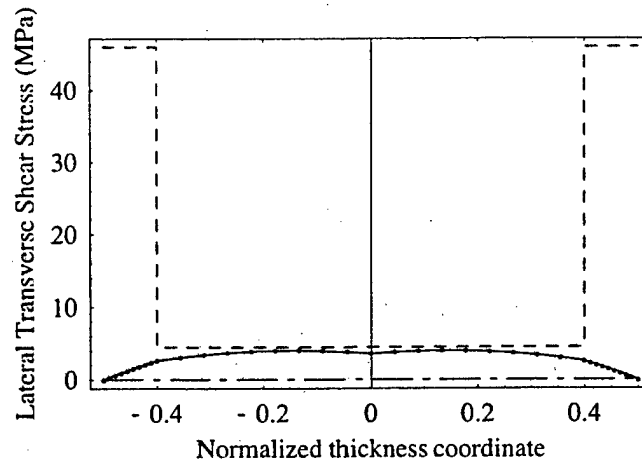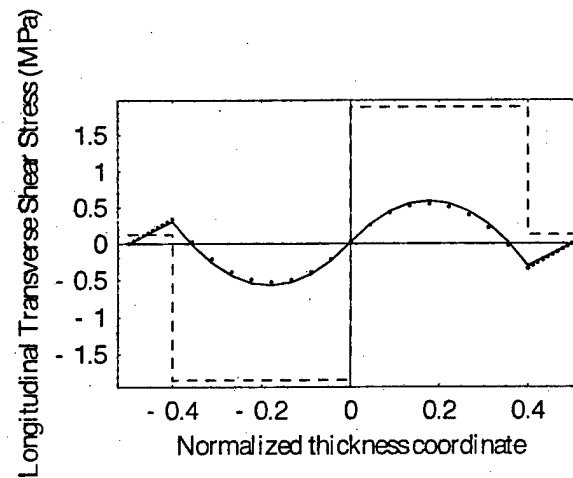

Figure 9. Distribution of the 3-D stress σ_{22} vs the thickness coordinate. Solid line: exact solution; dots: VAPAS; dashed line: FOSDT; long-dash/short-dash line: CLT.
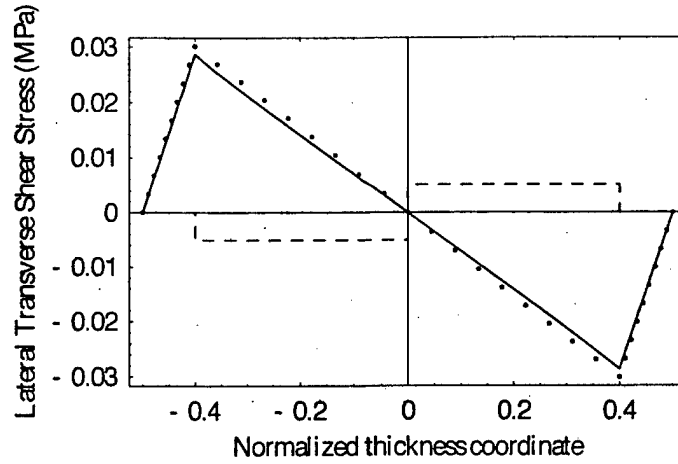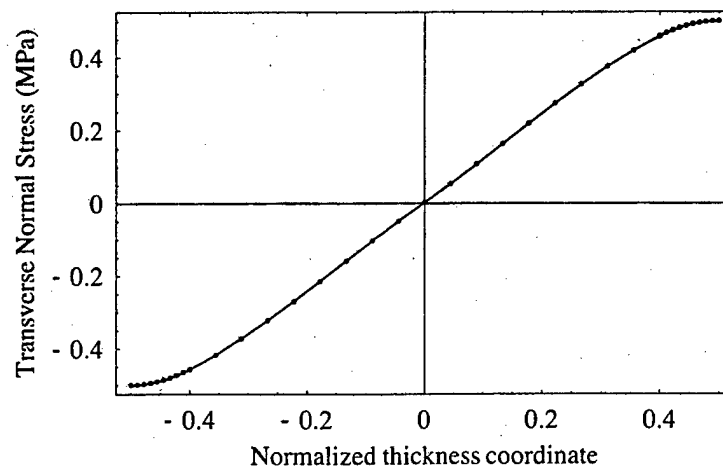
Figure 10. Distribution of the 3-D stress σ_{13} vs the thickness coordinate. Solid line: exact solution: dots: VAPAS; dashed line: FOSDT; long-dash/short-dash line: CLT.
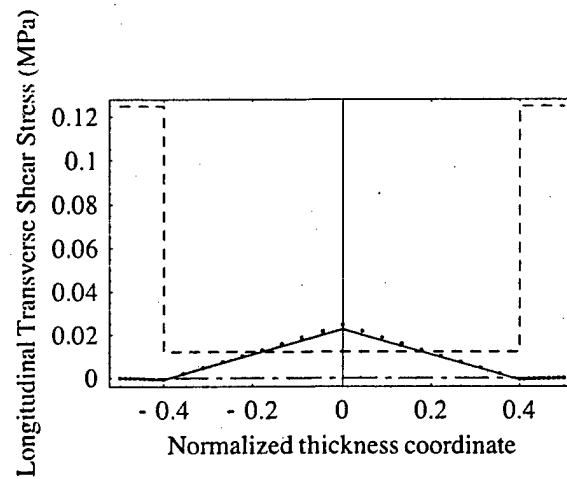
Figure 11. Distribution of the 3-D stress σ_{23} vs the thickness coordinate. Solid line: exact solution; dots: VAPAS; dashed line: FOSDT; long-dash/short-dash line: CLT.

Figure 12. Distribution of the 3-D stress σ_{33} vs the thickness coordinate. Solid line: exact solution; dots: VAPAS; dashed line: FOSDT; long-dash/short-dash line: CLT.

Figure 13. Distribution of the 3-D stress σ_{11} vs the thickness coordinate. Solid line: exact solution; dots: VAPAS; dashed line: FOSDT; long-dash/short-dash line: CLT.

Figure 14. Distribution of the 3-D stress σ_{12} vs the thickness coordinate. Solid line: exact solution; dots: VAPAS; dashed line: FOSDT; long-dash/short-dash line: CLT.

Figure 15. Distribution of the 3-D stress σ_{22} vs the thickness coordinate. Solid line: exact solution; dots: VAPAS; dashed line: FOSDT; long-dash/short-dash line: CLT.

Figure 16. Distribution of the 3-D stress σ_{13} vs the thickness coordinate. Solid line: exact solution; dots: VAPAS; dashed line: FOSDT; long-dash/short-dash line: CLT.

Figure 17. Distribution of the 3-D stress σ_{23} vs the thickness coordinate. Solid line: exact solution; dots: VAPAS; dashed line: FOSDT; long-dash/short-dash line: CLT.

Figure 18. Distribution of the 3-D stress σ_{33} vs the thickness coordinate. Solid line: exact solution; dots: VAPAS; dashed line: FOSDT; long-dash/short-dash line: CLT.

7. Conclusion

A thermopiezoelastic model of composite piezoeletric plates has been developed by use of the variational asymptotic method. A general 2-D constitutive law that is as close to asymptotical correctness as possible has been obtained by solving the 1-D through-the-thickness analysis. The original 3-D results have been reproduced as accurately as possible from a Reissner-Mindlin type plate analysis. Numerical examples show that, although the resulting theory is as simple and efficient as a single-layer first order shear deformation theory, it can approximate the 3-D exact solution very accurately.

The present work differs from previous work on this topic in the literature in the following five aspects:

(i) The present formulation is in an intrinsic form which is suitable for both geometrically nonlinear and linear plate theories.

(ii) Without using any kinematical *ad hoc* assumptions, the dimensional reduction from 3-D to 2-D is carried out systematically by using the variational asymptotic method.

(iii) The Reissner-Mindlin type model proposed in the present theory is *not* a FOSDT. The present theory differs from FOSDT by representing all the deformations that are purposely eliminated in the development of FOSDT. This is accomplished through allowing all possible deformation in the 3-D warping functions, which are solved in turn by the variational asymptotic method.

(iv) All the loads (mechanical, thermal, and electric) that can be applied to a piezoelectric plate can be handled by the present theory. Moreover, all the load distribution through the thickness can be arbitrary and is approximated in VAPAS by a layerwise fourth-degree polynomial. This is more realistic and accurate than most existing models, in which only a constant or linear distribution is allowed.

(v) The present theory decouples the modeling process of the plate completely from the 2-D plate problem described on the reference plane so that the obtained 2-D generalized constitutive model can be used as input for any other 2-D standard plate solver. The flexibility of VAPAS connecting to standard plate and shell solvers can help the structural analysts focus more on solving 2-D problem for different situations.

The computer program VAPAS can now be used along with a 2-D Reissner-Mindlin type plate solver to perform an efficient yet accurate and detailed analysis for thermopiezoelastic behavior of laminated piezoelectric composite plates. Such a tool will be very useful for designers of piezoelectric plates to more efficiently carry out accurate tradeoff studies. It has to be emphasized that the present work only deals with thermal and/or piezoelectric actuation of smart plates. Changes of temperature and electric fields caused by deformation of the plate, which is the so-called sensing capability of smart plates, cannot be treated by means of the present theory. To extend the theory to deal with this class of problems is possible but requires significant effort.

Acknowledgments

References

[1] Loewy, R. G., "Recent Developments in Smart Structures with Aeronautical Applications," *Proceedings of the 37th Israel Annual Conference on Aerospace Sciences, Tel Aviv, Israel*, February 1996.

[2] Saravanos, D. A. and Heyliger, P. R., "Mechanics and Computational Models for Laminated Piezoelectric Beams, Plates, and Shells," *Applied Mechanics Review*, Vol. 52, No. 11, 1999, pp. 305 – 319.

[3] Tauchert, T. R., Ashida, F., Noda, N., Adali, S., and Verijenko, V., "Developments in Thermopiezoelasticity with Relevance to Smart Composite Structures," *Composite Structures*, Vol. 48, 2000, pp. 31 – 38.

[4] Chopra, I., "Status of Application of Smart Structures Technology to Rotorcraft Systems," *Journal of the American Helicopter Society*, Vol. 45, No. 4, 2000, pp. 228 – 252.

[5] Giurgiutiu, V., "Review of Smart Materials Actuation Solutions for Aeroelastic and Vibration Control," *Journal of Intelligent Material Systems and Structures*, Vol. 11, 2000, pp. 525 – 544.

[6] Tauchert, T. R., "Piezothermoelastic Behavior of a Laminated Plate," *Journal of Thermal Stresses*, Vol. 15, No. 1, 1992, pp. 25 – 37.

[7] Lee, H.-J. and Saravanos, D. A., "Generalized Finite Element Formulation for Smart Multilayered Thermal Piezoelectric Composite Plates," *International Journal of Solids and Structures*, Vol. 34, 1997, pp. 3355 – 71.

[8] Chattopadhyay, A., Li, J., and Gu, H., "Coupled Thermo-Piezoelectric-Mechanical Model for Smart Composite Laminates," *AIAA Journal*, Vol. 37, No. 12, 1999, pp. 1633 – 38.

[9] Lee, C. K., "Theory of Laminated Piezoelectric Plates for the Design of Distributed Sensors/Actuators," *Journal of the Acoustical Society of America*, Vol. 87, No. 3, 1990, pp. 1144 – 1158.

[10] Tzou, H. S. and Zhong, J. P., "Electromechanics and Vibrations of Piezoelectric Shell Distributed Systems," *Journal of Dynamic Systems, Measurement and Control*, Vol. 115, No. 4, 1993, pp. 506 – 517.

[11] Mitchell, J. A. and Reddy, J. N., "A Refined Hybrid Plate Theory for Composite Laminates with Piezoelectric Laminae," *International Journal of Solids and Structures*, Vol. 32, No. 16, 1995, pp. 2345 – 2367.

[12] Yu, W., Hodges, D. H., and Volovoi, V. V., "Asymptotic Construction of Reissner-like Models for Composite Plates with Accurate Strain Recovery," *International Journal of Solids and Structures*, Vol. 39, No. 20, 2002, pp. 5185 – 5203.

[13] Yu, W., Hodges, D. H., and Volovoi, V. V., "Asymptotically Accurate 3-D Recovery from Reissner-like Composite Plate Finite Elements," *Computers and Structures*, Vol. 81, No. 7, 2003, pp. 439–454.

[14] Yu, W., Hodges, D. H., and Volovoi, V. V., "Asymptotic Generalization of Reissner-Mindlin Theory: Accurate Three-Dimensional Recovery for Composite Shells," *Computer Methods in Applied Mechanics and Engineering*, Vol. 191, No. 44, 2002, pp. 4971–5112.

[15] Yu, W. and Hodges, D. H., "An Asymptotic Approach for Thermoelastic Analysis of Laminated Composite Plates," *Journal of Engineering Mechanics*, October 2002, submitted.

[16] Berdichevsky, V. L., "Variational-Asymptotic Method of Constructing a Theory of Shells," *PMM*, Vol. 43, No. 4, 1979, pp. 664 – 687.

[17] Bauchau, O., "Computational Schemes for Flexible, Nonlinear Multi-Body Systems," *Multibody System Dynamics*, Vol. 2, 1998, pp. 169–225.

[18] Danielson, D. A., "Finite Rotation with Small Strain in Beams and Plates," *Proceedings of the 2nd Pan American Congress of Applied Mechanics*, Valparaiso, Chile, January 2 – 4 1991, Valparaiso Chile.

[19] Danielson, D. A. and Hodges, D. H., "Nonlinear Beam Kinematics by Decomposition of the Rotation Tensor," *Journal of Applied Mechanics*, Vol. 54, No. 2, 1987, pp. 258 – 262.

[20] Hodges, D. H., Atilgan, A. R., and Danielson, D. A., "A Geometrically Nonlinear Theory of Elastic Plates," *Journal of Applied Mechanics*, Vol. 60, No. 1, March 1993, pp. 109 – 116.

[21] Reddy, J. N., *Mechanics of Laminated Composite Plates: Theory and Analysis*, CRC Press, Boca Raton, Florida, 1997.

[22] Sutyrin, V. G. and Hodges, D. H., "On Asymptotically Correct Linear Laminated Plate Theory," *International Journal of Solids and Structures*, Vol. 33, No. 25, 1996, pp. 3649 – 3671.

[23] Shang, F., Wang, Z., and Li, Z., "Analysis of thermally induced cylindrical flexure of laminated plates with piezoelectric layers," *Composites Part B*, Vol. 28B, 1997, pp. 185–193.

An Energy Decaying Scheme for Nonlinear Dynamics of Shells*

Carlo L. Bottasso,
Dipartimento di Ingegneria Aerospaziale, Politecnico di Milano
Milano, Italy.
Olivier A. Bauchau and Jou-Young Choi
Georgia Institute of Technology, School of Aerospace Engineering
Atlanta, GA, USA.

Abstract

A novel integration scheme for nonlinear dynamics of geometrically exact shells is developed based on the inextensible director assumption. The new algorithm is designed so as to imply the strict decay of the system total mechanical energy at each time step, and consequently unconditional stability is achieved in the nonlinear regime. Furthermore, the scheme features tunable high frequency numerical damping and it is therefore stiffly accurate. The method is tested for a finite element spatial formulation of shells based on mixed interpolations of strain tensorial components and on a two-parameter representation of director rotations. The robustness of the scheme is illustrated with the help of numerical examples.

1   Introduction

The formulation of integration algorithms for nonlinear dynamics of geometrically exact shells is the focus of this work. The partial differential equations governing this class of problems are known to present a rich mathematical structure. In particular, the resulting models are Hamiltonian systems characterized by a symplectic nature and associated with conservation laws that stem from symmetries of the Hamiltonian. The linear and angular momentum as well as the total mechanical energy are conserved for free motions of such systems.

The understanding of the geometric characteristics of the governing equations has been historically confined to the fields of analytical mechanics and pure mathematics. Surprisingly, this knowledge has been seldom used for the development of numerical methods. Indeed, the study of new integration algorithms has been traditionally preoccupied with the development of methods applicable to vast classes of problems, for example the class of differential/algebraic equations, or hyperbolic conservation laws. Consequently, classical methods rarely preserve the underlying structure of the problem being solved, and hence, such structure is *lost* in the numerical solution.

This approach also limits the possible theoretical analyses of the schemes, which are, more often than not, confined to linear or model cases. For instance, it is customary to characterize integration schemes for structural dynamics by studying their behavior when applied to a linear oscillator. This approach is clearly not adequate when dealing with highly nonlinear problems such as the dynamics of geometrically exact shells.

A new approach to the design of integration algorithms attempts to bridge the divide between theoretical and numerical mechanics. Under this new paradigm, numerical schemes are "backward-engineered" to preserve some important qualitative features of the governing equations. Fittingly, this approach is now called *geometric integration* in the mathematical community [20]. Attempts at designing "geometry-aware" algorithms for structural dynamics problems can be traced back to the work of Simo and co-workers who analyzed the problems of rigid body dynamics [32], nonlinear elasto-dynamics [29], geometrically exact

---

shells [30], and geometrically exact beams [31]. In all cases, the idea was to design algorithms that ensure the discrete preservation of the total mechanical energy and of the linear and angular momenta of the system.

When integrating linear and nonlinear finite element models, the implications of the discrete equations stiffness must be carefully considered. Indeed, high frequencies are an artifact of the spatial discretization process and do not reflect the high frequencies of the original infinite dimensional problem. The need for high frequency numerical dissipation has been recognized in the past for linear problems [23]. When dealing with complex nonlinear systems, numerical dissipation becomes indispensable. Indeed, nonlinearities provide a mechanism for transferring energy from low to high frequency modes. Consequently, numerical solutions feature violent oscillations of a purely numerical origin that will eventually play havoc with the convergence characteristics of the nonlinear equation solver.

Among the various geometric characteristics of shell equations, energy preservation appears to be the most important for the development of robust time integration schemes. In fact, strict energy preservation at the discrete level leads to *unconditional stability in the nonlinear regime*, whereas the classical approach based on the analysis of the spectral radius leads to unconditional stability *in the linear regime only*. An energy preserving (EP) scheme for geometrically exact shell is developed in this paper. In addition, the scheme also preserves both linear and angular momenta of the system at the discrete level. Unfortunately, preservation of energy and high frequency dissipation cannot coexist, unless energy is transferred from high to low frequency modes, a transfer that has no physical basis. To solve this problem, a family of energy decaying (ED) schemes that imply a controllable energy decay within each time step is proposed in this work. In geometric terms, this means that the evolution of the system is not confined to the level set of constant energy, but is allowed to drift away from it in a monotonic and controllable manner. Since the energy remains bounded at all times, the scheme is unconditionally stable for nonlinear systems. Furthermore, it can be shown that the energy dissipation mechanism of the algorithm is the result of the removal of the higher frequencies from the computed response.

In related papers, various energy preserving and decaying geometric integrators were developed for rigid bodies and geometrically exact beams [11, 12, 15, 7, 8], and nonlinear elastodynamics [10]. The concepts were extended to multibody systems featuring nonlinear holonomic constraints [4, 16, 13, 17, 18, 14]; non-holonomic and unilateral constraints were treated in [6, 5]. The integration of the present shell model in a general finite element based multibody framework is discussed in [9]. The proposed scheme is independent of the choice of spatial discretization applied to the governing partial differential equations. In the present implementation, the finite element method is used, and the mixed interpolation of tensorial components [2, 3, 19] is implemented to avoid the shear locking problem. The orientation of unit shell directors is described by a special family of two-parameter rotations.

Nonlinearly energy decaying schemes have also been considered by other authors. Notably, a modification of the Energy-Momentum schemes of Simo and co-authors was pursued for beams and shells in refs. [22, 26], following on an idea proposed in ref. [1] for contact problems. Unfortunately, although not always explicitly noted in the cited papers, the resulting algorithms are only first-order accurate, and therefore of little use in practical applications. In refs. [27, 26], standard high frequency damping numerical integrators are combined with the explicit enforcement of conservation laws, in particular the total energy with the possible addition of the system momenta, resulting in the Constrained Energy Method (CEM) or the Constrained Energy-Momentum Algorithm (CEMA), respectively. However, this does not seem to be an appropriate manner of achieving nonlinear unconditional stability: since the higher modes are dissipated while the total system energy must remain constant, the algorithm effectively transfers energy from the artificial high modes to the physically meaningful low frequency modes. This un-natural transfer was pointed out in [26].

In contrast to the published approaches, the method here proposed is the only one to our knowledge that: *a)* is higher order accurate (between two and four [8]), *b)* removes the higher modes, as demonstrated by a spectral analysis [8], while at the same ensuring a strict algorithmic total energy decay in the nonlinear regime.

The paper is laid out as follows. The classical equations of motion for geometrically exact shells based on inextensible unit directors are presented in section 2. Next, an EP scheme is developed in section 3. Section 4 then presents an ED algorithm with tunable high frequency dissipation that is constructed from the EP scheme. Finally, numerical examples are presented in section 5 to demonstrate the efficiency and robustness of the proposed scheme. A discussion section concludes the paper.

2

2 Formulation of the Equations of Motion

2.1 Kinematics of the Shell Problem

Consider a shell of thickness h and reference surface area Ω, as depicted in fig. 1. An inertial frame of reference $\mathcal{S}$ consisting of three mutually orthogonal unit vectors i_1, i_2, i_3 is used. Let $\underline{r}_0$ be the position vector of an arbitrary point on the reference surface of the shell, and let ζ be the material coordinate along $\underline{n}$, the normal to the reference surface. The position vector $\underline{r}$ of an arbitrary point on the shell in its reference configuration is then

$$\underline{r}(\xi^1,\xi^2,\zeta) = \underline{r}_0(\xi^1,\xi^2) + \zeta\,\underline{n}(\xi^1,\xi^2), \tag{1}$$

where ξ^1 and ξ^2 are the material coordinates used to represent the shell reference surface. The coordinates ξ^1, ξ^2 and ζ form a set of curvilinear coordinates that are a natural choice to represent the shell geometry. The coordinates ξ^1 and ξ^2 are assumed to be lines of curvatures of the shell reference surface. The base vectors are then

$$g = \left[\underline{g}_1,\ \underline{g}_2,\ \underline{g}_3\right] = \left[\underline{r}_{,1},\ \underline{r}_{,2},\ \frac{\partial \underline{r}}{\partial \zeta}\right] = \left[(1 - \frac{\zeta}{R_1})\,\underline{a}_1,\ (1 - \frac{\zeta}{R_2})\,\underline{a}_2,\ \underline{n}\right], \tag{2}$$

where R_1 and R_2 are the principal radii of curvature, $\underline{a}_\alpha = \underline{r}_{0,\alpha}$, and the notation $(\cdot)_{,\alpha}$ is used to denote a derivative with respect to ξ^α. It is convenient to introduce a set of three mutually orthogonal unit vectors at the shell reference surface (i.e. at $\zeta = 0$)

$$\underline{e}_1 = \frac{\underline{a}_1}{\sqrt{a_{11}}}; \quad \underline{e}_2 = \frac{\underline{a}_2}{\sqrt{a_{22}}}; \quad \underline{e}_3 = \underline{n}, \tag{3}$$

where $a_{\alpha\alpha} = \underline{a}_\alpha \cdot \underline{a}_\alpha$.

Two fundamental assumptions will be made concerning the deformation of the shell, i.e. the material line initially normal to the reference surface of the shell remains a straight line and suffers no extension. This is the classical inextensible director model. With these assumptions, the position vector of a material point of the shell writes

$$\underline{R}(\xi^1,\xi^2,\zeta) = \underline{r}_0(\xi^1,\xi^2) + \underline{u}(\xi^1,\xi^2) + \zeta\,\underline{E}_3(\xi^1,\xi^2), \tag{4}$$

where $\underline{u}(\xi^1,\xi^2)$ is the reference surface displacement vector. In the deformed configuration, the base vectors at the shell reference surface are

$$G = [\underline{G}_1,\ \underline{G}_2,\ \underline{G}_3] = \left[\underline{R}_{,1},\ \underline{R}_{,2},\ \frac{\partial \underline{R}}{\partial \zeta}\right]. \tag{5}$$

Introducing the position vector, eq. (4), then yields

$$\hat{G} = \left[\frac{\underline{G}_1}{\sqrt{a_{11}}},\ \frac{\underline{G}_2}{\sqrt{a_{22}}},\ \underline{G}_3\right] = E + \zeta\,H, \tag{6}$$

where

$$E = [\underline{E}_1,\ \underline{E}_2,\ \underline{E}_3] = \left[\underline{e}_1 + \frac{\underline{u}_{,1}}{\sqrt{a_{11}}},\ \underline{e}_2 + \frac{\underline{u}_{,2}}{\sqrt{a_{22}}},\ \underline{E}_3\right]; \quad H = \left[\frac{\underline{E}_{3,1}}{\sqrt{a_{11}}},\ \frac{\underline{E}_{3,2}}{\sqrt{a_{22}}},0\right]. \tag{7}$$

Note that $\underline{E}_3(\xi^1,\xi^2)$ is a unit vector, whereas $\underline{E}_1$ and $\underline{E}_2$ are not unit vectors, nor are they orthogonal to $\underline{E}_3$, as axial and transverse shearing strains develop during deformation.

2.2 Equations of Motion

The Green-Lagrange strain tensor e is defined as

$$e = \frac{1}{2}(G^T G - g^T g). \tag{8}$$

The strain tensor e is defined in the curvilinear coordinate system defined by coordinates ξ^1, ξ^2 and ζ. However, it is more convenient to work with the strain tensor e defined in the locally rectangular system

3

defined by triad $\underline{e}_1$, $\underline{e}_2$, $\underline{e}_3$, see eqs. (3). For *shallow shells* (*i.e.* $\zeta/R_1 \ll 1$ and $\zeta/R_2 \ll 1$) undergoing large displacements and rotations but *small strains* (all strain components are assumed to be small compared to unity), the strain-displacement relationships can be written as

$$e = \frac{1}{2}\left[E^T E - I + \zeta\left(E^T H + H^T E + \kappa\right)\right],$$ (9)

where

$$\kappa = \begin{bmatrix} 1/R_1 & 0 & 0 \\ 0 & 1/R_2 & 0 \\ 0 & 0 & 0 \end{bmatrix}.$$ (10)

It is clear that the strains can be expressed in terms of five parameters: the three components of the displacement field $\underline{u}$ (through $\underline{E}_1$ and $\underline{E}_2$) and the two parameters defining the orientation of the unit director $\underline{E}_3$. Virtual changes in the strain energy of the structure are given by

$$\delta V = \int_\Omega \int_h \delta \bar{V} \, \mathrm{d}\zeta \mathrm{d}\Omega = \int_\Omega \int_h \delta e \cdot \tau \, \mathrm{d}\zeta \mathrm{d}\Omega,$$ (11)

where $\delta \bar{V}$ is the virtual strain energy density, and τ the second Piola-Kirchhoff stress tensor. Introducing the strains, eq. (9), and taking into account the symmetry of the stress tensor then yields

$$\delta \bar{V} = \delta E \cdot (E + \zeta H)\tau + \delta H \cdot \zeta E \tau.$$ (12)

The existence of a strain energy density function $\bar{V}$ is postulated here, hence the constitutive laws are of the form $\tau = \partial \bar{V}/\partial e$.

The velocity vector of material point P of the shell is obtained by differentiating the position vector, eq. (4), with respect to time, to find $\underline{v} = \underline{\dot{u}} + \zeta \underline{\dot{E}}_3$. The kinetic energy of the system is now

$$K = \int_\Omega \int_h \bar{K} \, \mathrm{d}\zeta \mathrm{d}\Omega = \frac{1}{2}\int_\Omega \int_h \rho \, \underline{v} \cdot \underline{v} \, \mathrm{d}\zeta \mathrm{d}\Omega,$$ (13)

where $\bar{K}$ is the kinetic energy density. Introducing the velocity vector then yields

$$\bar{K} = \frac{1}{2}\rho\left(\underline{\dot{u}} + \zeta \underline{\dot{E}}_3\right) \cdot \left(\underline{\dot{u}} + \zeta \underline{\dot{E}}_3\right).$$ (14)

Hamilton's Principle can now be expressed as

$$\int_{t_i}^{t_f} \int_\Omega \int_h (\delta \bar{K} - \delta \bar{V}) \, \mathrm{d}\zeta \mathrm{d}\Omega \mathrm{d}t$$

$$= -\int_{t_i}^{t_f} \int_\Omega \int_h \left[\rho(\delta\underline{u} + \zeta\delta\underline{E}_3)\cdot(\underline{\ddot{u}} + \zeta\underline{\ddot{E}}_3) + \delta E \cdot (E + \zeta H)\tau + \delta H \cdot \zeta E\tau\right] \, \mathrm{d}\zeta \mathrm{d}\Omega \mathrm{d}t$$

$$= 0. \quad (15)$$

Integrating through the thickness of the shell, we get

$$\int_{t_i}^{t_f} \int_\Omega \left\{\delta\underline{u} \cdot \left[\underline{\dot{h}} - (\underline{N}_{1,1} + \underline{N}_{2,2})\right] + \delta\underline{E} \cdot \left[\underline{\dot{g}}_f - (\underline{M}_{1,1} + \underline{M}_{2,2}) + \underline{N}_3\right]\right\} \, \mathrm{d}\Omega \mathrm{d}t = 0.$$ (16)

In this expression, $\underline{h} = m\underline{\dot{u}} + s^*\underline{\dot{E}}_3$, and $\underline{g} = s^*\underline{\dot{u}} + I^*\underline{\dot{E}}_3$ are the linear and angular momentum vectors of the shell, respectively; the mass coefficients are defined as $m = \int_h \rho \, \mathrm{d}\zeta$, $s^* = \int_h \rho\zeta \, \mathrm{d}\zeta$, $I^* = \int_h \rho\zeta^2 \, \mathrm{d}\zeta$. The in-plane forces are $\underline{N}_\alpha = (E\underline{N}_\alpha^* + H\underline{M}_\alpha^*)/\sqrt{a_{\alpha\alpha}}$, the out-of-plane forces $\underline{N}_3 = E\underline{N}_3^*$, and the bending moments $\underline{M}_\alpha = (E\underline{M}_\alpha^*)/\sqrt{a_{\alpha\alpha}}$. The convected forces are $N^* = [\underline{N}_1^*, \underline{N}_2^*, \underline{N}_3^*] = \int_h \tau \, \mathrm{d}\zeta$, and the convected bending moments $M^* = [\underline{M}_1^*, \underline{M}_2^*, \underline{M}_3^*] = \int_h \tau\zeta \, \mathrm{d}\zeta$.

The equations of motion of shells could be derived from this principle by expressing the variations $\delta\underline{E}_3$ in terms of two components of virtual rotation.

4

3   Energy Preserving Scheme

Discrete equations of motion that imply discrete conservation laws for the total mechanical energy, linear momentum and angular momentum of the system will now be developed. The resulting scheme is closely related to that of ref. [30], with the slight difference of more general definitions of the local mass and stiffness tensors which are useful for many engineering applications. Similar energy preserving schemes for geometrically exact shells with extensible directors are given in ref. [28].

Times t_i and t_f denote the initial and final times for a time step, respectively, and the subscripts $(\cdot)_i$ and $(\cdot)_f$ indicate quantities at t_i and t_f, respectively. The time step size is denoted $\Delta t = t_f - t_i$. Furthermore, the subscript $(\cdot)_m$ is used to denote mid-point average quantities defined as

$$(\cdot)_m = \frac{1}{2} \left[(\cdot)_f + (\cdot)_i \right].$$

(17)

The following matrix identity will be used extensively

$$A_f^T B_f - A_i^T B_i = (A_f - A_i)^T B_m + A_m^T (B_f - B_i).$$

(18)

Hamilton's Principle, eq. (15), is now approximated in time in the the following manner

$$\int_\Omega \int_h \left\{ \rho \left[(\underline{u}_f - \underline{u}_i) + \zeta(\underline{E}_{3f} - \underline{E}_{3i}) \right] \cdot \left[\frac{\underline{\dot{u}}_f - \underline{\dot{u}}_i}{\Delta t} + \zeta \frac{\underline{\dot{E}}_{3f} - \underline{\dot{E}}_{3i}}{\Delta t} \right] \right.$$
$$\left. + (E_f - E_i) \cdot (E_m + \zeta H_m)\tau_a + (H_f - H_i) \cdot \zeta E_m \tau_a \right\} \, \mathrm{d}\zeta \mathrm{d}\Omega = 0.$$

(19)

The change in strain components from t_i to t_f is evaluated with the help of identity (18) to find

$$e_f - e_i = \frac{1}{2} \left[(E_f - E_i)^T (E_m + \zeta H_m) + (E_m + \zeta H_m)^T (E_f - E_i) \right.$$
$$\left. + (H_f - H_i)^T \zeta E_m + \zeta E_m^T (H_f - H_i) \right].$$

(20)

Over one time step, the strain components can be approximated as $e(\eta) = e_m + \eta(e_f - e_i)/2$, where $\eta = 2(t - t_m)/\Delta t$ is the non-dimensional time. If the strain energy density function $\bar{V}$ is viewed as a function of the scalar variable η, the mean value theorem then implies the existence of a $\bar{\eta} \in [-1, 1]$ such that

$$\bar{V}_f = \bar{V}_i + \left. \frac{\partial \bar{V}}{\partial e} \right|_{\bar{\eta}} \frac{de}{d\eta} 2 = \bar{V}_i + \tau_a \cdot (e_f - e_i).$$

(21)

This relationship defines the average second Piola-Kirchhoff stress tensor, $\tau_a = \partial \bar{V}/\partial e|_{\bar{\eta}}$. Combining this result with eq. (20) then leads to

$$(E_f - E_i) \cdot (E_m + \zeta H_m)\tau_a + (H_f - H_i) \cdot \zeta E_m \tau_a = (e_f - e_i) \cdot \tau_a = \bar{V}_f - \bar{V}_i,$$

(22)

where the symmetry of the stress tensor was taken into account. For linear constitutive laws of the form $\tau = C^* e$, where C^* is the stiffness matrix, the average stress tensor simply becomes $\tau_a = C^* e_m$.

The following configuration updates are now defined

$$\frac{\underline{u}_f - \underline{u}_i}{\Delta t} = \underline{\dot{u}}_m; \quad \frac{\underline{E}_{3f} - \underline{E}_{3i}}{\Delta t} = \underline{\dot{E}}_{3m}.$$

(23)

Introducing eqs. (22) and (23) into the approximate expression for Hamilton's Principle, eq. (19), then leads to

$$\int_\Omega \int_h \left\{ \rho \left(\underline{\dot{u}}_m + \zeta \underline{\dot{E}}_{3m} \right) \cdot \left[(\underline{\dot{u}}_f - \underline{\dot{u}}_i) + \zeta(\underline{\dot{E}}_{3f} - \underline{\dot{E}}_{3i}) \right] + (\bar{V}_f - \bar{V}_i) \right\} \, \mathrm{d}\zeta \mathrm{d}\Omega$$
$$= \int_\Omega \int_h \left\{ \frac{\rho}{2} \left(\underline{\dot{u}}_f + \zeta \underline{\dot{E}}_{3f} \right) \cdot \left(\underline{\dot{u}}_f + \zeta \underline{\dot{E}}_{3f} \right) - \frac{\rho}{2} \left(\underline{\dot{u}}_i + \zeta \underline{\dot{E}}_{3i} \right) \cdot \left(\underline{\dot{u}}_i + \zeta \underline{\dot{E}}_{3i} \right) + (\bar{V}_f - \bar{V}_i) \right\} \, \mathrm{d}\zeta \mathrm{d}\Omega$$
$$= \int_\Omega \int_h \left[(\bar{K}_f - \bar{K}_i) + (\bar{V}_f - \bar{V}_i) \right] \, \mathrm{d}\zeta \mathrm{d}\Omega = 0.$$

(24)

5

This result clearly implies the conservation of the total mechanical energy of the system within a step. In summary, the approximate form of Hamilton's Principle given by eq. (19) leads to a discrete energy conservation statement, eq. (24), when the configuration updates are chosen according to eqs. (23), and the average stress according to eq. (21).

Integrating through the thickness of the shell leads to

$$\int_\Omega \left\{ (\underline{u}_f - \underline{u}_i) \cdot \left[\frac{\underline{h}_f - \underline{h}_i}{\Delta t} - (\underline{N}_{1m,1} + \underline{N}_{2m,2}) \right] \right. $$
$$\left. + (\underline{E}_{3f} - \underline{E}_{3i}) \cdot \left[\frac{\underline{g}_f - \underline{g}_i}{\Delta t} - (\underline{M}_{1m,1} + \underline{M}_{2m,2}) + \underline{N}_{3m} \right] \right\} \; d\Omega = 0. \quad (25)$$

In this expression, the in-plane forces are $\underline{N}_{\alpha m} = (E_m \underline{N}^*_{\alpha\alpha} + H_m \underline{M}^*_{\alpha\alpha})/\sqrt{a_{\alpha\alpha}}$, the out-of-plane forces $\underline{N}_{3m} = E_m \underline{N}^*_{3\alpha}$, and the bending moments $\underline{M}_{\alpha m} = (E_m \underline{M}^*_{\alpha\alpha})/\sqrt{a_{\alpha\alpha}}$. The discrete governing equations of motion for shells are then

$$\frac{\underline{h}_f - \underline{h}_i}{\Delta t} - (\underline{N}_{1m,1} + \underline{N}_{2m,2}) = \underline{p}_m; \quad (26)$$

$$Q_m^T \frac{\underline{g}_f - \underline{g}_i}{\Delta t} - Q_m^T (\underline{M}_{1m,1} + \underline{M}_{2m,2} - \underline{N}_{3m}) = \underline{q}^*_m, \quad (27)$$

where $\underline{p}$ are the externally applied loads, and $\underline{q}^*$ the externally applied moments measured in the local system. The finite change in director orientation $\underline{E}_{3f} - \underline{E}_{3i}$ was expressed in terms of the two parameter incremental rotation vector, see B.

Invariance of the system Hamiltonian under spatial translations and rotations implies the conservation of the linear and angular momenta. Although discrete preservation of momenta is less crucial than discrete preservation of energy, it is interesting to note that eqs. (26) and (27) also imply the discrete preservation of this invariant. At first, eqs. (26) are projected onto the test functions $\tilde{\pi} (\underline{r}_0 + \underline{u}_m)$ and eqs. (27) onto the test functions $\tilde{\pi} \underline{E}_{3m}$, where $\underline{\pi}$ is an arbitrary vector and $\tilde{\pi}$ is its associated skew-symmetric matrix. Next, integration over the shell reference surface yields

$$\int_\Omega \left\{ \tilde{\pi} (\underline{r}_0 + \underline{u}_m) \cdot \left[\frac{\underline{h}_f - \underline{h}_i}{\Delta t} - (\underline{N}_{1m,1} + \underline{N}_{2m,2}) \right] \right. $$
$$\left. + \tilde{\pi} \underline{E}_{3m} \cdot \left[\frac{\underline{g}_f - \underline{g}_i}{\Delta t} - (\underline{M}_{1m,1} + \underline{M}_{2m,2}) + \underline{N}_{3m} \right] \right\} \; d\Omega = 0. \quad (28)$$

Straightforward algebraic manipulations then lead to

$$\frac{\underline{\pi}}{\Delta t} \cdot \int_\Omega \left[(\tilde{\underline{r}}_0 + \tilde{\underline{u}}_f) \, \underline{h}_f - (\tilde{\underline{r}}_0 + \tilde{\underline{u}}_i) \, \underline{h}_i + \tilde{\underline{h}}_m (\tilde{\underline{u}}_f - \tilde{\underline{u}}_i) \right. $$
$$\left. + \tilde{\underline{E}}_f \underline{g}_f - \tilde{\underline{E}}_i \underline{g}_i + \tilde{\underline{g}}_m (\tilde{\underline{E}}_f - \tilde{\underline{E}}_i) \right] d\Omega = 0, \quad (29)$$

where the following result was used

$$\tilde{\underline{E}}_{1m} \underline{N}_{1m} + \tilde{\underline{E}}_{2m} \underline{N}_{2m} + \tilde{\underline{E}}_{3,1m} \underline{M}_{1m} + \tilde{\underline{E}}_{3,2m} \underline{M}_{2m} + \tilde{\underline{E}}_{3m} \underline{N}_{3m} = 0. \quad (30)$$

Inserting the configuration updates, eqs. (23), into eq. (29) then yields

$$\frac{\underline{\pi}}{\Delta t} \cdot \int_\Omega \left[(\tilde{\underline{r}}_0 + \tilde{\underline{u}}_f) \, \underline{h}_f - (\tilde{\underline{r}}_0 + \tilde{\underline{u}}_i) \, \underline{h}_i + \tilde{\underline{E}}_{3f} \underline{g}_f - \tilde{\underline{E}}_{3i} \underline{g}_i + \left(\tilde{\underline{h}}_m \dot{\underline{u}}_m + \tilde{\underline{g}}_m \dot{\underline{E}}_{3m} \right) \right] d\Omega = 0. \quad (31)$$

It is easily verified that $\tilde{\underline{h}}_m \dot{\underline{u}}_m + \tilde{\underline{g}}_m \dot{\underline{E}}_{3m} = 0$. Hence, since $\underline{\pi}$ is arbitrary, eq. (31) implies the discrete conservation of the total angular momentum, $\int_\Omega [(\tilde{\underline{r}}_0 + \tilde{\underline{u}}) \, \underline{h} + \tilde{\underline{E}} \, \underline{g}] \; d\Omega$. Finally, projecting eqs. (26) onto the test functions $\underline{\pi}$ and eqs. (27) onto the null test functions gives the discrete conservation of the total linear momentum $\int_\Omega \underline{h} \; d\Omega$.

It is important to note that any spatial discretization of the discrete equations of motion will inherit the discrete energy and momentum conservation statements just proved, when the configuration updates are chosen according to eqs. (23), and the average stress according to eq. (21).

6

4 Energy Decaying Scheme

As discussed in the introduction, energy preservation, *per se*, is not sufficient to yield robust time integration schemes. High frequency numerical dissipation must be added as an inherent feature of the scheme. Such a scheme will now be constructed for the shell equations of motion using the EP scheme as a basic building block. Further details on the scheme are given in ref. [8].

First, an additional state is introduced at time $t_j = \lim_{\epsilon \to 0}(t_i + \epsilon)$, and the subscript $(\cdot)_j$ is used to denote quantities at this time. The following averages are now defined

$$(\cdot)_g = \frac{1}{2}\left[(\cdot)_f + (\cdot)_j\right]; \quad (\cdot)_h = \frac{1}{2}\left[(\cdot)_j + (\cdot)_i\right]. \tag{32}$$

The ED scheme proceeds from the initial to the final time by means of two coupled steps: one step from t_i to t_f, the other from t_i to t_j. The time-discrete equations of dynamic equilibrium are

$$\frac{\underline{h}_f - \underline{h}_i}{\Delta t} - \left(\underline{N}_{1g,1} + \underline{N}_{2g,2}\right) = \underline{p}_g;$$

$$Q_m^T \frac{\underline{g}_f - \underline{g}_i}{\Delta t} - Q_g^T \left(\underline{M}_{1g,1} + \underline{M}_{2g,2} - \underline{N}_{3g}\right) = \underline{q}_g^*; \tag{33}$$

$$\frac{\underline{h}_j - \underline{h}_i}{\Delta t} + \frac{1}{3}\left[\left(\underline{N}_{1g,1} + \underline{N}_{2g,2}\right) - \left(\underline{N}_{1p,1} + \underline{N}_{2p,2}\right)\right] = \underline{p}_h;$$

$$Q_h^T \frac{\underline{g}_j - \underline{g}_i}{\Delta t} + \frac{1}{3}\left[Q_g^T\left(\underline{M}_{1g,1} + \underline{M}_{2g,2} - \underline{N}_{3g}\right) - Q_h^T\left(\underline{M}_{1p,1} + \underline{M}_{2p,2} - \underline{N}_{3p}\right)\right] = \underline{q}_h^*. \tag{34}$$

The configuration update relationships are given as

$$\underline{u}_f = \underline{u}_i + \Delta t\,(\dot{\underline{u}}_f + \dot{\underline{u}}_j)/2, \qquad \underline{u}_j = \underline{u}_i - \Delta t\left[\dot{\underline{u}}_f - \dot{\underline{u}}_i - \alpha(\dot{\underline{u}}_j - \dot{\underline{u}}_i)\right]/6;$$

$$\underline{E}_{3f} = \underline{E}_{3i} + \Delta t\,(\dot{\underline{E}}_{3f} + \dot{\underline{E}}_{3j})/2, \quad \underline{E}_{3j} = \underline{E}_{3i} - \Delta t\left[\dot{\underline{E}}_{3f} - \dot{\underline{E}}_{3i} - \alpha(\dot{\underline{E}}_{3j} - \dot{\underline{E}}_{3i})\right]/6, \tag{35}$$

where α is a tuning parameter that controls the amount of numerical dissipation provided by the scheme, while the forces $\underline{N}_{\alpha p}$ and moments $\underline{M}_{\alpha p}$ are given by

$$\underline{N}_{\alpha p} = \underline{N}_{\alpha h} + \alpha\,(\underline{N}_{\alpha j} - \underline{N}_{\alpha i})/2; \quad \underline{M}_{\alpha p} = \underline{M}_{\alpha h} + \alpha\,(\underline{M}_{\alpha j} - \underline{M}_{\alpha i})/2. \tag{36}$$

Using developments similar to those exposed for the EP scheme, it can be easily shown that the proposed discrete equations imply

$$(K_f + V_f) - (K_i + V_i) + \alpha\,c^2 = 0. \tag{37}$$

c^2 is a positive quantity given by

$$c^2 = \int_\Omega \frac{1}{2}\left[m \parallel \dot{\underline{u}} \parallel \cdot \parallel \dot{\underline{u}} \parallel + 2s^* \parallel \dot{\underline{u}} \parallel \cdot \parallel \dot{\underline{E}}_3 \parallel + I^* \parallel \dot{\underline{E}}_3 \parallel \cdot \parallel \dot{\underline{E}}_3 \parallel\right]\,d\Omega$$

$$+ \int_\Omega \frac{1}{2} \parallel \underline{\varepsilon} \parallel C^* \parallel \underline{\varepsilon} \parallel\,d\Omega \geq 0, \tag{38}$$

where $\parallel \cdot \parallel = (\cdot)_j - (\cdot)_i$ is the jump between t_i and t_j. This result implies the decay of the total mechanical energy over one step of the algorithm, $(K_f + V_f) \leq (K_i + V_i)$. The parameter α clearly controls the amount of energy that is dissipated within the step. Two such parameters could be used, controlling the amount of dissipated kinetic and strain energies, respectively, but this level of complexity does not seem to be necessary. The property of preservation of momentum observed in the EP case is lost in the ED algorithm.

If the above ED scheme is applied to a single degree of freedom linear oscillator, the asymptotic value of the spectral radius of the amplification matrix, ρ_∞, is found to be $\rho_\infty = (1 - \alpha)/(1 + \alpha)$. For $\alpha = 1$, $\rho_\infty = 0$, and asymptotic annihilation is achieved. If $\alpha = 0$, $\rho_\infty = 1$, and in view of eq. (37), energy is exactly preserved. Hence, the ED scheme is in fact a family of schemes with a single tuning parameter, α, that controls the amount of high frequency numerical dissipation; both asymptotic annihilation or exact energy

preservation can be achieved with the same scheme by using $\alpha = 1$ or 0, respectively. The spectral radius, algorithmic damping ratio and relative period error, as defined in ref. [24], are plotted in figs. 2 through 4 for varying α.

An error analysis based on Taylor series expansions for the linear harmonic oscillator model problem determined that the ED($\alpha = 0$) scheme is fourth order accurate. For the same model problem, ED($\alpha = 1$) is third order accurate. For general nonlinear problems, numerical experiments show that all methods exhibit convergence rates ranging between two and three.

5 Numerical Examples

All the examples described in this section will be treated with the proposed ED family of schemes corresponding to values of the tuning parameter $\alpha \in [0, 1]$. Although any value of α within this range can be used, the examples described here will contrast the two extreme choices. For $\alpha = 1$ ($\rho_\infty = 0$), asymptotic annihilation is obtained. On the other hand, for $\alpha = 0$ ($\rho_\infty = 1$), exact energy preservation is achieved.

5.1 Clamped Half-Cylinder under Point Load

Consider the half-cylinder of radius $R = 1.2$ m and width $b = 2$ m depicted in fig. 5. The shell has a thickness $t = 6$ mm, is build-in along edge BC and free along the other. The structure is made of aluminum; Young's modulus $E = 73$ GPa, Poisson's ratio $\nu = 0.30$ and density $\rho = 2700$ kg/m^3. At point D, the shell is subjected to a concentrated load $\underline{P} = -P_0(t)(\underline{i}_1 + \underline{i}_2 + \underline{i}_3)$. The magnitude of the load is

$$P_0(t) = \begin{cases} P \, (1 - \cos 2\pi t/T)/2 & t \leq T, \\ 0 & t > T, \end{cases} \tag{39}$$

where $P = 0.1$ kN and $T = 2.0$ s. The shell was modeled by a regular 8×4 mesh of quadratic elements. All simulations were run with a time step $\Delta t = 5.0 \; 10^{-03}$ s, for a total time of 6 s.

Under the effect of the applied loads, the shell bends predominantly in the vertical direction, its direction of least bending stiffness, as illustrated in fig. 6 that shows the configuration of the system at various instants in time. The three components of displacements at point D are shown in fig. 7; vertical displacements of up to 0.6 m are observed. The components of transverse shearing forces are shown in fig. 8.

Next, the same problem was simulated with $\rho_\infty = 1$, i.e. with no high frequency dissipation. The corresponding results are shown in figs. 7 to 8. Displacement and moment results are found to be in excellent agreement. At the scale of the figures, they are, in fact, indistinguishable. For the period of time $2 < t < 6$ s, the system is not subjected to any loading, and the total mechanical energy of the system should remain constant. For the ED($\alpha = 0$) scheme, the energy is indeed preserved, as expected; for the ED($\alpha = 1$) scheme, 0.3% of the energy is numerically dissipated in this period, as depicted in fig. 9. It could be concluded that the ED($\alpha = 0$) and ED($\alpha = 1$) solutions are nearly identical, and that numerical dissipation is not necessary. However, the ED($\alpha = 1$) and ED($\alpha = 0$) scheme predictions for the transverse shearing forces, shown in fig. 8, are markedly different. ED($\alpha = 0$) predictions for force components F_{13} show high frequency oscillations that are absent in the corresponding ED($\alpha = 1$) predictions. A simulation using the ED($\alpha = 1$) scheme with a time step $\Delta t = 1.0 \; 10^{-03}$ s showed that the ED($\alpha = 1$) predictions are converged. A simulation using the ED($\alpha = 0$) scheme and the same smaller time step yielded results with increased high frequency oscillations for the force predictions. It should be noted that the dynamic response of this simple system is very smooth; yet even here, high frequency numerical dissipation appears to be necessary to obtain a smooth, converged solution.

5.2 Dynamic Response of a Plate with Edge Beams

Consider the rectangular plate of length $L = 2$ m, width $b = 0.05$ m and thickness $t = 2$ mm as depicted in fig. 10. Two circular beams of radius $r = 2$ mm are attached at the plate edges. A third circular beam is located at the center of the plate. All components are made of aluminum; Young's modulus $E = 73$ GPa, density $\rho = 2700$ kg/m^3. The total mass of the edge beams is 10 kg each, and that of the central beam is 1 kg. The plate is subjected to uniformly distributed loads F_m and F_ℓ along FE and CB, respectively. The

components of these loads along the $\underline{i}_1$ and $\underline{i}_3$ axes are $F_{1m} = 40$ N/m and $F_{3m} = 80$ N/m, respectively, and $F_{1\ell} = -20$ N/m and $F_{3\ell} = -60$ N/m, respectively. The common time history of each loading component is

$$F_i(t) = \begin{cases} F_i \, (1 - \cos 2\pi t/T)/2 & t \le T, \\ 0 & t > T, \end{cases} \tag{40}$$

where $T = 3.0$ s. The plate is discretized with 10 quadratic plate elements along its length. A constant time step $\Delta t = 6 \; 10^{-03}$ s was used for all simulations.

At time $t > 3$ s the applied load vanishes, and the system total mechanical energy should remain constant. The evolution of the energy of the system for three different cases is shown in fig. 11: the plate model using the ED($\alpha = 1$) scheme, the same plate model using the ED($\alpha = 0$) scheme, and a simplified model of the system using beam elements and the ED($\alpha = 1$) scheme. For times $t > 3$ s, the total energy remains a constant for the ED($\alpha = 0$) scheme and nearly constant for the ED($\alpha = 1$) schemes. The relative energy loss is also presented in the figure: 0.6% of the energy was dissipated by the ED($\alpha = 1$) scheme in the period $t \in [3, 20]$ s. This figure clearly demonstrates the non-increasing property of the energy evolution for the proposed ED($\alpha = 1$) schemes, as opposed the constant energy predicted in ED($\alpha = 0$) simulations. The trajectory of the plate mid-span point is shown in fig. 12: good correlation is observed between the predictions of the three models. The beam model is slightly off due to the inherent simplifying assumptions. The behavior of the quarter-span axial force and transverse shear force are shown in fig. 13 and 14, respectively. The poor predictions of the ED($\alpha = 0$) schemes are obvious in these two plots. The history of axial force presents violent oscillations with amplitudes an order of magnitude larger than those observed for the ED($\alpha = 1$) scheme. The history of the transverse shear force predicted by the ED($\alpha = 0$) scheme quickly diverges from the ED($\alpha = 1$) predictions for both beam and plate models. To ascertain the accuracy of the ED($\alpha = 1$) predictions, a convergence study was performed. Nearly identical results were found with smaller time step sizes $\Delta t = 3.0$ and $1.0 \; 10^{-03}$ s, or when using the time adaptivity procedure. On the other hand, oscillations of increasing amplitude were found as the time step size is reduced in the ED($\alpha = 0$) scheme. Furthermore, the time adaptivity procedure failed to yield any results because the time step size was driven to unreasonably small values, $\Delta t = 10^{-07}$ s, as the procedure tries to cope with increasingly violent oscillations.

5.3 Dynamic Response of a Cruciform

Consider a cruciform consisting of four thin panels (*Panels A, B, C,* and *D*) connected to a central beam, as depicted in fig. 15. Each panel is of thickness $t = 4$ mm, length $L = 1.2$ m, and width $b = 0.1$ m. The central beam has a square cross-section of width $a = 8$ mm. A mass $M = 12$ kg is attached at the tip of the central beam at point T. Panels and beam are simply supported at the root of the cruciform. A concentrated load $P(t)$ is applied at point T. The load acts in the plane defined by axes $\underline{i}_2$ and $\underline{i}_3$ and makes a 30 degree angle with axis $\underline{i}_2$. All components are made of aluminum with properties given in the previous example. The time history of the applied load is

$$P(t) = \begin{cases} P_0 \, (1 - \cos 2\pi t/T)/2 & t \le T, \\ 0 & t > T, \end{cases} \tag{41}$$

where $P_0 = 1.2$ kN and $T = 0.1$ s.

As the applied load increases, in-plane stresses in the panels rapidly increase and buckling takes place in those panels subjected to compression, as can be observed in fig. 16 that depicts the configuration of the cruciform at two instants in time. The trajectory of point T projected onto plane $\underline{i}_2$, $\underline{i}_3$ is shown in fig. 17. For reference, the corresponding trajectory of a beam with cross-sectional properties equivalent to those of the cruciform is also presented. Of course, the equivalent beam model is much stiffer since it does not allow buckling to take place. Furthermore, the motion remains confined to the plane defined by axis $\underline{i}_1$ and the line of action of the applied load. When each panel is modeled individually, the stiffness of system varies both spatially and temporally, giving rise to the more complex motion shown in fig. 17. The total mechanical energy of the system is shown in fig. 18. From time $t = 0.1$ to 0.2 s, the system is free and its total mechanical energy should remain constant. Due the dissipative nature of the integration scheme, a small amount of energy is dissipated over that period of time: 2.7% of the energy was dissipated over the 2435 time step period.

The root shear force and quarter-span bending moment in *Panels A* and *C* are shown in fig. 19 and 20, respectively. Each panel undergoes alternating phases of tensile and compressive loading. During the compressive phases, buckling takes place, and large shear forces and bending moments are observed in contrast with the tensile phases during which these quantities remain much smaller.

5.4 Snap-Through of a Cylindrical Shell

The snap-through behavior of a cylindrical shell under a concentrated load was investigated in ref [27]. The shell consists of a 60 degree sector of a cylinder of height $h = 5$ m, radius $R = 5$ m and thickness $t = 0.1$ m, as shown in fig. 21. Material properties are: Young's modulus $E = 210$ GPa, Poisson ratio $\nu = 0.25$ and density $\rho = 10^4$ kg/m^3. The two straight edges of the shell are simply supported, while the two curved edges are free.

A concentrated force F is applied at the shell's apex. This force linearly increases from 0 to $5\ 10^7$ N in 0.2 s, then is held constant at that value. The simulation ends at time $t = 0.3$ s. Due to the symmetry of the problem, a quarter shell only is modeled; a regular 4×4 mesh of quadratic elements was used. The time step size was selected as $\Delta t = 10^{-3}$ s.

As the load increases, the shell apex displacement increases, then suddenly, snap-through takes place and curvature reverses. Curvature reversal initiates in the region of the applied load, then quickly propagates throughout the entire structure, which undergoes subsequent violent oscillations. Snapshots of the system at various instants in time are given in fig. 22. The vertical displacements of the point of application of the load computed with the ED($\alpha = 1$) scheme is shown in fig. 23. Note the gradual increase of the shell deflection, until collapse at buckling and the resulting vibratory response in the inverted configuration.

Ref. [27] presents simulations of this problem using various schemes: the generalized-α [21] and the CEMA [27] schemes. The former scheme features high frequency numerical dissipation and linear stability properties, while the latter adds to the generalized-α method a constraint on the total mechanical energy of the system. CEMA is therefore both energy preserving and high frequency dissipative. The results presented in fig. 23 are in close agreement with those obtained with the generalized-α scheme, but quite different from those predicted by CEMA in the post buckling regime. It is important to realize that the higher modes are only an artifact of the discretization process, and should therefore be *removed* from the computed response. A standard scheme like the generalized-α method accomplishes this goal through the characteristic low-pass shape of its spectral radius; however, there is no guarantee that energy will not be allowed to grow within one step for nonlinear problems. In contrast, CEMA enforces the exact conservation of energy in the nonlinear regime, but at the same time inherits high frequency dissipation from the underlying generalized-α algorithm. Consequently, an artificial mechanism for transferring energy from the higher (artificial) modes to the lower modes is created that drives the response to an erroneous solution. In contrast, the proposed ED scheme achieves both nonlinear stability and high frequency dissipation.

Next, the same problem was simulated with $\rho_\infty = 1$, *i.e.* with no high frequency dissipation. In this case, two refinements in time step size were required to successfully complete the simulation, one at time $t = 0.1665$ s ($\Delta t = 5\ 10^{-4}$ s), the other at time $t = 0.2142$ s ($\Delta t = 2.5\ 10^{-4}$ s). Deflections predicted by the ED($\alpha = 0$) and ED($\alpha = 1$) schemes, shown in fig. 23, are in good agreement during the initial snap-through phase, but become increasingly different during the subsequent oscillations. The force and velocity fields are markedly different. The plate center forces for both ED($\alpha = 0$) and ED($\alpha = 1$) schemes are shown in fig. 24. The forces predicted by the ED($\alpha = 0$) scheme present violent oscillations of amplitude up to an order of magnitude larger than those predicted by the ED($\alpha = 1$) scheme. These violent oscillations hamper the convergence of the Newton process at each time step, leading to the need for smaller time steps. The same observations can be made about fig. 25 which compares the plate center vertical velocity. Violent oscillations are initiated at snap-through and the strict preservation of energy implied by the ED($\alpha = 0$) scheme prevents any subsequent decay of these vibrations. Since vibratory stresses are a great importance to designers, it is essential to assess the ability of new integration schemes to reliably predict these quantities. It is unfortunate that many scientific publications about geometric integration only present responses for preserved quantities such as total mechanical energy or momentum. The above plots demonstrate that while ED($\alpha = 0$) scheme might perform very well for the prediction of total energy, momentum, or even displacement fields, they are unable to reliably predict other important fields such as velocities and internal stresses. Consequently, such schemes are of little values in real life applications.

10

6 Conclusions

In this work, a robust algorithm for the dynamic analysis of geometrically exact shell structures was presented. The method is geometry-based, *i.e.* it incorporates knowledge about specific qualitative features of the underlying partial differential equations. However, departing from the classical approaches based on strict preservation of energy, the method presented here allows the system to drift away from the level set of constant energy in a controlled and tunable manner.

This feature achieves two goals. First, a bound is placed on the total mechanical energy of the discrete system, leading to the concept of nonlinear unconditional stability; this stability criterion is stronger than that obtained through the classical analysis of numerical schemes. The resulting numerical procedure is endowed with superior robustness, an important feature when dealing with complex engineering problems. Second, the monotonic energy drift is associated with numerical dissipation of the high frequency modes. This tunable dissipation makes the algorithm stiffly accurate, and avoids the build up of energy in the higher modes that are an artifact of the spatial discretization process.

The proposed scheme can deal with general shell structures and is not tied to a specific spatial discretization of the governing partial differential equations. Kinematic nonlinearities are treated in a rigorous manner, and material nonlinearities can be handled when the constitutive laws stem from the existence of a strain energy density function. The efficiency and robustness of the proposed approach were demonstrated with specific numerical examples.

[1] F. ARMERO AND E. PETÖCZ, *Formulation and analysis of conserving algorithms for frictionless dynamic contact/impact problems*, Computer Methods in Applied Mechanics and Engineering, 158 (1998), pp. 269–300.

[2] K. BATHE AND E. DVORKIN, *A four-node plate bending element based on Mindlin/ Reissner plate theory and a mixed interpolation*, International Journal for Numerical Methods in Engineering, 21 (1985), pp. 367–383.

[3] ——, *A formulation of general shell elements - The use mixed interpolation of tensorial components*, International Journal for Numerical Methods in Engineering, 22 (1986), pp. 697–722.

[4] O. BAUCHAU, *Computational schemes for flexible, nonlinear multi-body systems*, Multibody System Dynamics, 2 (1998), pp. 169–225.

[5] ——, *On the modeling of friction and rolling in flexible multi-body systems*, Multibody System Dynamics, 3 (1999), pp. 209–239.

[6] ——, *Analysis of flexible multi-body systems with intermittent contacts*, Multibody System Dynamics, 4 (2000), pp. 23–54.

[7] O. BAUCHAU AND C. BOTTASSO, *On the design of energy preserving and decaying schemes for flexible, nonlinear multi-body systems*, Computer Methods in Applied Mechanics and Engineering, 169 (1999), pp. 61–79.

[8] O. BAUCHAU, C. BOTTASSO, AND L. TRAINELLI, *Robust integration schemes for flexible multibody systems*, Computer Methods in Applied Mechanics and Engineering, 192 (2003), pp. 395–420.

[9] O. BAUCHAU, J. CHOI, AND C. BOTTASSO, *On the modeling of shells in multibody dynamics*, Multibody System Dynamics, 8 (2002), pp. 459–489.

[10] O. BAUCHAU AND T. JOO, *Computational schemes for nonlinear elasto-dynamics*, International Journal for Numerical Methods in Engineering, 45 (1999), pp. 693–719.

[11] O. BAUCHAU AND N. THERON, *Energy decaying scheme for non-linear beam models*, Computer Methods in Applied Mechanics and Engineering, 134 (1996), pp. 37–56.

[12] ——, *Energy decaying schemes for nonlinear elastic multi-body systems*, Computers and Structures, 59 (1996), pp. 317–331.

[13] M. BORRI, C. BOTTASSO, AND L. TRAINELLI, *A novel momentum-preserving energy-decaying algorithm for finite element multibody procedures*, in Proceedings of Computational Aspects of Nonlinear Structural Systems with Large Rigid Body Motion, NATO Advanced Research Workshop, Pultusk, Poland, July 2-7, J. Ambrósio and M. Kleiber, eds., 2000, pp. 549–568.

[14] M. BORRI, L. TRAINELLI, AND C. BOTTASSO, *On representations and parameterizations of motion*, Multibody Systems Dynamics, 4 (2000), pp. 129–193.

[15] C. BOTTASSO AND M. BORRI, *Energy preserving/decaying schemes for non-linear beam dynamics using the helicoidal approximation*, Computer Methods in Applied Mechanics and Engineering, 143 (1997), pp. 393–415.

[16] ——, *Integrating finite rotations*, Computer Methods in Applied Mechanics and Engineering, 164 (1998), pp. 307–331.

[17] C. BOTTASSO, M. BORRI, AND L. TRAINELLI, *Integration of elastic multibody systems by invariant conserving/dissipating algorithms. Part I: formulation*, Computer Methods in Applied Mechanics and Engineering, 190 (2001), pp. 3669–3699.

[18] ——, *Integration of elastic multibody systems by invariant conserving/dissipating algorithms. Part II: numerical schemes and applications*, Computer Methods in Applied Mechanics and Engineering, 190 (2001), pp. 3701–3733.

[19] M. BUCALEM AND K. BATHE, *Higher-order MITC general shell elements*, International Journal for Numerical Methods in Engineering, 36 (1993), pp. 3729–3754.

[20] C. BUDD AND A. ISERLES, *Geometric integration: Numerical solution of differential equations on manifolds*, Philosophical Transactions of the Royal Society of London Series A-Mathematical Physical and Engineering Sciences, 357 (1999), pp. 945–956.

[21] J. CHUNG AND G. HULBERT, *A time integration algorithm for structural dynamics with improved numerical dissipation: The generalized-α method*, Journal of Applied Mechanics, 60 (1993), pp. 371–375.

[22] M. CRISFIELD, U. GALVANETTO, AND G. JELENIĆ, *Dynamics of 3-d co-rotational beams*, Computational Mechanics, 20 (1997), pp. 507–519.

[23] H. HILBER, T. HUGHES, AND R. TAYLOR, *Improved numerical dissipation for time integration algorithms in structural dynamics*, Earthquake Engineering and Structural Dynamics, 5 (1977), pp. 282–292.

[24] T. HUGHES, *Analysis of transient algorithms with particular reference to stability behavior*, in Computational Methods for Transient Analysis, T. Belytschko and T. Hughes, eds., North-Holland, Amsterdam, 1983, pp. 67–155.

[25] T. KANE AND D. LEVINSON, *Dynamics: Theory and Applications*, McGraw-Hill, Inc., New York, 1985.

[26] D. KUHL AND M. CRISFIELD, *Energy conserving and decaying algorithms in non-linear structural dynamics*, International Journal for Numerical Methods in Engineering, 45 (1999), pp. 569–599.

[27] D. KUHL AND E. RAMM, *Constraint energy momentum algorithm and its application to non-linear dynamics of shells*, Computer Methods in Applied Mechanics and Engineering, 136 (1996), pp. 293–315.

[28] C. SANSOUR, P. WRIGGERS, AND J. SANSOUR, *Nonlinear dynamics of shells: Theory, finite element formulation and integration schemes*, Nonlinear Dynamics, 13 (1997), pp. 279–305.

[29] J. SIMO AND N. TARNOW, *The discrete energy-momentum method. Conserving algorithms for nonlinear dynamics*, ZAMP, 43 (1992), pp. 757–792.

[30] ———, *A new energy and momentum conserving algorithm for the nonlinear dynamics of shells*, International Journal for Numerical Methods in Engineering, 37 (1994), pp. 2527–2549.

[31] J. SIMO, N. TARNOW, AND M. DOBLARE, *Non-linear dynamics of three-dimensional rods: Exact energy and momentum conserving algorithms*, International Journal for Numerical Methods in Engineering, 38 (1995), pp. 1431–1473.

[32] J. SIMO AND K. WONG, *Unconditionally stable algorithms for rigid body dynamics that exactly preserve energy and momentum*, International Journal for Numerical Methods in Engineering, 31 (1991), pp. 19–52.

A Rodrigues Parameters

It is clear that any parameterization of finite rotations [25] could be used with the present shell formulation. In particular, we have used the Rodrigues parameters $\underline{r} = 2\underline{k} \tan\phi/2$, where ϕ is the magnitude of the finite rotation and $\underline{k}$ the components of the unit vector about which it takes place. The following notation is introduced $r_0 = \cos^2\phi/2 = 1 / (1 + \underline{r}^T \underline{r}/4)$, and the finite rotation tensor R then writes

$$R(\underline{r}) = I + r_0\, \tilde{r} + \frac{r_0}{2}\, \widetilde{r}\widetilde{r}. \tag{1}$$

The following decomposition of the rotation tensor is extensively used in this work

$$R = \left(I + \frac{\tilde{r}}{2}\right)\left(I + \frac{\tilde{r}}{2}\right)^{-T} = \left(I + \frac{\tilde{r}}{2}\right)^{-T}\left(I + \frac{\tilde{r}}{2}\right); \quad \left(I + \frac{\tilde{r}}{2}\right)^{-T} = \frac{R + I}{2}. \tag{2}$$

B Orientation of a Unit Director

Consider a unit vector $\underline{i}_3$, called a *director*, that rotates to a final orientation $\underline{e}_3$. For convenience, this director is considered to be the third unit vector of a triad $\mathcal{S}$ defined by $\underline{i}_1, \underline{i}_2, \underline{i}_3$, rotating to a triad $\mathcal{S}^*$ with orientation $\underline{e}_1, \underline{e}_2, \underline{e}_3$. The relationship between these two triads is $\underline{e}_\alpha = R\,\underline{i}_\alpha$, where R is an orthogonal rotation tensor. If one solely focuses on the director, this rotation tensor is not uniquely defined, as any rotation about the director leaves its orientation unchanged. A virtual change in the director orientation is

$$\delta\underline{e}_3 = \widetilde{e}_3^T\,\delta\underline{\psi}, \tag{1}$$

where $\delta\underline{\psi}$ is the virtual rotation vector, $\widetilde{\delta\psi} = \delta R R^T$.

The components of the virtual change in director orientation measured in $\mathcal{S}^*$ become

$$R^T\delta\underline{e}_3 = R^T\widetilde{e}_3^T\delta\underline{\psi} = \widetilde{i}_3^T R^T\delta\underline{\psi} = \widetilde{i}_3^T\delta\underline{\psi}^* = \begin{vmatrix} -\delta\psi_2^* \\ \delta\psi_1^* \\ 0 \end{vmatrix}, \tag{2}$$

where $\delta\underline{\psi}^*$ are the components of the virtual rotation vector in $\mathcal{S}^*$. This relationship clearly demonstrates that arbitrary values of $\delta\psi_3^*$, corresponding to virtual rotations of the director about its own orientation, will not affect virtual changes in the director orientation, and hence, setting $\delta\psi_3^* = 0$ is a valid choice. The following notation is adopted

$$\delta\underline{\psi}^* = \underline{i}_1\delta\alpha_1^* + \underline{i}_2\delta\alpha_2^* = b\,\delta\underline{\alpha}^*; \quad b = [\underline{i}_1, \underline{i}_2]. \tag{3}$$

$\delta\underline{\alpha}^*$ is a 2×1, "two parameter" virtual rotation vector. It follows that $\delta\underline{\psi} = R\,\delta\underline{\psi}^* = Rb\,\delta\underline{\alpha}^*$, and hence

$$\delta\underline{e}_\alpha = R\,\widetilde{i}_\alpha^T\, b\,\delta\underline{\alpha}^*. \tag{4}$$

If Rodrigues parameters are used to parameterize R, an equivalent expression can be obtained for finite changes in director orientation with the help of eq. (2)

$$\underline{e}_{\alpha f} - \underline{e}_{\alpha i} = R_m\,\widetilde{i}_\alpha^T\, b\,\underline{s}^* = Q_m\,\underline{s}^*; \quad \underline{r}^* = b\,\underline{s}^*, \tag{5}$$

where $\underline{r}^*$ are the Rodrigues parameter measured in $\mathcal{S}^*$, and $\underline{s}^*$ the corresponding "two parameter" incremental rotation vector.

14
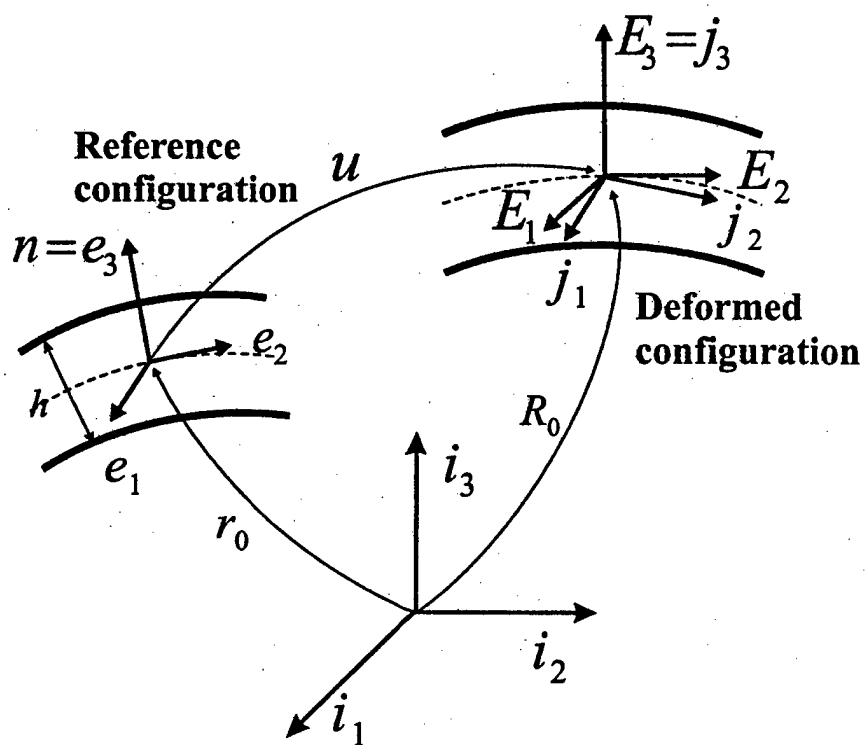
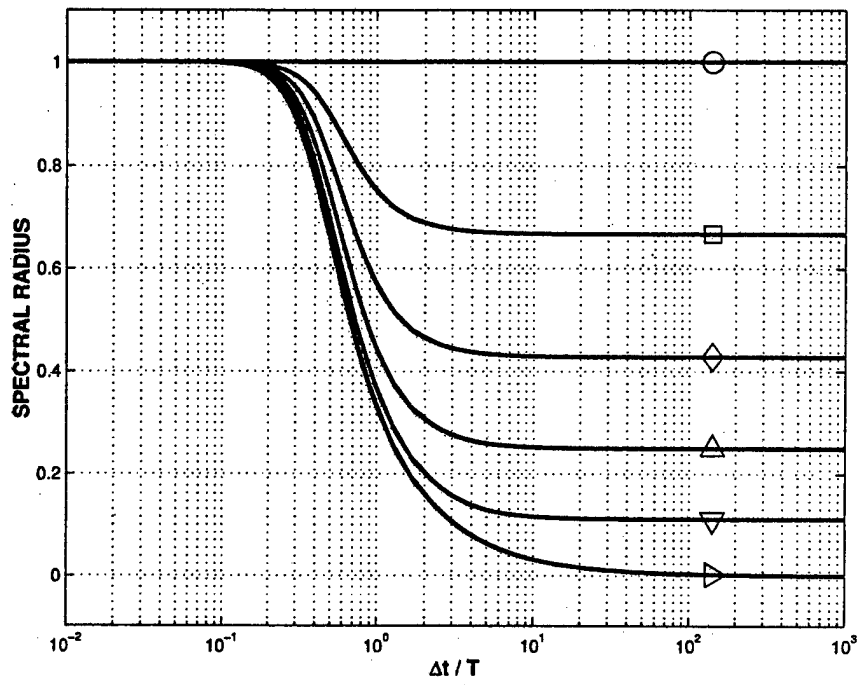Figure 1: Configuration of the shell in the reference and deformed configurations.

Figure 2: Spectral radius of the ED scheme for varying α: $\circ = 0.0, \square = 0.2, \lozenge = 0.4, \triangle = 0.6, \nabla = 0.8, \triangleright = 1.0$.
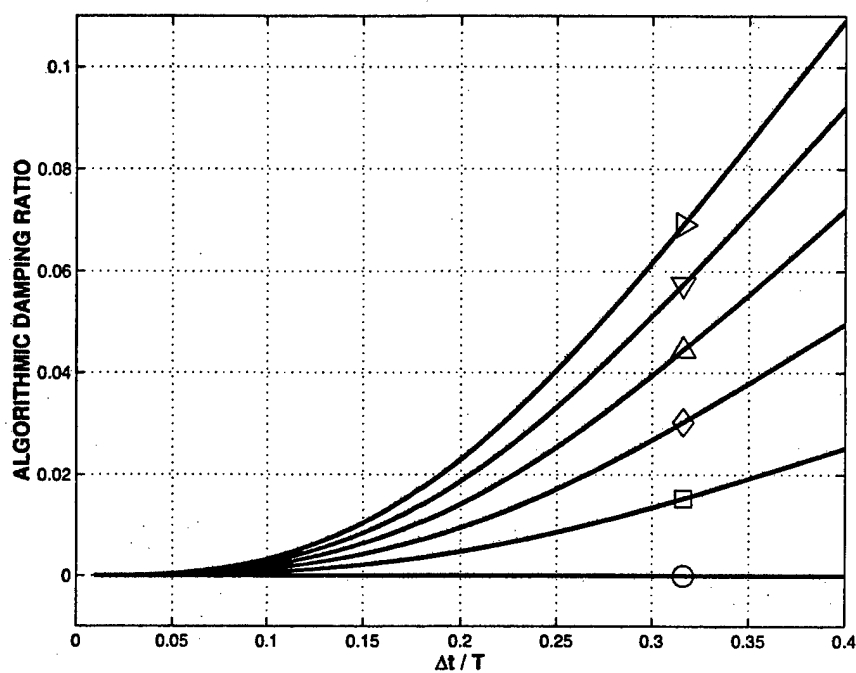
Figure 3: Algorithmic damping ratio of the ED scheme for varying α: $\circ = 0.0, \square = 0.2, \Diamond = 0.4, \triangle = 0.6, \nabla = 0.8, \triangleright = 1.0$.
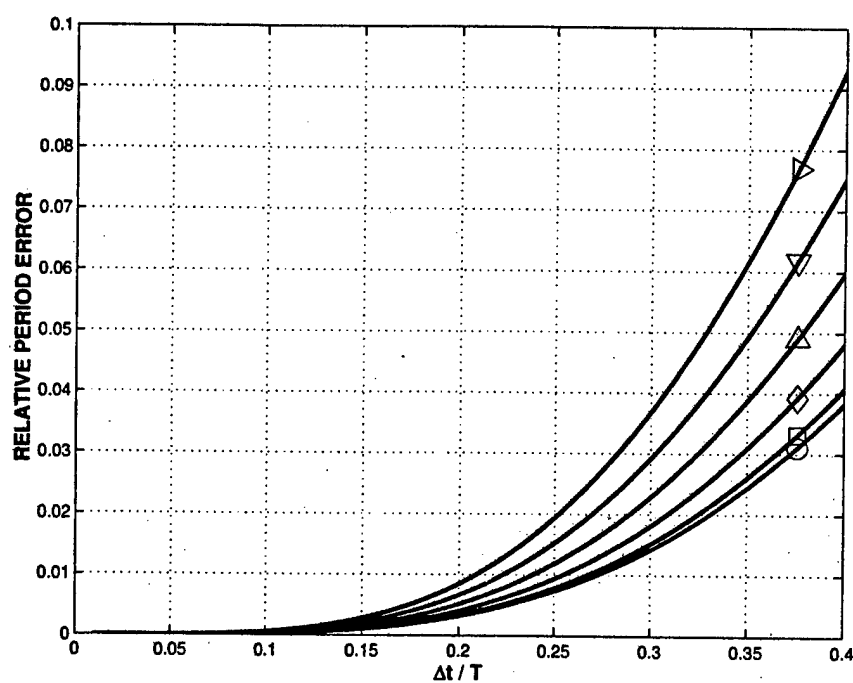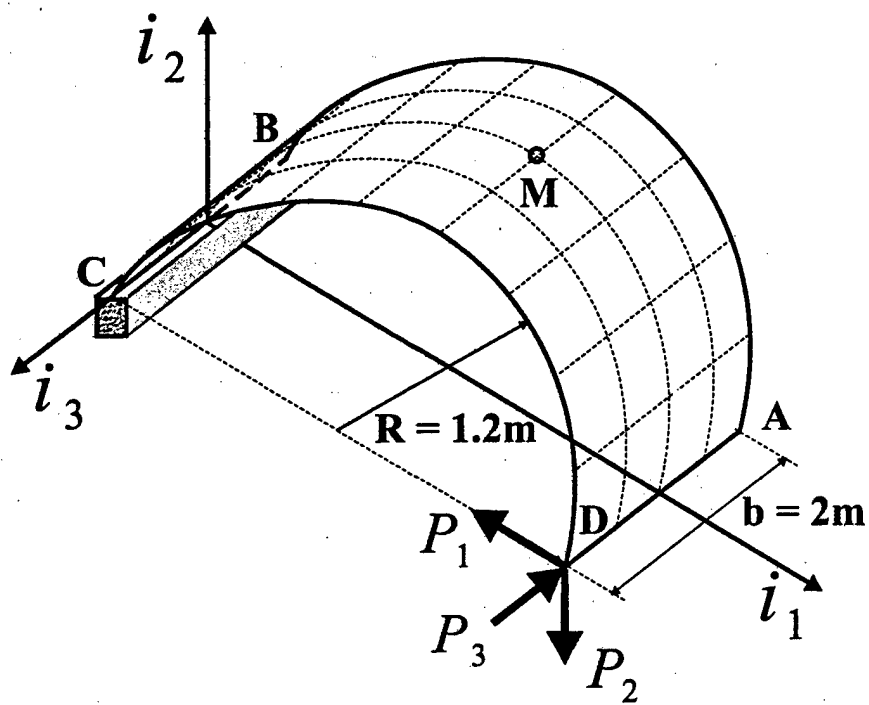
Figure 4: Relative period error of the ED scheme for varying α: $\circ = 0.0, \square = 0.2, \Diamond = 0.4, \triangle = 0.6, \nabla = 0.8, \triangleright = 1.0$.

Figure 5: Configuration of the clamped half-cylinder.
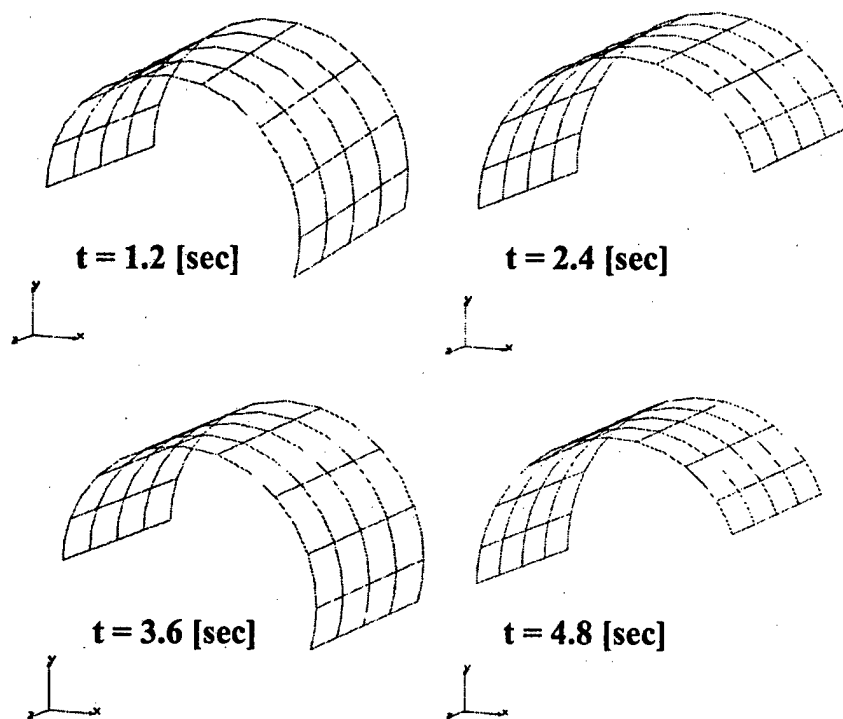
Figure 6: Configuration of the system at various instants in time.
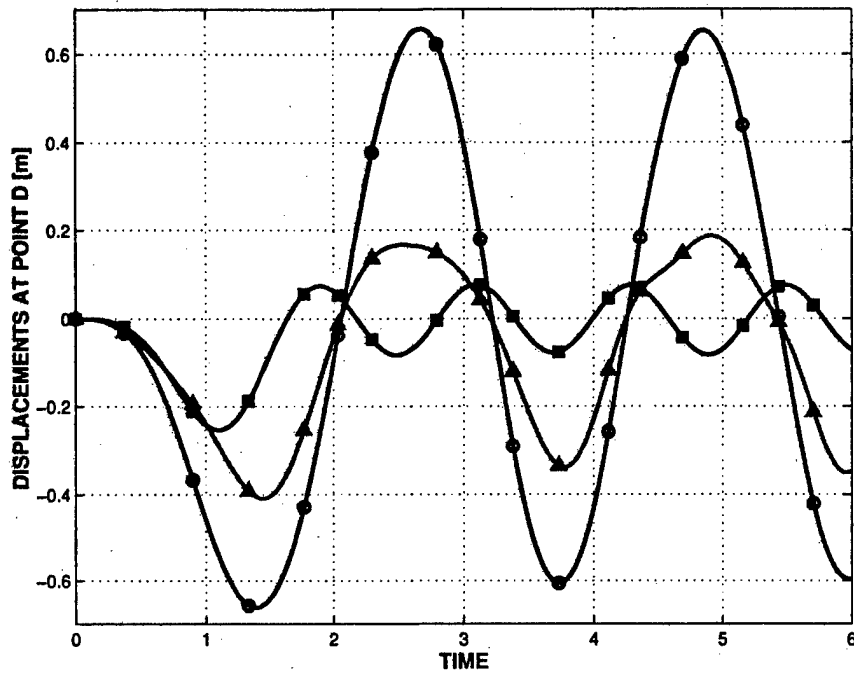
Figure 7: Displacement components at point D. U_1: $\triangle$; U_2: $\circ$; U_3: $\square$. ED($\alpha = 1$) scheme: solid line; ED($\alpha = 0$) scheme: dashed line.
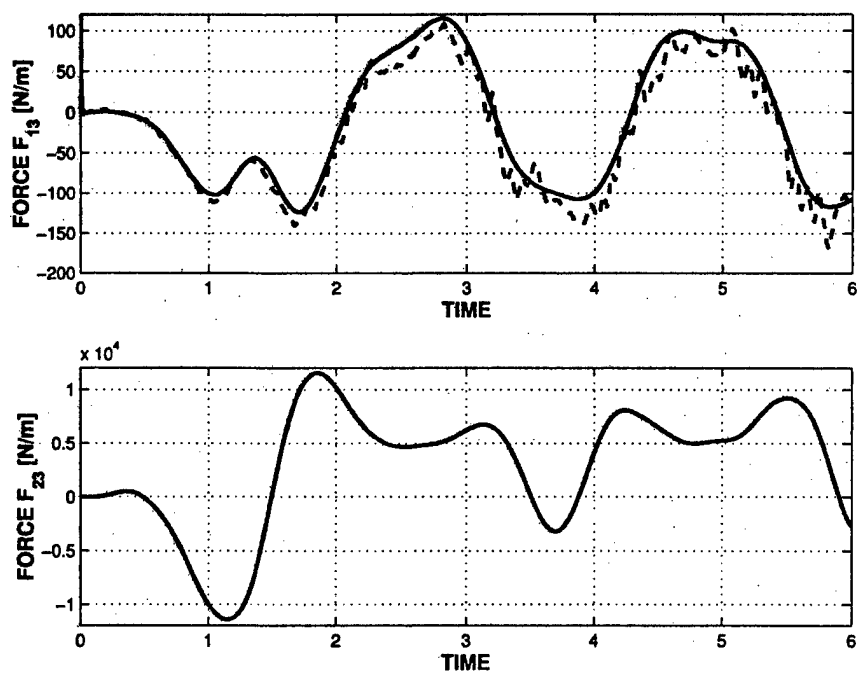
Figure 8: Time history of transverse shear forces at point M. F_{13}: top figure; F_{23}: bottom figure. ED($\alpha = 1$) scheme: solid line; ED($\alpha = 0$) scheme: dashed line.

22
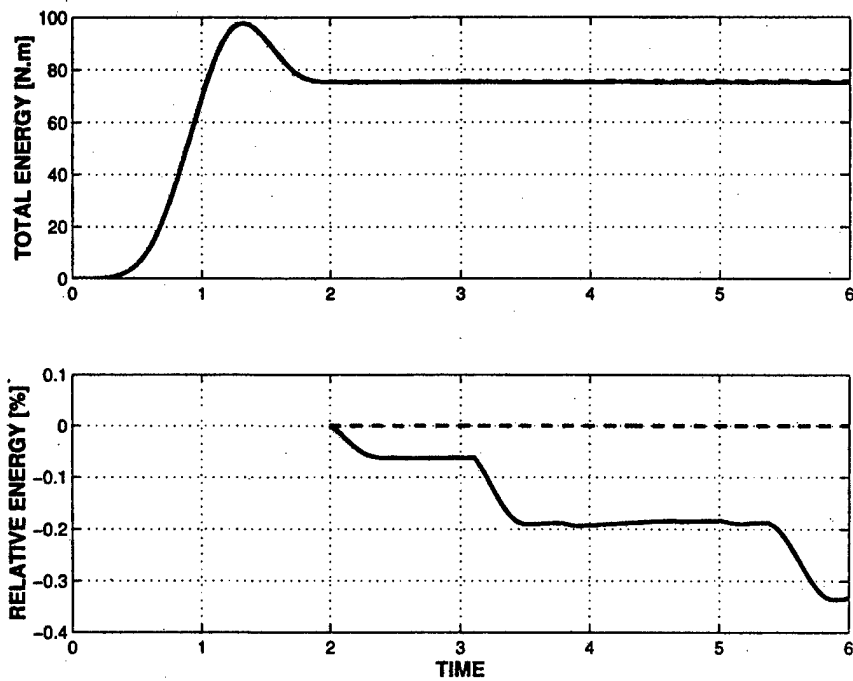
Figure 9: Time history of total energy of the system (top figure). Relative total energy loss from time $t \in [2,6]$ sec (bottom figure). ED($\alpha = 1$) scheme: solid line; ED($\alpha = 0$) scheme: dashed line.
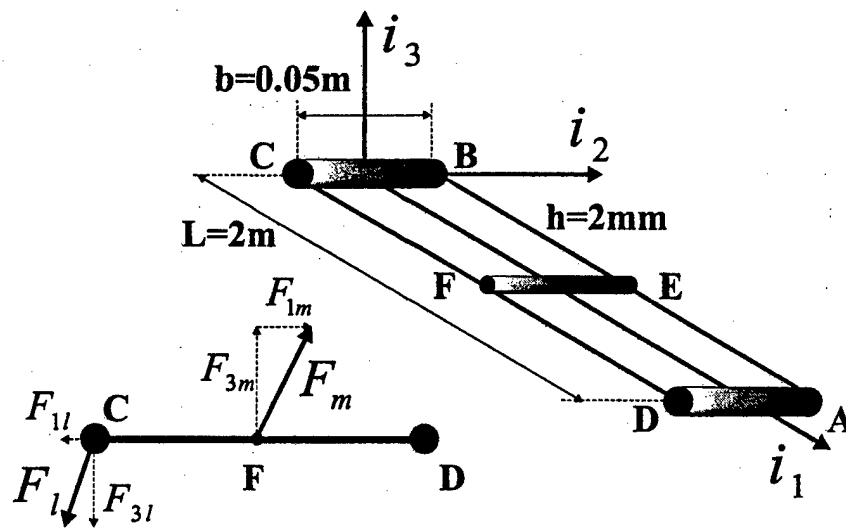
Figure 10: Configuration of the plate with concentrated masses.
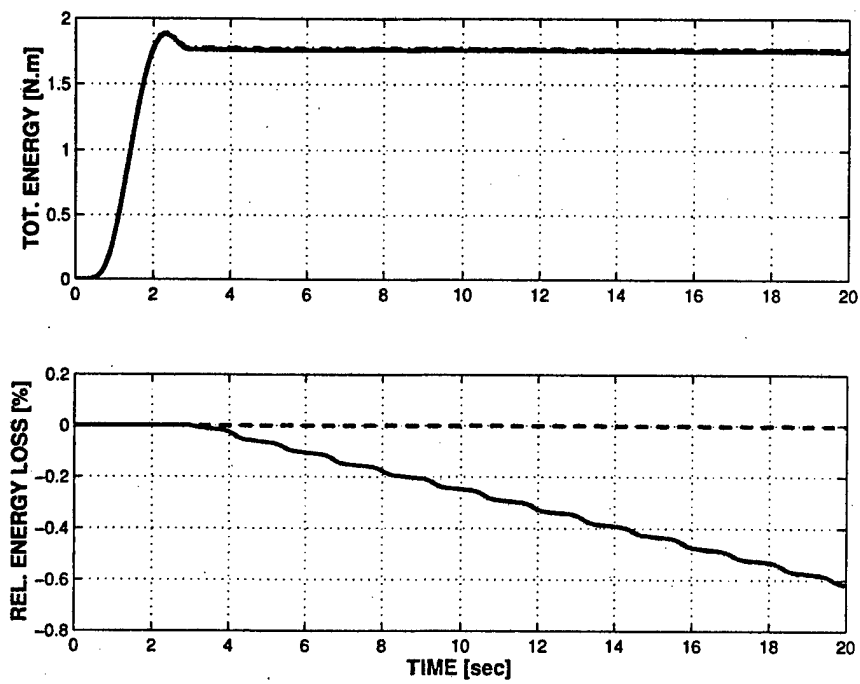
Figure 11: Time history of the total mechanical energy (top figure) and relative energy loss (bottom figure). Plate model (ED($\alpha = 1$)): solid line; Plate model (ED($\alpha = 0$)): dashed line; Beam model (ED($\alpha = 1$)): dashed-dot line.
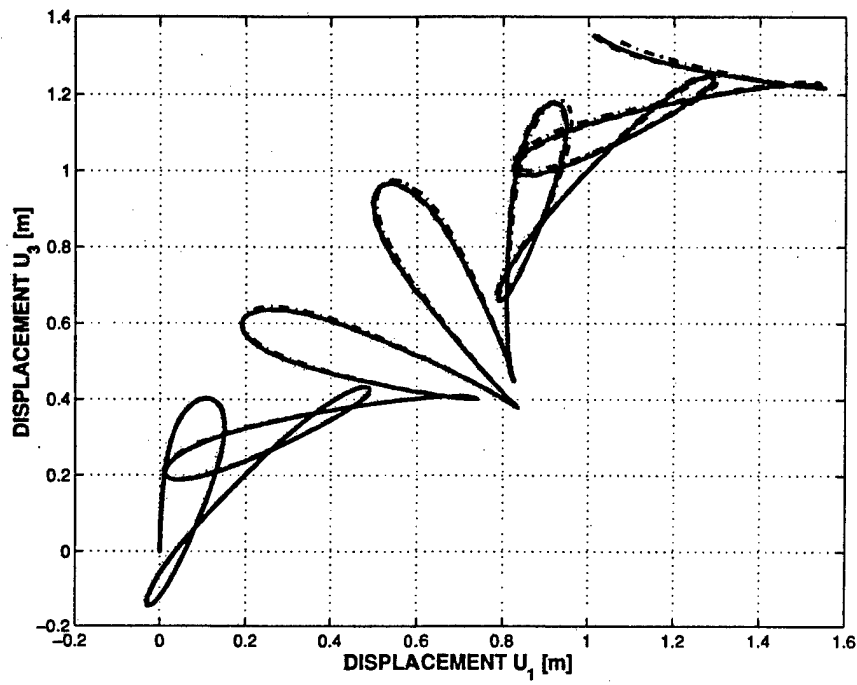
Figure 12: Trajectory of the plate mid-span point. Plate model (ED($\alpha = 1$)): solid line; Plate model (ED($\alpha = 0$)): dashed line; Beam model (ED($\alpha = 1$)): dashed-dot line.
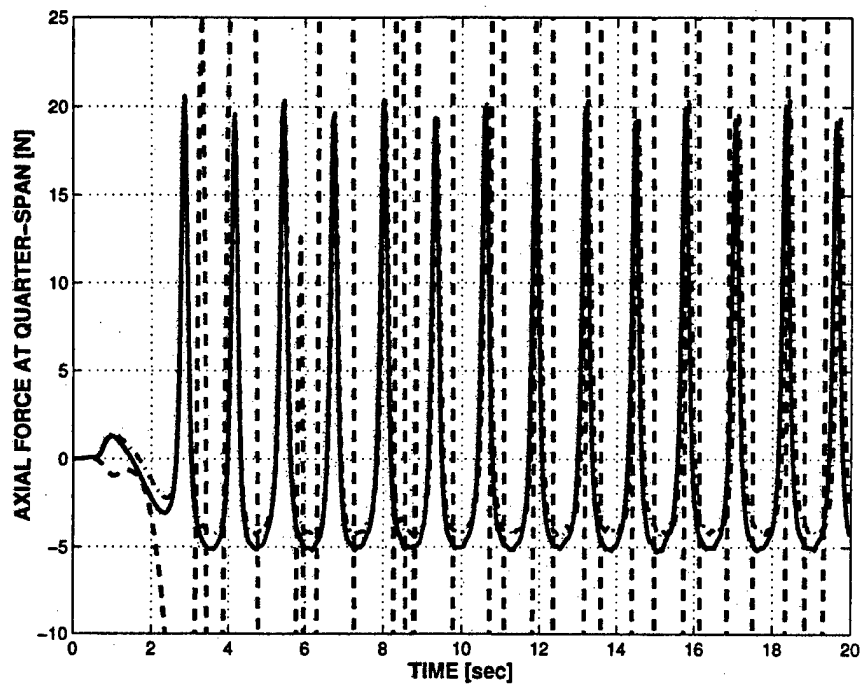
Figure 13: Time history of the quarter-span axial force. Plate model (ED($\alpha = 1$)): solid line; Plate model (ED($\alpha = 0$)): dashed line; Beam model (ED($\alpha = 1$)): dashed-dot line.
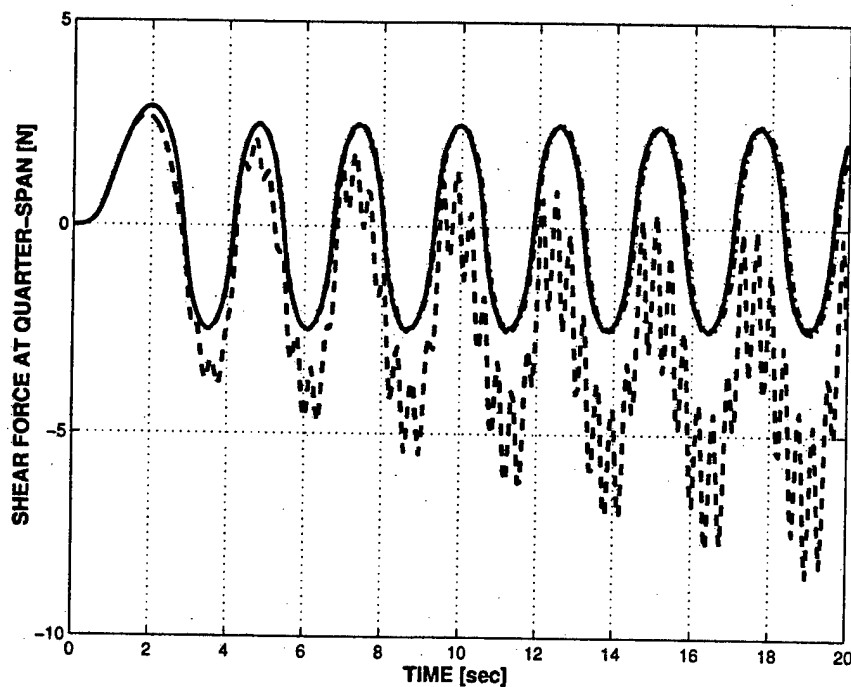
Figure 14: Time history of the quarter-span transverse shear force. Plate model (ED($\alpha = 1$)): solid line; Plate model (ED($\alpha = 0$)): dashed line; Beam model (ED($\alpha = 1$)): dashed-dot line.
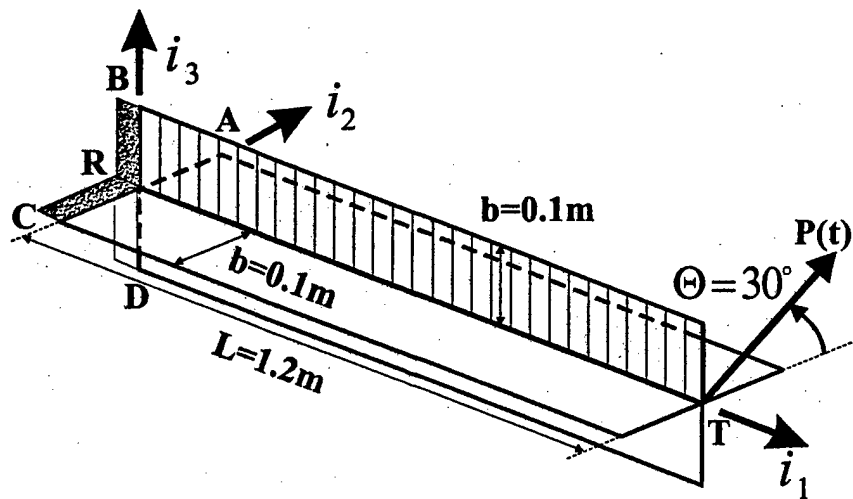
Figure 15: Configuration of the cruciform problem.

t=0.062 sec.

t=0.093sec
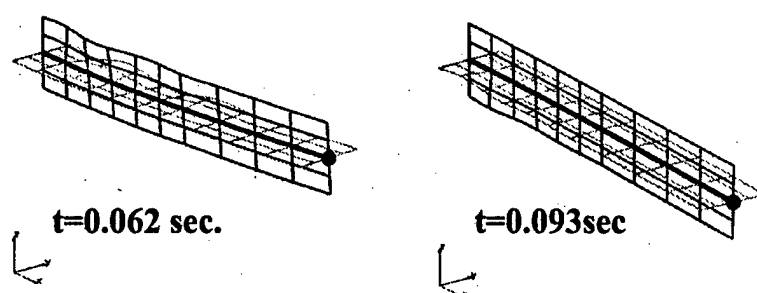
Figure 16: Configuration of the cruciform at times $t = 0.062$ and 0.093 s.
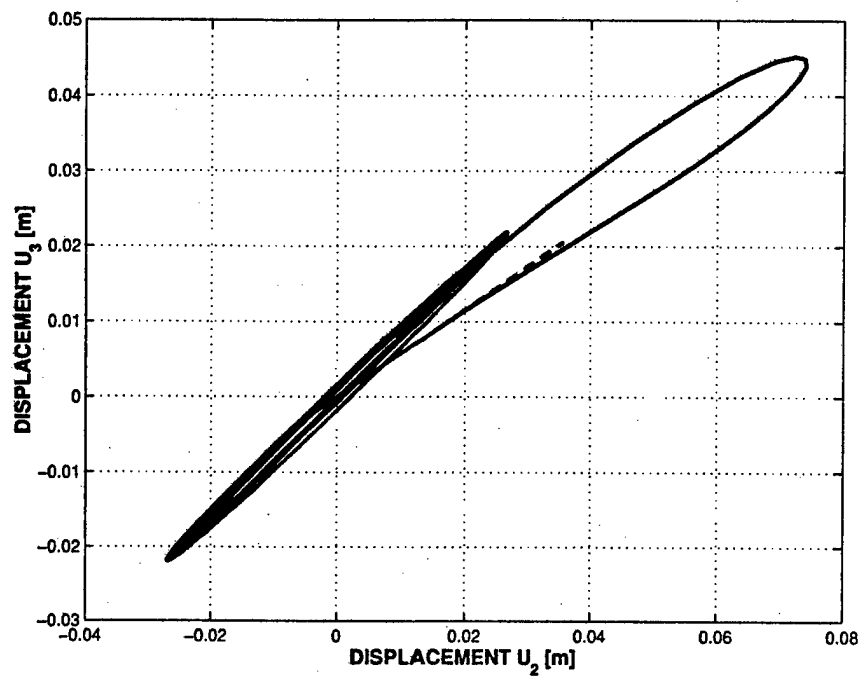
Figure 17: Trajectory of point T of the cruciform projected in the plane i_2, i_3. Solid line: shell model; dashed line: beam model.
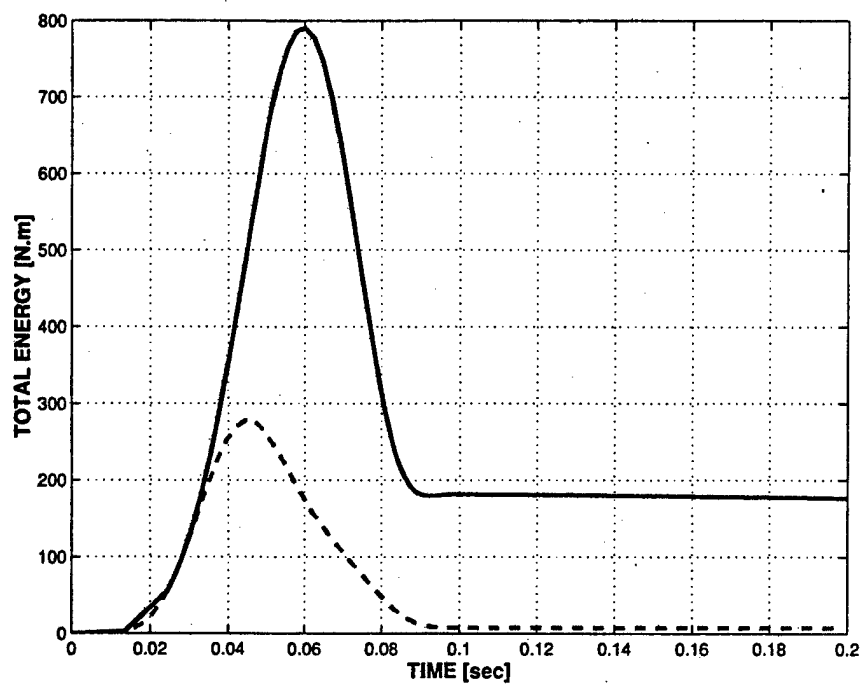
Figure 18: Total mechanical energy of the system. Solid line: shell model; dashed line: beam model.
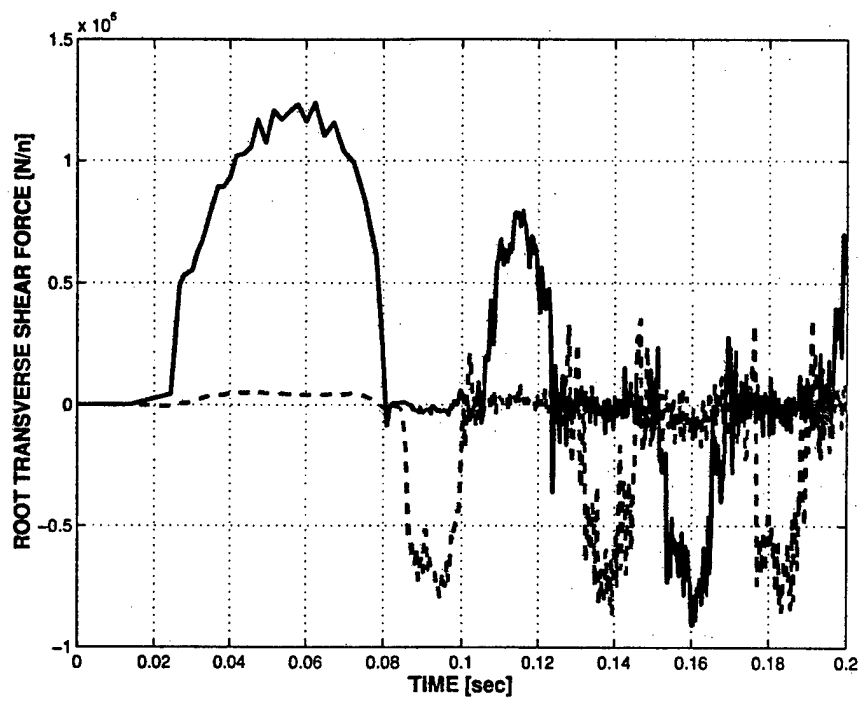
Figure 19: Time history of the root shear force in *Panel A* (solid line) and *Panel C* (dashed line).
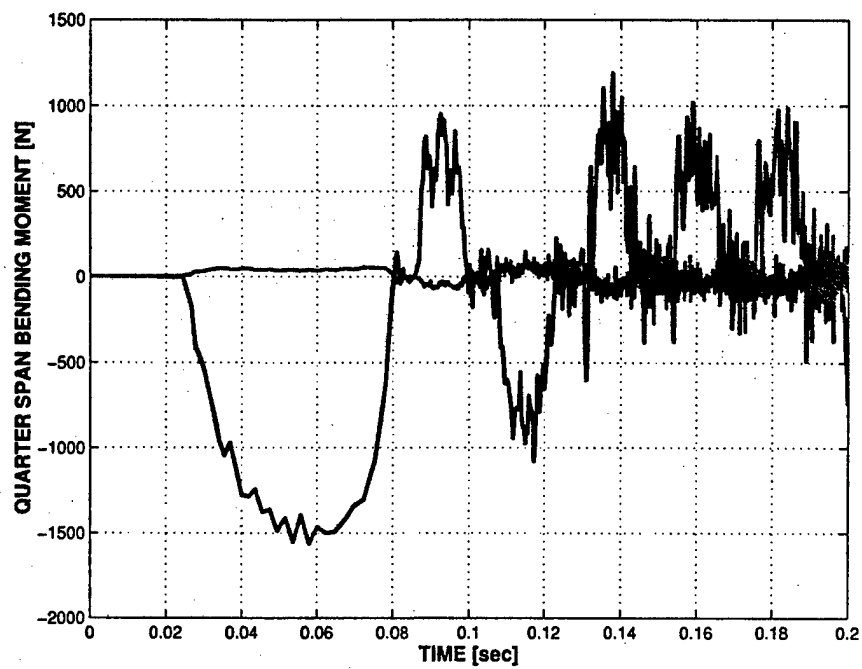
Figure 20: Time history of the quarter-span bending moment in *Panel A* (solid line) and *Panel C* (dashed line).
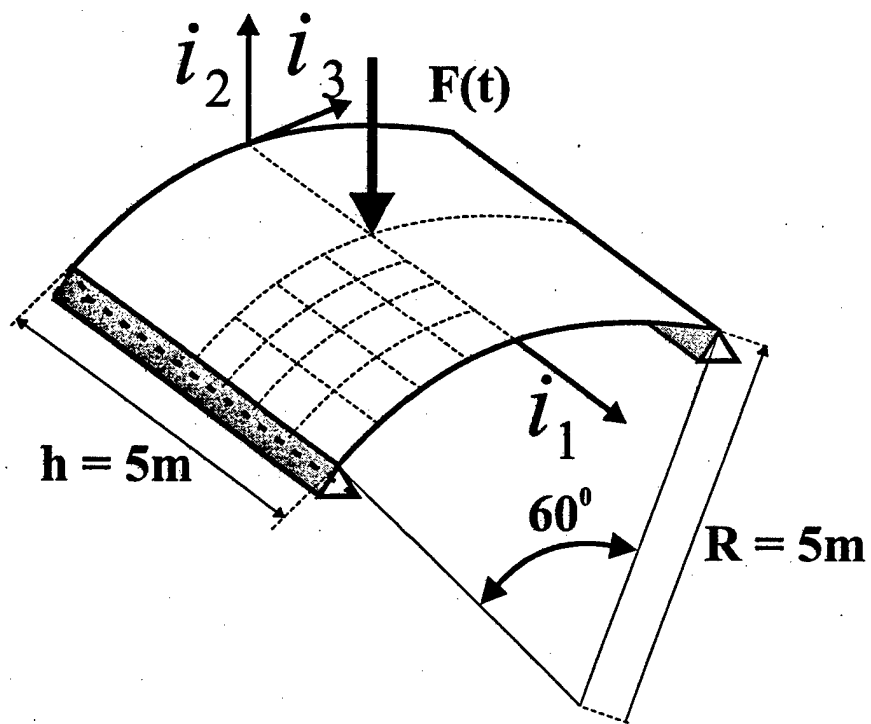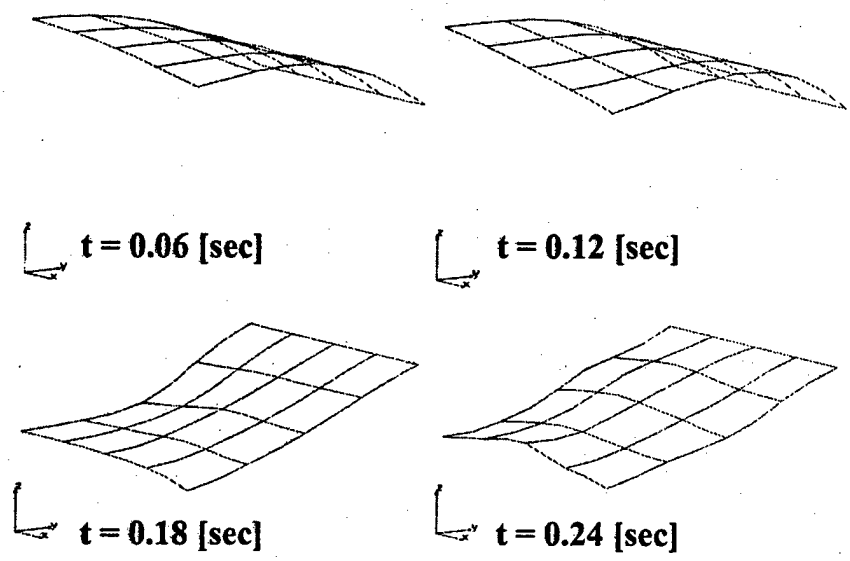
Figure 21: Configuration of the snap-through problem.

t = 0.06 [sec]   t = 0.12 [sec]

t = 0.18 [sec]   t = 0.24 [sec]

Figure 22: System configurations at various time instants during the simulation.
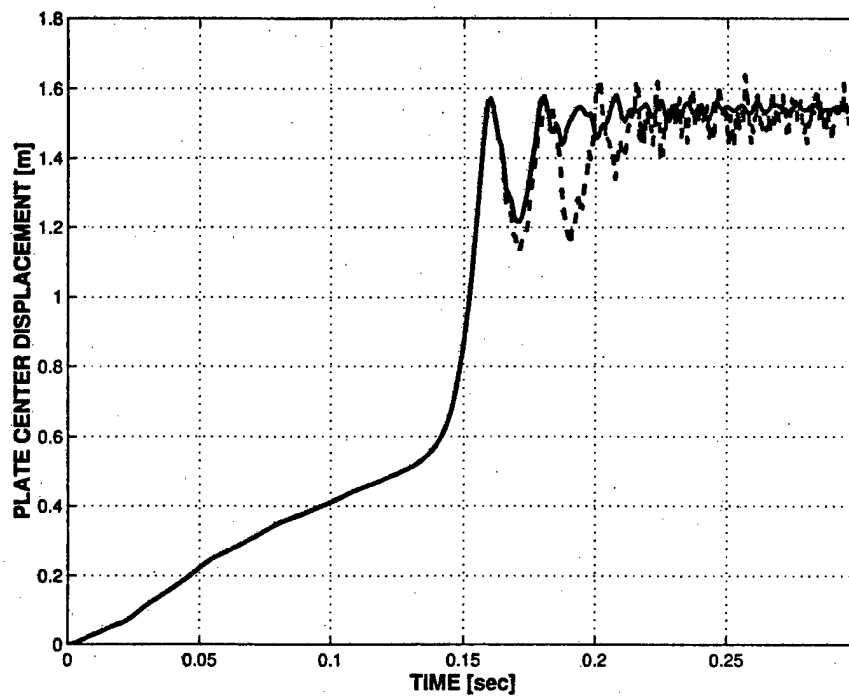
Figure 23: Time history of the plate center vertical displacement. ED($\alpha = 1$) scheme: solid line; ED($\alpha = 0$) scheme: dashed line.
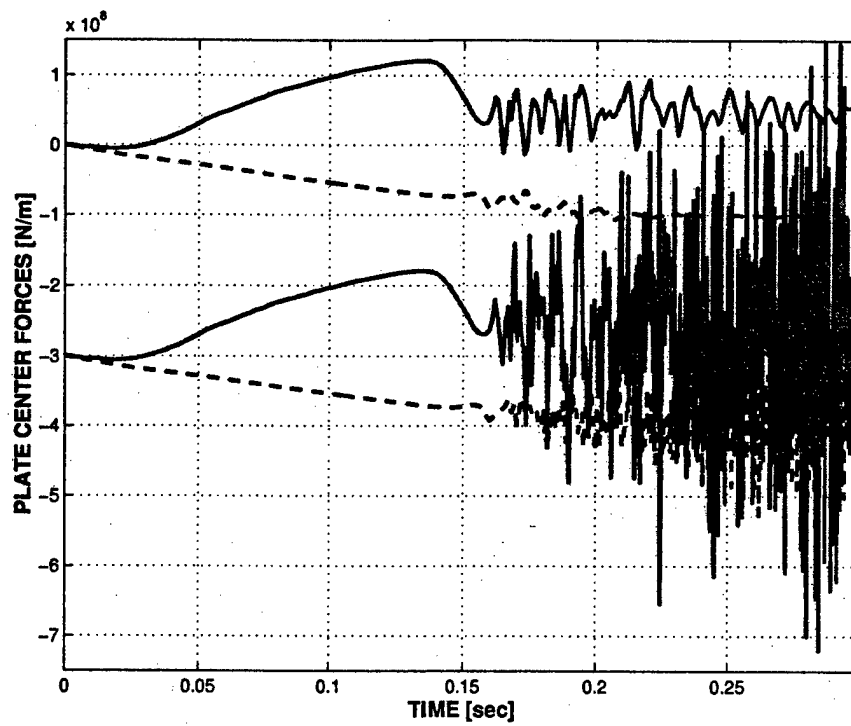
Figure 24: Time history of the plate center forces for the ED($\alpha = 1$) and ED($\alpha = 0$) schemes. Force F_1: solid line; F_3: dashed line. For clarity the ED($\alpha = 0$) results are shifted downwards 3 10^8 N.
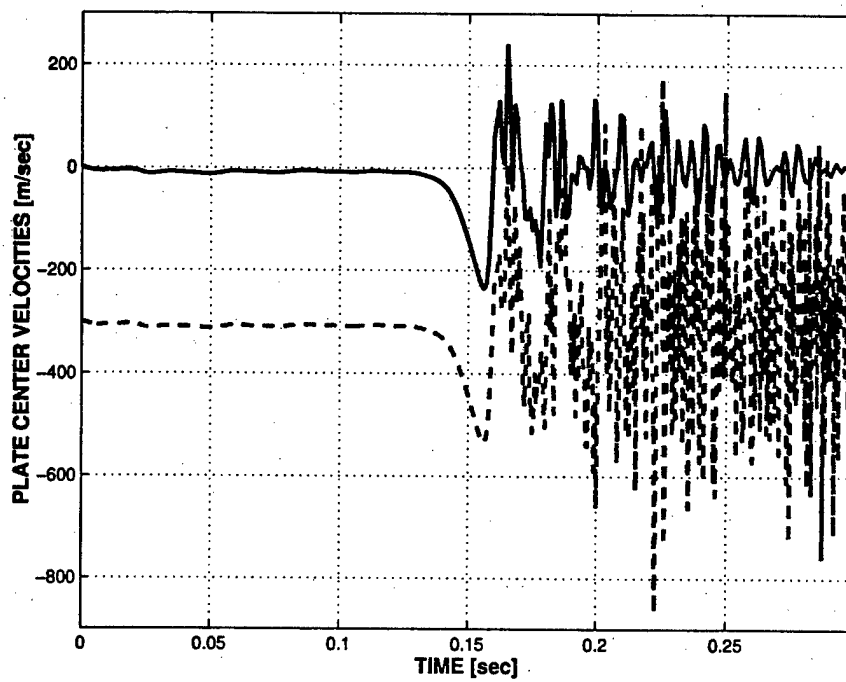
Figure 25: Time history of the plate center vertical velocity. ED($\alpha = 1$) scheme: solid line; ED($\alpha = 0$) scheme: dashed line, shifted downwards $3\ 10^2$ m/s for clarity.